Non-contrast-enhanced Magnetic Resonance Imaging and Computational Fluid Dynamics for Carotid Atherosclerosis

Yuanyuan Dai (M.D.)

A thesis submitted to Macquarie University for the degree of Doctor of Philosophy, Department of Biomedical Sciences, Faculty of Medicine and Health Sciences

Supervisor:

Professor Itsu Sen (Yi Qian)

Co-Supervisor (Fudan University):

Professor Jiang Lin

MACQUARIE University
SYDNEY·AUSTRALIA

Statement of Originality

This thesis is my original work except where acknowledgement has been made and where due reference is stated otherwise. The contents in this thesis, to the best of my knowledge, has not been accepted for the award for any other degree or diploma at a university or any other tertiary institution. The thesis has obtained the approval of the Ethics Committee approvals from Macquarie University (Reference No.: 5201700885) and Shanghai Zhongshan Hospital of Fudan University (Approval No.: B2014-004).

Yuanyuan Dai

July 2018

Contents

Acknowledgements

Firstly, I would like to express my deepest and sincerest gratitude to my supervisor Professor Itsu Sen (Yi Qian), who has been supportive and inspiring on the academic field in my doctorate candidate period. His expertise and knowledgeable words have enlightened me through my study life. I also am very appreciated for his patience and inclusive manners.

My greatest gratitude should also be given to Professor Jiang Lin. Thanks for his guidance and suggestions helped me all through my research journey, and for allowing me to have such a long-time experience in the high degree research and culture life in Australia.

In addition, I would like to thank all my friends and colleagues: Anna Guller, Olivia Leuang, David Verrelli, Yujie Li, Mingzi Zhang and Adam Chakos. Thanks for their academic discussion, accompanied and these talks that help me go through the difficulties during this journey, as well as the good times shared together.

My grateful thanks must be given to Peng Lv, who helped me with the clinical data collection and shared with me his intellectual and resourceful ideas when conducting my research. Thanks also need to be given to Aihua Ji and Xueqin Bai, who supported me to a great extent during my doctoral study.

I am very thankful of Dr. Xi Zhao for his technical and academic supports in Computational Fluid Dynamics study, which made my research progressing successively and timely.

I acknowledge the contributions from Dr. Askan Javadzadegan, who gave me considerable academic help for my PhD study.

Great thanks must be given to these amazing mates in our office. Thanks for the great chats, board games, and these memorable moments and experiences that we had together.

I would like to acknowledge the financial support from Macquarie Research Excellence Scholarship (iMQRES) for my tuition fee and living costs.

Most of all, I am very grateful to my family, for your endless support and love through this challenging journey. Your support and contributions allows me to pursuit the knowledge and life without any worries. Your love beyond any words.

List of Publications

Journal Papers

1. **Y. Dai**, P. Lv, J. Lin, R. Luo, A. Ji, H. Liu, C. Fu. Comparison study between multicontrast atherosclerosis characterization (MATCH) and conventional multicontrast MRI of carotid plaque with histology validation. J Magn Reson Imaging. 2017; 45(3):764-770. (**IF = 3.612**)
2. **Y. Dai**, Y. Qian, P. Lv, A. Javadzadegan, X. Tang, Y. Qian, J. Lin. Hamodyanmics analysis of carotid artery after endarterectomy: A study based on CFD and MRA. Quantitative Imaging in Medicine and Surgery. 2018; 8(4):399-409. (**IF = 2.23**)
3. **Y. Dai**, M. Zhang, Y. Li, P. Lv, A. Ji, X. Bai, Y. Qian, J. Lin. Associations between local haemodynamics and carotid intraplaque haemorrhage with different stenosis severities: a preliminary study based on MRI and CFD. J Clin Neurosci. Revised.
4. P. Lv, **Y. Dai,** J. Lin, W. Zhang, H. Liu, H. Liu, X. Tang. A comparison study between 3D T2-weighted SPACE and conventional 2D T2-weighted turbo spin echo in assessment of carotid plaque. Int J Cardiovasc Imaging. 2017; 33(3):395-400. (IF = 1.896)
5. S. Yang, J. Lin, F. Lu, **Y. Dai**, Z. Han, C. Fu, F. Hu, H. Gu. Contrast-enhanced susceptibility weighted imaging with ultrasmall superparamagnetic iron oxide improves the detection of tumor vascularity in a hepatocellular carcinoma nude mouse model. J Magn Reson Imaging. 2016; 44(2):288-95. (IF = 3.612)

Conference proceeding

1. Y. Dai, P. Lv, A. Javadzadegan, X. Tang, Y. Qian, J. Lin. Haemodynamic Analysis of Carotid Artery before and after Carotid Endarterectomy Surgery. The 5th International Conference on Mechanics in Medicine and Biology (ICMMB), 2017.

List of abbreviations

2D	two-dimensional
3D	three-dimensional
4D	four-dimensional
AUC	areas under curve
BB	black-blood
CA	calcification
CAS	carotid artery stenting
CCA	common carotid artery
CEA	carotid endarterectomy
CFD	computational fluid dynamics
CAVATAS	carotid and vertebral artery transluminal angioplasty study
CT	computed tomography
CTA	computed tomography angiography
CREST	carotid revascularisation endarterectomy versus stenting trial
DIR	double inversion recovery
DWI	diffuse-weighted imaging
DSA	digital subtraction angiography
DUS	Doppler/duplex ultrasonography
ECA	external carotid artery
ECST	European carotid surgery trial
EGG	electrocardiogram
FSE	fast spin echo
FLASH	fast low angle shot
FOV	field of view
IPH	intraplaque haemorrhage
IMT	intimal-medial thickness
ICA	internal carotid artery
ICC	intraclass correlation coefficient

ICSS	international carotid stenting study
LDL	low-density lipoprotein
LRNC	lipid-rich necrotic core
LM	loose matrix
MATCH	multi-contrast atherosclerosis characterization
MRI	magnetic resonance imaging
MRA	magnetic resonance angiography
NASCET	north American symptomatic carotid endarterectomy trial
NWI	normal wall index
PC	phase contrast
RF	repeated radiofrequency
ROI	region-of-interest
SD	standard deviation
SNR	signal-noise-ratio
SMC	smooth muscle cell
SAPPHIRE	stenting and angioplasty with protection in patients at high risk for endarterectomy
EVA-3Sb	symptomatic severe carotid stenosis
T1w	T1 weighed imaging
T2w	T2 weighted imaging
TE	echo time
TI	inversion time
TOF	time-of-flight
TR	repetition time
TIA	transient ischemic attack
TSE	turbo spin-echo
VENC	encoding velocity
mWSS	maximum wall shear stress
WSS	wall shear stress
WSSG	wall shear stress gradient

List of Figures

List of Tables

Abstract

Atherosclerotic plaques of the carotid artery are considered to be one of the major risk factors for stroke. To efficiently and precisely characterise the major plaque components, a new magnetic resonance imaging (MRI) sequence has therefore been promoted in this project. Besides plaque components, haemodynamics also plays a critical role in the progress and rupture of atherosclerotic plaques. Therefore, a new methodology that combines computational fluid dynamics (CFD) with non-contrast-enhanced magnetic resonance angiography (MRA) has been developed in this study to provide quantitative haemodynamic analysis for the diagnosis of carotid atherosclerosis and assessment of the outcomes of surgery.

In the first part of this research, a newly-developed plaque sequence termed 'MATCH' is introduced. The MATCH sequence has the advantages of short acquisition time and ability to identify plaque components. The MATCH sequence has been utilised to characterise the major plaque components, which include intraplaque haemorrhage (IPH), a large lipid-rich necrotic core, loose matrix, and calcification. The performance of MATCH in differentiating plaque components was compared with that of conventional multi-contrast MRI and confirmed by histological evidence in this study. The results indicate that the MATCH was comparable if not superior to conventional protocol in identification and quantification of major carotid plaque components.

In the second part, the relationship between haemodynamics and carotid plaques with IPH was investigated. We hypothesised that haemodynamics plays a pivotal role in the development of IPH. For this purpose, the maximum wall shear stress (mWSS) at the surface

of plaques was compared for the groups with and without IPH under different severities of carotid artery stenosis. The results demonstrated that the higher mWSS was exhibited in carotids with IPH for cases with stenosis less than 70%, and the magnitude of mWSS was positively correlated with the volume of IPH. However, there was no significant relationship between mWSS and IPH when the stenosis exceeded 70%. Our results indicate that mWSS is a promising parameter to evaluate plaque vulnerability for carotids with stenosis of less than 70%.

In the last part of this thesis, CFD simulation was performed to analyse blood flow changes after carotid endarterectomy (CEA). The morphological characteristics and haemodynamic parameters were compared before and after CEA, as well as for healthy carotids as a control group. The major haemodynamic parameters were restored after surgery in short-term follow-up. This study indicates that CFD analysis can provide valuable information for the evaluation of physiological functions after CEA.

Chapter 1

Introduction

Introduction

Carotid atherosclerosis is considered as the leading cause of stroke in developed countries, effecting thousands of millions people in the world. It is well acknowledged that the treatment of carotid atherosclerosis could markedly reduce the risk of subsequent stroke. The clinical guidelines of carotid atherosclerosis take stenosis severity as the criteria, which recommend that the carotids with stenosis over 70 % and symptomatic stenosis between 50 and 69 % are subject to revascularisation [1]. However, as described by large randomised clinical trials that patients with carotid stenosis less than 50% still experience the cerebrovascular events [2]. In this regard, the risk stratification of carotid atherosclerosis is essential to provide extra information beyond stenosis severity for the decision-making before revascularisation.

Medical imaging is commonly applied in the diagnosis and evaluation of carotid atherosclerosis. The advancement of magnetic resonance imaging (MRI) technology has promoted the morphological analysis of atherosclerotic plaques [3, 4]. The ability and the accuracy to analyse plaque burden and components is the key to assess plaque stability [5]. However, the clinical application of MRI in plaque analysis is restricted due to the inherent limitations of conventional MRI including long acquisition time (around 10 minutes) and difficulty in interpretation. Therefore, the improvement of MRI in the diagnosis of carotid atherosclerosis is necessary for broad clinical application.

Follow the rapidly development of medical imaging and computer technology, computational fluid dynamics (CFD) is applicable to simulate the complex haemodynamic flows. Image-based CFD, which is the combination of medical imaging and simulation methodology, has been applied to evaluate the haemodynamic information in vascular diseases [6, 7]. Previous investigators have made considerable progress in understanding the role haemodynamics

played in the initiation and development of atherosclerosis by using image-based CFD [8, 9]. However, before the CFD technology could be applied in clinical practice, comprehensive understanding of plaque morphologic and haemodynamic relationship and the assessment on interventions is required. In general, the capability for risk stratification of carotid atherosclerosis needs to be improved from conventional imaging modality and the functional assessment needs to be improved and evaluated.

I conducted this research from a radiologist's view aiming to improve the accuracy of diagnosis and post-surgery assessment for carotid atherosclerosis. In this study, a new MRI sequence was introduced and the CFD technology together with the non-contrast MRI was investigated to develop a diagnosis tool to assess the risk stratifications of carotid atherosclerosis. Herein, a brief overview and contents of each chapter are provided below.

Chapter 2

This chapter by reviewing the recent studies of carotid atherosclerosis to provide background information to this thesis. The vasculature of carotid artery is briefly introduced and then the recent studies on carotid atherosclerosis are comprehensively reviewed in regards to the clinical characteristics, aetiology, diagnosis, and treatments of carotid atherosclerosis.

Chapter 3

In this chapter, the MRI techniques applied for the evaluation of carotid atherosclerosis were introduced. The major principle of carotid MRI techniques used in the current study were reviewed as well as their clinical and advanced application. In addition, some novel techniques in the carotid atherosclerosis were also introduced aiming to provide new insights for the future study.

Chapter 4

In this chapter, we introduced a new non-contrast MRI sequence termed as MATCH to analyse plaque morphology and characterise the major plaque compositions including intraplaque haemorrhage (IPH), lipid-rich necrotic core, loose matrix and calcification. The performance of MATCH in measuring plaque burden and identifying plaque compositions were compared with conventional multi-contrast MRI, with histology as a reference.

Chapter 5

This chapter provided an overview of CFD application in cerebrovascular diseases, particularly in carotid atherosclerosis, as well as the major haemodynamic parameters. Then, the methodology of CFD used in this project were presented , including basic CFD theories, CFD modelling, meshing generation, boundary conditions, CFD simulation, post-processing.

Chapter 6

In this chapter, we analyse the relationships between IPH and local haemodynamics by using non-contrast-enhanced MRI and CFD. The maximum wall shear stress between plaques with and without IPH related to the severities of carotid arteries, as well as the relationship between the volume of IPH and maximum wall shear stress.

Chapter 7

In this chapter, we explored the haemodynamics after carotid endarterectomy by using non-contrast-enhanced MRI and CFD. The comparison of haemodynamics changes before and after carotid endarterectomy were performed with the control of a healthy group. The haemodynamic parameters including the maximum, mean, minimum and gradient of wall shear stress as well as morphological characteristics were compared and analysed.

Chapter 8

This chapter provides an overview of the findings of this thesis regarding the plaque imaging techniques and quantitative haemodynamic analysis in the pre-surgery risk stratification and the post-surgery assessment by using non-enhance MRI and CFD. The application of the plaque sequence and CFD technologies will have the potential to be generalised into clinical practice. Overall, plaque component and haemodynamic analysis techniques would be available to provide information for the diagnosis and post-surgery follow-ups of carotid atherosclerosis.

Reference

1. Barnett HJ, Taylor DW, Eliasziw M, et al. Benefit of carotid endarterectomy in patients with symptomatic moderate or severe stenosis. North American Symptomatic Carotid Endarterectomy Trial Collaborators. N Engl J Med. 1998;339(20):1415-1425.

2. Rothwell PM, Gutnikov SA, Warlow CP, Trialists ECS. Reanalysis of the final results of the European Carotid Surgery Trial. Stroke. 2003;34(2):514-523.

3. Saam T, Hatsukami TS, Takaya N, et al. The vulnerable, or high-risk, atherosclerotic plaque: noninvasive MR imaging for characterization and assessment. Radiology. 2007;244(1):64-77.

4. Millon A, Mathevet JL, Boussel L, et al. High-resolution magnetic resonance imaging of carotid atherosclerosis identifies vulnerable carotid plaques. J Vasc Surg. 2013;57(4):1046-1051.

5. Hosseini AA, Simpson RJ, Altaf N, Bath PM, MacSweeney ST, Auer DP. Magnetic Resonance Imaging Plaque Hemorrhage for Risk Stratification in Carotid Artery Disease With Moderate Risk Under Current Medical Therapy. Stroke. 2017;48(3):678-685.

6. Cebral J, Mut F, Sforza D, et al. Clinical Application of Image-Based CFD for Cerebral Aneurysms. Int J Numer Method Biomed Eng. 2011;27(7):977-992.

7. Jia Q, Liu HB, Li YP, Wang XX, Jia JJ, Li YY. Combination of Magnetic Resonance Angiography and Computational Fluid Dynamics May Predict the Risk of Stroke in Patients with Asymptomatic Carotid Plaques. Medical Science Monitor. 2017;23:479-488.

8. Birchall D, Zaman A, Hacker J, Davies G, Mendelow D. Analysis of haemodynamic disturbance in the atherosclerotic carotid artery using computational fluid dynamics. Eur Radiol. 2006;16(5):1074-1083.

9. Martin D, Zaman A, Hacker J, Mendelow D, Birchall D. Analysis of haemodynamic factors involved in carotid atherosclerosis using computational fluid dynamics. Br J Radiol. 2009;82:S33-S38.

Chapter 2

Literature Review

2.1 Introduction

Carotid atherosclerosis is a well-established risk factor for transient ischaemic attack (TIA) and stroke, affecting millions of people both in developing and developed countries. These ischaemic events may be caused by reduced blood supply to the brain caused by the narrowing lumen or the emboli from carotid plaques [1, 2], and so carotid plaque removal and stenosis correction can definitely decrease the risk of stroke [3]. Therefore, great interest has been aroused in the diagnosis and management of carotid atherosclerosis. This chapter will give a brief review of the vasculature, pathology, and aetiology of carotid atherosclerosis, followed by a detailed examination of relevant research studies on the diagnosis and management of carotid atherosclerosis, providing background information for the whole project.

2.2 Carotid bifurcation

The carotid bifurcation is the most common site for atherosclerotic plaques [4]. The vasculature of the carotid bifurcation comprises the distal common carotid artery (CCA), the proximal internal carotid artery (ICA), the external carotid artery (ECA), and the carotid sinus or so-called carotid bulb (the dilation of the region where ICA arises from CCA).

The CCA rises from the aortic arch or brachiocephalic trunk, up to the level of the C4 vertebra where it is enlarged to form the carotid sinus, and then then splits into two branches, namely the ICA and the ECA. Blood flow from the ICA supplies the brain, together with flow from the contralateral ICA and vertebral arteries through the circle of Willis, which is the underlying reasons by which embolization occurs in the brain. The blood from the ECA and its branches, including the superior thyroid artery, the facial artery, the occipital artery and so on, support the superficial structures in the head and neck region [5]. An illustration of the

carotid artery and its proximal and distal connections is provided in **Figure 2-1**, which is a three-dimensional (3D) reconstruction based on computed tomographic angiography (CTA).

Due to the structure of the carotid bifurcation, disturbed or helical flows occur [6]. Unlike normal developed flow, these types of flows are considered to be involved in the development of atherosclerosis [6]. The carotid bulb, where atherosclerotic plaques most frequently develop, is subject to formation of helical flow patterns in large regions, whereas the inner region of the bifurcation area and the distal ICA maintains normal bulk flows [7].

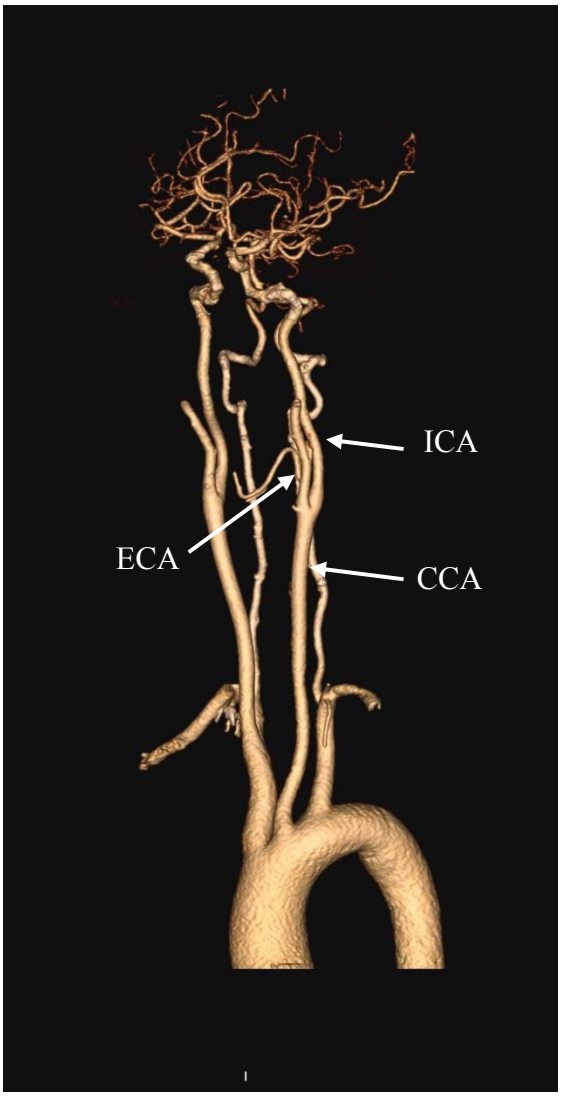

Figure 2-1. Computed tomography angiography showing a complete view of a normal carotid artery, including common carotid artery (CCA), carotid bifurcation, internal carotid artery (ICA) and external carotid artery (ECA), which is the critical pathway of blood flow from the thoracic aorta to vessels in the brain. (From Zhongshan Hospital of Fudan University, Shanghai, China)

2.3 Pathology

Atherosclerosis is a chronic inflammatory disease characterised by the local development of atherosclerotic plaques on the artery wall. The process of atherosclerosis begins in the early stages of life and takes decades to form the plaques [8].

A normal carotid artery wall is composed of three layers: tunica intima, tunica media and tunica adventitia. The process of atherosclerosis is initiated by low-density lipoprotein (LDL) sinking into the tunica intima. Inflammatory cells including monocytes, macrophages and other immune cells are then activated and accumulated through the cooperation of endothelial cells and smooth muscle cells (SMCs). These inflammatory cells extend, oxidise and modify the LDL, leading to accumulation of lipoprotein [9]. With the cohesion of lipoproteins, lipid pools form. Eventually those lipid pools together with SMCs become embedded in an extracellular matrix, this is termed fatty streak formation (an early stage of atherosclerosis) which induces artery wall thickening [8]. As the wall thickens, the local vessel wall diameter increases in order to compensate for the reduction of lumen calibre, known as a remodelling process.

The advanced stage of atherosclerosis manifests more complex processes, with the further accumulation of lipid coupled with inflammation. During this stage, the fatty streaks develop into fibroatheromata. As the SMCs and lipid pools accumulate, the formation of an atherosclerotic plaque progresses and necrosis began to occur [10]. The necrotic lesion promotes further inflammation and exacerbates the atheroma development. On the surface of a necrotic plaque, a thin fibrous cap is often seen. The fibrous plaques were reported in the same places where necrotic plaques developed, hence it may indicate the same provenance of these two types of plaque [11].

The occurrence of intraplaque haemorrhage (IPH) is thought to originate from the disruption of microvessels (vasa vasorum) within an atheroma. New microvessels developed from the tunica media penetrate into the plaque. Erythrocytes may leak from such new microvessels, which lack strong support from pericytes, resulting in haemorrhage within plaques [8]. It is also reported that fibrin and carotid plaque fissure can also stimulate haemorrhage inside plaques [12, 13]; the underlying mechanism, however, is not fully understood.

2.4 Aetiology

2.4.1 Conventional risk factors

The aetiology of atherosclerosis is not fully elucidated. Chronic infection was considered to be a possible pathogenesis of atherogenesis. It was proposed that chronic infections may induce systematic inflammation and autoimmune responses, which are eventually subject to the development of atherosclerosis [14]. Yamashita *et al.* investigated the products from gram-negative organisms in atherosclerotic plaques, and suggested that there exist links between systemic infection and local atherosclerotic inflammation [15]. A study by DeGraba *et al.* showed that inflammation, including expression of inflammatory cytokines, was commonly seen in symptomatic carotid plaques [16]. The level of high-sensitivity C-reactive protein, a systematic biomarker of inflammation, is related at a statistically significant level to the development of carotid atherosclerosis [17]. Some other studies also indicated that other inflammatory or autoimmune diseases, such as rheumatoid arthritis [18], lupus erythematosus [19], and psoriasis [20], were involved in the development of atherosclerosis.

Several systematic risk factors affect the development of atherosclerosis by provoking or intensifying the inflammation process. Male gender, age, obesity, smoking, hypertension,

diabetes, hyperlipidaemia, fibrinogen, and low levels of high-density lipoprotein cholesteroland are frequently considered to be independent predictors of atherosclerosis [21-23]. A study by Rovella *et al.* [24] showed that for obese patients with age < 70 years, the odds ratio of unstable plaque formation was 5.91. While in males with age ≥ 70 years, the odds ratio of unstable plaque formation decreased to 4.61; however, the odds ratio in females with age ≥ 70 years was 0.93. A study of Chinese type 2 diabetics showed that age over 60, hypertension, and dyslipidaemia were associated with intimal–medial thickness (IMT) [25]. Both active and passive smoking were able to increase the IMT [26]. A 3-year follow-up study showed that systolic blood pressure, especially raised daytime systolic blood pressure variability (>15 mm Hg), was significantly related to the progression of IMT [27]. A study by Crouse *et al.* [28] demonstrated that the active treatment of cholesterol could significantly reduce the IMT of the carotid artery by 35%. A meta-analysis including 10 trials and 3443 individuals in an age range of 30 to 70 years old proved that statin therapy was significantly related to the increase of IMT during a relatively long-term follow-up [29].

Each of these risk factors contributes to atherosclerosis through specific mechanisms. It is recognized that smoking can cause inflammation responses, especially in the activation of high-sensitivity C-reactive protein and fibrinogen, which are important in cardiovascular diseases [30, 31]. Hypertension and hyperglycaemia can induce oxidative stress through overproduction of reactive oxygen species, resulting in oxidative DNA changes and deterioration of medial thickness [32, 33]. However, the mechanisms underlying some other risk factors still need to be unravelled.

2.4.2 Genetic risk factors

The genetic factors involved in the process of atherogenesis are not conclusively understood.

However, studies from siblings, twins, and families showed that genetic factors account for a substantial proportion of atherosclerosis [34, 35]. Ethnic predisposition to atherosclerosis was also observed. In a recent study, results showed that for Mexican-Americans and European-Americans different genes from different chromosomes were associated with intimal thickening and plaque development [36]. Hence, genetic factors are considered to be associated with the occurrence of atherosclerosis.

It is thought that the genetic factors play a role in the inflammatory process and interact with conventional risk factors in atherosclerosis [37]. To be specific, certain genotypes, such as matrix metalloproteinase 3 (MMP3) [38, 39], interleukin 6 (IL-6) [40, 41], hepatic lipase, apolipoprotein E (APOE) [42, 43], angiotensinogen [44], paraoxonase [45], and cholesterylester transfer protein (CETP) [35, 39], are considered to play a critical role in atherosclerosis. However, more studies are needed to further confirm the role of these genetic factors.

2.4.3 Haemodynamic factors

Although the aforementioned factors are well acknowledged to characterise the development of atherosclerotic diseases, haemodynamic factors are thought to play a critical role in their localization and progression [46]. Haemodynamic factors are involved in the initiation of atherosclerosis. For example, plaque formation is preferred to occur in recirculation areas, *i.e.* downstream of arterial bifurcations and bends. It also has been observed that local haemodynamic parameters can advance plaque growth and rupture [47]. Low wall shear stresses and long residence times are thought to exacerbate the chemical processes of wall thickening and clotting especially in complex flow areas [48]. A longitudinal study showed the plaque ruptured in regions exposure to high wall shear stress [49].

2.5 Clinical characteristics

Carotid atherosclerosis is traditionally classified into symptomatic and asymptomatic types. Symptomatic carotid atherosclerosis is usually defined as transient ischaemic attack (TIA) or stroke ipsilateral to the carotid stenosis in the preceding 6 months [50, 51]. However, some symptoms such as amaurosis (vision loss) and aphasia are often seen. The symptoms vary depending upon which segments of the vessel have been blocked by the emboli detached from carotid plaques. If the anterior cerebral circulation is involved, contralateral symptoms including hemianopia, visuospatial neglect, weakness, or paraesthesia in the face, arm or leg are manifested [51]. However, due to the circulation through the circle Willis, in some cases carotid arteries with significant atherosclerotic plaques may remain asymptomatic. An indicative scan (**Figure 2-2**) from diffusion weighted imaging shows the ipsilateral ischaemic symptoms in the left hemisphere due to carotid atherosclerosis.

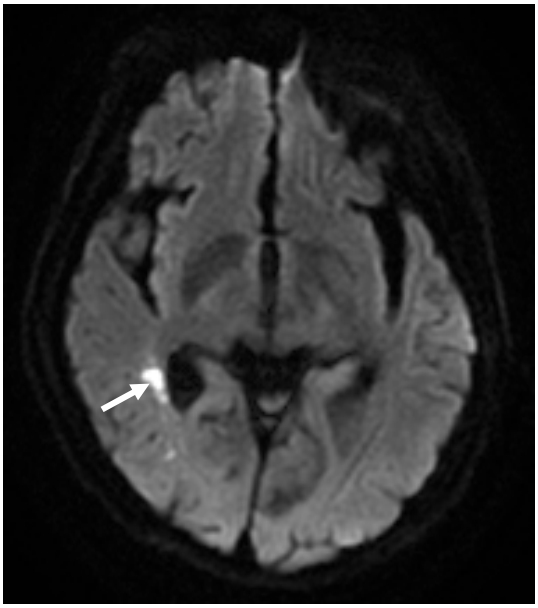

Figure 2-2. Scan from diffusion-weighted imaging (DWI) showing acute embolic infarcts (white arrow) of the right middle cerebral artery territory associated with carotid atherosclerosis. This image is from a 51-year-old male with left carotid atherosclerosis, who had experienced dizziness and headache for one week. (From Zhongshan Hospital of Fudan University, Shanghai, China)

2.6 Diagnosis of carotid stenosis

2.6.1 Clinical guidelines

The severity of luminal stenosis is the reference criterion for the management of carotid atherosclerosis. In line with the criterion, investigations into accurate calculation of the percentage of the lumen stenosis have been explored widely. Several randomised clinical trials including the European Carotid Surgery Trial (ECST) and the North American Symptomatic Carotid Stenosis Trial (NASCET) have proposed different standards to measure the severity of stenosis [49, 52]. Currently, the NASCET criteria provide the consensus method to quantify stenosis of the carotid artery [53, 54]. The percentage stenosis according

to NASCET is calculated from the following formula [54, 55]:

Percentage stenosis = (1 − minimal diameter / distal normal diameter) × 100. (2-1)

According to the range within which the calculated percentage falls, the stenosis can be graded as mild (0–30%), low–moderate (30–50%), high–moderate (50–69%), or severe (70–99%) occlusion [54]. The earlier European Carotid Surgery Trial (ECST) measurement procedure used the estimated normal lumen diameter at the site of the lesion instead of the distal normal diameter in the above formula [2, 56]. An illustration of the NASCET and ECST methods is provided in **Figure 2-3**.

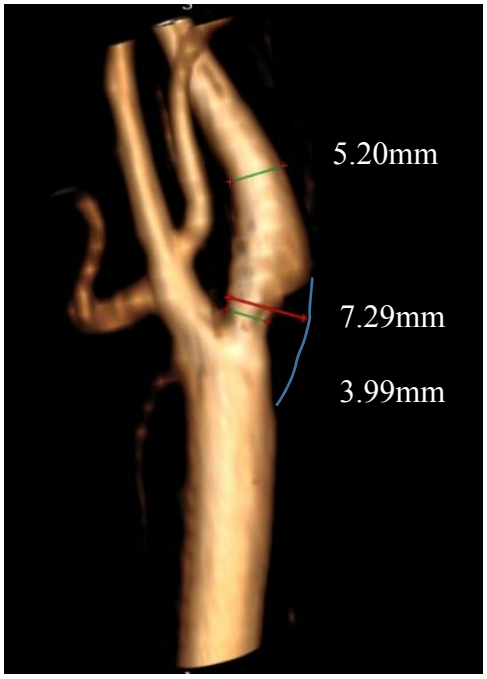

NASCET = (1 – 3.99/5.20) × 100

= 23.26 %

ECST = (1 – 3.99/7.29) × 100

= 45.27 %

Figure 2-3. Illustration of two different measurement methods from NASCET and ECST. (From Zhongshan Hospital of Fudan University, Shanghai, China)

The existence of two different measurement protocols causes a certain mismatch between the two trials. The degree of stenosis calculated in the NASCET tended to be smaller than that calculated in the ESCT [57]. In order to better compare the results from the two trials, Rothwell *et al.* in 1994 introduced a formula establishing a concordance between stenosis measurements in the two trials: the stenosis degree measured by the ECST protocol was equal to 0.6 times the percentage stenosis measured by the NASCET method plus 40 [56].

2.6.2 Plaque burden

The efficacy of using the surrogate marker of luminal narrowing in predicting embolism events is being challenged. The landmark European trial, ESCT, showed that 43.8% of the 2018 trial participants with symptomatic carotid disease had stenosis of under 30% [58], and 61% of the 2226 recently symptomatic subjects had less than 50% carotid stenosis in the NASCET [54]. In this regard, many factors in addition to stenosis were proposed to stratify the high risks of carotid atherosclerosis. Plaque burden is considered to be one of the risk factors that are closely related to the occurrence of ischaemic stroke [59]. Previous studies reported that plaque burden can be evaluated in terms of plaque thickness, plaque area and volume, normal wall index (NWI), and so on [60]. Measurement of plaque burden may enable assessment of individual responses to therapy [61]. However, no consensus has been made on the choice of the different parameters and the methods of measurement, as the contrast between outer and internal vessel wall is relatively low. Current imaging modalities might have practical difficulties and biases in the delineations of the wall features and volumetric calculations.

2.6.3 Plaque compositions

The differentiation of plaque types has garnered increasing interest in risk stratification

analyses and in assessing the effects of therapy. Some compositions are considered to be associated with TIA or ischaemic stroke risks. Thus, the term “vulnerable plaques” appeared to describe such plaques. However, the “vulnerable” concept was first described by Muller to categorize plaques with a disruptive nature and causing acute clinical events in coronary arteries [62]. The consensus definition of the vulnerable plaque was established for the carotid artery in 2003 [63]. Presence of vulnerable plaque was proved to increase the risk of stroke [64]. The vulnerable plaques feature intraplaque haemorrhage (IPH), a large lipid-rich necrotic core (LRNC), and a thin fibrous cap. However, beyond the common vulnerable plaques, controversies have been raised regarding calcification. Some studies showed relations to embolism events [65, 66], while other researchers held different opinions [67]. A recent systematic review suggested that calcification might be slightly useful in predicting cerebrovascular ischaemic events [68]. Although assessment of plaque components has not been written into the guidelines for carotid atherosclerosis management, plaque composition still plays a pivotal role in guiding clinicians’ decision-making.

2.6.4 Diagnostic tools

The diagnosis of carotid atherosclerosis mainly depends on imaging modalities. For many years, different imaging methods, including digital subtraction angiography (DSA), Doppler/duplex ultrasonography (DUS), computed tomography angiography (CTA) and magnetic resonance angiography (MRA), have been used to monitor the degree of luminal stenosis [69].

DSA is considered to be the reference standard for evaluating the severity of carotid stenosis [70]. The major disadvantages of DSA are the unable to visualise the vessel wall structure, thereby it is unable to provide plaque information. Besides that, DSA carries a relatively high

risk of causing neurological dysfunctions and other complications, leading to a certain proportion of morbidities and mortalities. A large study of 2,899 patients showed the incidence of neurological events is about 1.3%, and 0.5% were permanent [71]. The occurrence rate of major neurological complications ranges from 0.26 to 0.43% [72].

DUS is the primary non-invasive imaging modality used for screening of carotid atherosclerosis [73]. The velocity of blood flow measured at different locations within the artery could vary according to the degree of carotid stenosis. To better indicate the severity of carotid disease, the velocity measurements were translated into stenosis 'cut points' which are broadly used in clinical practice. A peak systolic velocity (PSV) of 125 to 230 cm/s is said to suggest a 50% to 69% stenosis, while a PSV of >230 cm/s suggests a >70% carotid stenosis [74]. A meta-analysis showed that a peak systolic velocity of 130 cm/s or larger could suggestively have a sensitivity of 98% and specificity of 88% in the identification of stenoses over 50%, and a peak systolic velocity of 200 cm/s or over can provide a sensitivity of 90% and specificity of 94% for the diagnosis of stenoses over 70% [75]. However, how to interpret the DUS criteria is still of concern, and a standardization of this should be set up [76]. Furthermore, the measurement varies considerably among different users and could be affected by heavy calcification of the artery.

CTA as a non-invasive method is widely used to evaluate carotid artery stenosis [77, 78]. It has been applied frequently in the initial evaluation of patients with carotid stenosis. The advantages of CTA lie in its fast and non-invasive nature. In addition, it permits visualization of the arterial lumen, display of multiple-plane views, and rendering of the 3D reconstruction of the artery. However, unlike DUS, CTA has issues of radiation exposure and a contrast medium requirement. A study of 81 carotid arteries compared CT with DSA and found that

CT had a high sensitivity and a high negative predictive value in the measurement of stenosis [79]. A study of historical specimens confirmed that CTA had the best accuracy in detecting carotid stenosis compared with DUS, DSA, and MRA [80].

MRA is a commonly accepted method in evaluation of carotid stenosis, with wide applications. The advantages of MRA are its non-invasiveness and high spatial resolution. MRA is considered to be able to accurately diagnose carotid stenosis as efficiently as CT [81]. However, the sensitivity and specificity vary among different MRA sequences. Contrast enhanced (CE) MRA is considered to be the most accurate MRA sequence to evaluate artery narrowing; however, it can still overestimate the stenosis by 2.6 % using the ECST measurement and underestimate the stenosis by 0.6 % using the NASCET method [80]. Non-contrast-enhanced MRA, which does without contrast medium, recently emerged as a substitute for CE-MRA. As the most commonly used non-contrast MRA method, TOF-MRA is the most preferred sequence for routine clinical use due to the quick scan time. An early study showed that TOF-MRA only provides moderate accuracy in characterising mild stenosis, with DUS and DSA as references [82]. With the advancement of MR techniques, TOF-MRA could be accurately used in carotid stenosis grading, with a sensitivity of 95.5% and a specificity of 87.2% [83]. However, TOF-MRA is thought to misclassify high or severe stenosis as occlusion [84]. Three-dimensional (3D) black blood MRA is a newly developed sequence and was able to correctly assess moderate to severe stenosis, compared with DSA; however, due to long scan time, usage is not prevalent in clinical practice [85]. Recently, a review from Brinjikji *et al.* [86] nominated MRA as the gold standard for carotid imaging, as it is not only available for stenosis measurement but also has high sensitivity and specificity in the characterization of plaque compositions. High-resolution, multi-contrast carotid MRA protocols have been used to depict atherosclerotic components within carotid plaques; the

validity of these protocols have been evaluated by histopathology, and the protocols have been applied in multicentre trials. Despite the advantages of MRA, it must also be mentioned that the main limitation of MRA is its time constraints. Further disadvantages are the inability of MRA to examine the substantial proportion of patients who have claustrophobia, extreme obesity, or incompatible implanted devices such as pacemakers or defibrillators [87].

2.7 Treatment of carotid atherosclerosis

The guidelines recommend that patients with stenosis greater than or equal to 70% and symptomatic patients with stenosis of 50–69% undergo revascularisation [54, 88]. In carotid stenosis of <50% with or without symptoms, the medical therapy rather than revascularisation is the optimal choice [89]. To date, the first-line treatment for carotid stenosis is through surgery or stenting: carotid endarterectomy (CEA) and carotid artery stenting (CAS) [88]. Medical therapy is considered as to be a complementary method to CEA and CAS.

2.7.1 Carotid endarterectomy

The procedure for CEA is to mechanically remove the atherosclerotic plaque from an incision in the vessel wall. After heparin administration, the ICA, CCA, and ECA are sequentially closed using vascular clamps. Then a longitudinal incision is made in the anterior surface of the CCA near the bifurcation and extended anteriorly to the distal ICA, where the plaque transitions into normal intima tunica [89]. CEA is considered to be beneficial for older patients with symptomatic stenosis [90].

The benefits of CEA surgery in patients with severe (70% to 99%) stenosis have been demonstrated by several large randomised clinical trials, including the NASCET and ECST [54, 91, 92]. The NASCET, involving 659 patients with severe stenosis, was stopped after 2

years and the results showed that the 2-year risk of ipsilateral stroke was 26% in patients treated medically compared with 9% in patients treated surgically [54, 93]. The ECST, including more than 3000 patients, showed that the 3-year stroke or death risk for patients with stenosis of 70–99% was 26.5% for those that underwent non-surgical treatment and 14.9% for the surgical treatment [94]. These results were confirmed by a recent meta-analysis, which showed that an elderly population with stenosis over 70% benefits predominantly from CEA surgery [95]. The results of reanalysis of the ECST data showed that the 5-year absolute risk reduction is 21.2% in patients with stenosis of 70–99% [73]. Pooled analysis of the NASCET and ECST data by Rothwell *et al.*, which included 6902 patients and 35,000 patient-years of follow-up, yielded an absolute risk reduction of 16 % in severe symptomatic carotid disease with CEA as compared to the best medical management [96]. Furthermore, the 10-year follow-up showed that patients with severe stenosis maintain the benefits from CEA [92].

In terms of symptomatic carotid diseases with stenosis between 50 and 69%, moderate benefits from CEA were shown [54, 95]. The 5-year incidence of ipsilateral stroke was 15.7% in NASCET patients with stenoses of 50% to 69% [54]. The absolute 5-year rate decreased by 8.4% in the NASCET and a reduction of 5.7% was shown in the ESCT [73]. Reanalysis of the ESCT data showed no benefit to patients with near occlusion from CEA [73]. However, CEA surgery has uncertain merit to such nearly occluded arteries from a long-term perspective. Conversely, CEA surgery tended to have a hazardous impact on patients with stenoses of under 30% [95], while in another trial the percentage stenosis for which CEA was hazardous extended up to 50% [92].

There exist some controversies over the benefits to asymptomatic patients of carotid

revascularisation. Adults with asymptomatic carotid stenosis are at increased risk, 2–5% per year, of ipsilateral carotid territory ischaemic stroke in the absence of medical therapy [47]. Two large trials, ACAS and ACST, have explored this question by treating patients with a combination of CEA and medical therapy or medical therapy alone [97, 98]. ACAS considered that benefits from surgery for the asymptomatic disease with stenosis of 60% or more in a selected population of patients have been demonstrated if the surgical morbidity/mortality is 0.3% and the patient has at least a 5-year prognosis for a healthy life thereafter. However, some authors mentioned that these trials were performed two decades ago, and, with the development of medicine since then, some of this research should be repeated again. In 1998, a meta-analysis investigating five trials that had collectively enrolled 2440 patients with stenosis >50% showed that CEA could unequivocally reduce the chance of ipsilateral stroke in patients with asymptomatic carotid stenosis [99]. It has also been shown that CEA in asymptomatic carotid stenosis brings greater benefits to younger patients [100].

2.7.2 Carotid artery stenting

CAS has emerged as an alternative and less invasive approach for carotid atherosclerosis treatment in clinical practice [101, 102], especially for those patients with severe cardiac and cerebrovascular diseases, or with medical illnesses which have a high perioperative risk, or for those who wish to avoid undergoing traumatic surgeries [103]. However, patients with age over 75 are not recommended for CAS treatment [104]. The CAS procedure is less traumatic than the CEA procedure. After local anaesthesia and the injection of clopidogrel and aspirin, a directional catheter with a guidewire is used to select the CCA from the femoral artery. During this process, an embolic protection device (EPD) is recommended for the purpose of protecting distal circulation [89].

Two larger randomised clinical trials, the Stenting and Angioplasty with Protection in Patients at High Risk for Endarterectomy (SAPPHIRE) [105] and Stent-Protected Angioplasty versus Carotid Endarterectomy (SPACE) [106] studies, showed that CAS is comparable to CEA in terms of perioperative stroke and death risk in arteries with stenosis greater than 70%. The SAPPHIRE trial found the 30-day rates of stroke or death from myocardial infarctions (MI) were 4.8% in CAS and 9.8% in CEA [105], whereas the SPACE trial showed that the 2-year rates of ipsilateral or periprocedural stroke or death were 9.5% in CAS and 8.8% in CEA [106]. A recent meta-review including 3901 patients from five RCTs also confirmed this conclusion, showing that CAS and CEA had similar risks of periprocedural major stroke, periprocedural ipsilateral stroke or MI [107]. In addition, some studies showed that CAS can significantly reduce post-surgical MI compared with CEA [108, 109].

Another two large randomised trials, the International Carotid Stenting Study (ICSS) [110] and the Endarterectomy versus Angioplasty in Patients with Symptomatic Severe Carotid Stenosis program (EVA-3S) [111], favoured CEA over CAS. The ICSS, by comparing CAS and CEA outcomes for symptomatic carotid stenoses at over 50% stenosis, found that CEA had lower rates of stroke, death, or periprocedural MI compared with CAS (5.4% versus 8.5%). The EVA-3S trial compared the periprocedural risk of CAS with CEA in terms of stroke, death and MI and was aborted with a negative result after 30 days. The incomplete study showed the rates of disabling stroke and death were 1.5% after CEA and 3.4% after CAS. A meta-review by Meier *et al.* [112] encompassing 11 randomised clinical trials showed that the periprocedural risk of death or stroke is lower in CEA compared to CAS in the short-term (less than one year).

The Carotid Revascularisation Endarterectomy versus Stenting Trial (CREST), which is the

most highly regarded trial, showed that periprocedural stroke occurred more frequently after CAS compared with the rate after CEA [113]. Although the CREST did not show any statistically significant difference between CAS and CEA with respect to the incidence of 30-day MI, stroke, or death, nor in the 4-year ipsilateral stroke incidence rates, a subgroup analysis showed a higher rate of periprocedural stroke for CAS in symptomatic patients [114]. Furthermore, gender and age also affect the incidence rates of stroke and death due to CAS and CEA. Women [115] and patients aged over 65 years [116] tended to have higher rates of stroke and death with CAS than they did with CEA.

2.7.3 Medical therapy

Although the landmark NASCET studies of the 1990s and early 2000s established the advantages of CEA compared with medical therapy, medical treatments including antihypertensive therapy, lowering hyperlipidaemia by statin agents, controlling diabetes and smoking cession are suggested to be effective ways to reduce the risk of stroke. Mervick *et al.* [117] analysed rates of stroke incidence in patients with or without statin pre-treatment from over 2000 TIA patients; 387 of whom had significant carotid disease. Those authors found that the rate of stroke occurrence was 3.8 % in the statin-treated group as compared to 13.2 % in the non-treatment group. In 2008, the Society for Vascular Surgery reconfirmed that patients who have symptomatic <50% stenosis are well suited to optimal medical therapy alone [89]. Medical therapy are also considered to be the main treatment recommended for asymptomatic carotid arteries. A study by the Society for Vascular Surgery also showed that asymptomatic carotid arteries with < 60% stenosis are better suited for medical treatment [89].

2.8 Artery restenosis after treatment

Restenosis is the most common complication of carotid revascularisation. However, the medical community has not reached consensus on the definition of restenosis. Some studies use criteria of a reduction of lumen diameter ≥ 70% and a peak velocity exceeding 3.0 m/s by DUS [118], while some other studies use a ≥ 50% reduction for the first criterion [119, 120]. It has been shown that most of the restenosis occurs about 6 months after revascularisation [106]. However, the cause of restenosis after revascularisation remains an issue that is not yet fully understood. The Carotid and Vertebral Artery Transluminal Angioplasty Study (CAVATAS) results revealed that restenosis 1 year after CAS was partially due to residual stenosis. The anatomic structure and operative techniques could influence the restenosis after CAS and CEA, such as the original form of stenosis, lack of stent coverage area, and the stent type [121]. Other studies proposed that the closure techniques of CEA surgery may affect the restenosis rate. Direct suture could increase the restenosis rate after surgery [122].

Although restenosis rates after CEA are relatively low, it still affects between 1% and 5% of patients and many times leads to more risky and expensive reintervention [123]. It has been reported that patients who underwent CAS may experience higher restenosis risk compared with those on whom CEA was performed [124]. A study by Arquizan et al. [120] reported that the short-term rate of carotid restenosis of over 50% or complete occlusion is about 2.5-times higher after CAS (12.5%) than after CEA (5.0%). That study included 507 patients, with 242 treated by CAS and 265 by CEA, and a follow-up time of 2.5 years. A large randomised trial called CREST, including 2191 patients and a 2-year follow-up, showed that the restenosis rate was similar for CAS and CEA (6.0% versus 6.3%) [118]. Another study with 533 patients who underwent radiation therapy showed more restenosis in patients after CEA than after CAS [125]. The results of the CAVATAS showed the rate of restenosis ≥70% in the ipsilateral carotid artery was higher after CAS than after CEA during the 1-year follow-up (18.5%

versus 5.2%). In regard to the discrepancies among different studies, this may be caused by patient-selection bias.

2.8 Conclusion

Despite the thorough understanding of atherosclerotic plaques, they have not been added into the clinical criteria on guiding the treatment of carotid atherosclerosis, partly due to the imaging techniques in spotting different plaque components. New plaque imaging techniques is in demanding, so that the wide application of plaque components analysis could be available.

Reference

1. Bronnum-Hansen H, Davidsen M, Thorvaldsen P, Danish MSG. Long-term survival and causes of death after stroke. Stroke. 2001;32(9):2131-2136.

2. Rothwell PM, Eliasziw M, Gutnikov SA, et al. Analysis of pooled data from the randomised controlled trials of endarterectomy for symptomatic carotid stenosis. Lancet. 2003;361(9352):107-116.

3. Brott TG, Hobson RW, 2nd, Howard G, et al. Stenting versus endarterectomy for treatment of carotid-artery stenosis. N Engl J Med. 2010;363(1):11-23.

4. Grotta JC. Clinical practice. Carotid stenosis. N Engl J Med. 2013;369(12):1143-1150.

5. Michalinos A, Chatzimarkos M, Arkadopoulos N, Safioleas M, Troupis T. Anatomical Considerations on Surgical Anatomy of the Carotid Bifurcation. Anat Res Int. 2016;2016:6907472. doi: 10.1155/2016/6907472.

6. Gallo D, Steinman DA, Bijari PB, Morbiducci U. Helical flow in carotid bifurcation as surrogate marker of exposure to disturbed shear. Journal Of Biomechanics. 2012;45(14):2398-2404.

7. Ku DN, Giddens DP, Zarins CK, Glagov S. Pulsatile flow and atherosclerosis in the human carotid bifurcation. Positive correlation between plaque location and low oscillating shear stress. Arteriosclerosis. 1985;5(3):293-302.

8. Insull W, Jr. The pathology of atherosclerosis: plaque development and plaque responses to medical treatment. Am J Med. 2009;122(1 Suppl):S3-S14.

9. Kockx MM, De Meyer GR, Muhring J, Jacob W, Bult H, Herman AG. Apoptosis and related proteins in different stages of human atherosclerotic plaques. Circulation. 1998;97(23):2307-2315.

10. Virmani R, Ladich ER, Burke AP, Kolodgie FD. Histopathology of carotid atherosclerotic disease. Neurosurgery. 2006;59(5 Suppl 3):S219-227.

11. Eggen DA, Solberg LA. Variation of atherosclerosis with age. Lab Invest. 1968;18(5):571-579.

12. Kolodgie FD, Yahagi K, Mori H, et al. High-risk carotid plaque: lessons learned from histopathology. Semin Vasc Surg. 2017;30(1):31-43.

13. Daemen MJ, Ferguson MS, Gijsen FJ, et al. Carotid plaque fissure: An underestimated source of intraplaque hemorrhage. Atherosclerosis. 2016;254:102-108.

14. Kiechl S, Egger G, Mayr M, et al. Chronic infections and the risk of carotid atherosclerosis: prospective results from a large population study. Circulation.

2001;103(8):1064-1070.
15. Yamashita K, Ouchi K, Shirai M, Gondo T, Nakazawa T, Ito H. Distribution of Chlamydia pneumoniae infection in the atherosclerotic carotid artery. Stroke. 1998;29(4):773-778.
16. DeGraba TJ, Siren AL, Penix L, et al. Increased endothelial expression of intercellular adhesion molecule-1 in symptomatic versus asymptomatic human carotid atherosclerotic plaque. Stroke. 1998;29(7):1405-1410.
17. Hashimoto H, Kitagawa K, Hougaku H, et al. C-reactive protein is an independent predictor of the rate of increase in early carotid atherosclerosis. Circulation. 2001;104(1):63-67.
18. del Rincon I, Williams K, Stern MP, Freeman GL, O'Leary DH, Escalante A. Association between carotid atherosclerosis and markers of inflammation in rheumatoid arthritis patients and healthy subjects. Arthritis & Rheumatism. 2003;48(7):1833-1840.
19. Divard G, Abbas R, Chenevier-Gobeaux C, et al. High Sensitivity Cardiac Troponin T Is a Biomarker for Atherosclerosis In Systemic Lupus Erythematous Patients: A Cross-Sectional Controlled Study. Annals Of the Rheumatic Diseases. 2017;76:187-187.
20. Dinic MZ, Zecevic RD, Hajdukovic Z, et al. Psoriasis is the independent factor for early atherosclerosis: A prospective study of cardiometabolic risk profile. Vojnosanitetski Pregled. 2016;73(12):1094-1101.
21. Etesami M, Hoi Y, Steinman DA, et al. Comparison of carotid plaque ulcer detection using contrast-enhanced and time-of-flight MRA techniques. AJNR Am J Neuroradiol. 2013;34(1):177-184.
22. Woo SY, Joh JH, Han SA, Park HC. Prevalence and risk factors for atherosclerotic carotid stenosis and plaque: A population-based screening study. Medicine (Baltimore). 2017;96(4):e5999.
23. Zhang Y, Bai L, Shi M, et al. Features and risk factors of carotid atherosclerosis in a population with high stroke incidence in China. Oncotarget. 2017;8(34):57477-57488.
24. Rovella V, Anemona L, Cardellini M, et al. The role of obesity in carotid plaque instability: interaction with age, gender, and cardiovascular risk factors. Cardiovasc Diabetol. 2018;17(1):46.
25. Yuan C, Lai CW, Chan LW, Chow M, Law HK, Ying M. Cumulative effects of hypertension, dyslipidemia, and chronic kidney disease on carotid atherosclerosis in Chinese patients with type 2 diabetes mellitus. J Diabetes Res. 2014;2014:179686. doi:

10.1155/2014/179686.
26. Kiechl S, Werner P, Egger G, et al. Active and passive smoking, chronic infections, and the risk of carotid atherosclerosis: prospective results from the Bruneck Study. Stroke. 2002;33(9):2170-2176.
27. Sander D, Kukla C, Klingelhofer J, Winbeck K, Conrad B. Relationship between circadian blood pressure patterns and progression of early carotid atherosclerosis - A 3-year follow-up study. Circulation. 2000;102(13):1536-1541.
28. Crouse JR, 3rd, Byington RP, Bond MG, et al. Pravastatin, Lipids, and Atherosclerosis in the Carotid Arteries (PLAC-II). Am J Cardiol. 1995;75(7):455-459.
29. Kang S, Wu Y, Li X. Effects of statin therapy on the progression of carotid atherosclerosis: a systematic review and meta-analysis. Atherosclerosis. 2004;177(2):433-442.
30. Tibuakuu M, Kianoush S, DeFilippis AP, et al. Usefulness of Lipoprotein-Associated Phospholipase A2 Activity and C-Reactive Protein in Identifying High-Risk Smokers for Atherosclerotic Cardiovascular Disease (from the Atherosclerosis Risk in Communities Study). Am J Cardiol. 2018;121(9):1056-1064.
31. Al Rifai M, DeFillippis AP, McEvoy JW, et al. The relationship between smoking intensity and subclinical cardiovascular injury: The Multi-Ethnic Study of Atherosclerosis (MESA). Atherosclerosis. 2017;258:119-130.
32. Mahat RK, Singh N, Gupta A, Rathore V. Oxidative DNA Damage and Carotid Intima Media Thickness as Predictors of Cardiovascular Disease in Prediabetic Subjects. J Cardiovasc Dev Dis. 2018;5(1). pii: E15. doi: 10.3390/jcdd5010015.
33. Myburgh C, Huisman HW, Mels CMC. The relation of blood pressure and carotid intima-media thickness with the glutathione cycle in a young bi-ethnic population: the African-PREDICT study. J Hum Hypertens. 2018:32(4):268-277.
34. Fox CS, Polak JF, Chazaro I, et al. Genetic and environmental contributions to atherosclerosis phenotypes in men and women: heritability of carotid intima-media thickness in the Framingham Heart Study. Stroke. 2003;34(2):397-401.
35. Humphries SE, Morgan L. Genetic risk factors for stroke and carotid atherosclerosis: insights into pathophysiology from candidate gene approaches. Lancet Neurol. 2004;3(4):227-236.
36. Arya R, Escalante A, Farook VS, et al. A genetic association study of carotid intima-media thickness (CIMT) and plaque in Mexican Americans and European Americans with rheumatoid arthritis. Atherosclerosis. 2018;271:92-101.

37. Rost NS, Wolf PA, Kase CS, et al. Plasma concentration of C-reactive protein and risk of ischemic stroke and transient ischemic attack: the Framingham study. Stroke. 2001;32(11):2575-2579.
38. Woessner JF. Matrix Metalloproteinases And Their Inhibitors In Connective-Tissue Remodeling. Faseb Journal. 1991;5(8):2145-2154.
39. Newby AC, Southgate KM, Davies M. Extracellular matrix degrading metalloproteinases in the pathogenesis of arteriosclerosis. Basic Res Cardiol. 1994;89 Suppl 1:59-70.
40. Chumaeva N, Hintsanen M, Pulkki-Raback L, et al. Interleukin-6 gene polymorphism, chronic stress and atherosclerosis: interleukin-6-174G>C polymorphism, chronic stress and risk of early atherosclerosis in the Cardiovascular Risk in Young Finns Study. J Psychosom Res. 2014;76(4):333-338.
41. Eltoft A, Arntzen KA, Wilsgaard T, Mathiesen EB, Johnsen SH. Interleukin-6 is an independent predictor of progressive atherosclerosis in the carotid artery: The Tromso Study. Atherosclerosis. 2018;271:1-8.
42. Doliner B, Dong C, Blanton SH, et al. Apolipoprotein E Gene Polymorphism and Subclinical Carotid Atherosclerosis: The Northern Manhattan Study. J Stroke Cerebrovasc Dis. 2018;27(3):645-652.
43. Zhao LL, Su G, Chen LX, et al. Apolipoprotein E polymorphisms are associated with ischemic stroke susceptibility in a Northwest China Han population. Biosci Rep. 2017;37(6). pii: BSR20171088. doi: 10.1042/BSR20171088.
44. Bhuiyan AR, Chen W, Srinivasan SR, et al. G-6A polymorphism of angiotensinogen gene modulates the effect of blood pressure on carotid intima-media thickness. The Bogalusa Heart Study. Am J Hypertens. 2007;20(10):1073-1078.
45. Lioudaki S, Verikokos C, Kouraklis G, et al. Paraoxonase-1: Characteristics and role in atherosclerosis and carotid artery disease. Curr Vasc Pharmacol. 2017.
46. Malek AM, Alper SL, Izumo S. Hemodynamic shear stress and its role in atherosclerosis. JAMA. 1999;282(21):2035-2042.
47. Meissner I, Wiebers DO, Whisnant JP, O'Fallon WM. The natural history of asymptomatic carotid artery occlusive lesions. JAMA. 1987;258(19):2704-2707.
48. Dilley RJ, Mcgeachie JK, Prendergast FJ. A Review Of the Histologic-Changes In Vein-To-Artery Grafts, with Particular Reference To Intimal Hyperplasia. Arch Surg. 1988;123(6):691-696.
49. Groen HC, Gijsen FJ, van der Lugt A, et al. Plaque rupture in the carotid artery is

localized at the high shear stress region: a case report. Stroke. 2007;38(8):2379-2381.
50. Markl M, Schnell S, Wu C, et al. Advanced flow MRI: emerging techniques and applications. Clin Radiol. 2016;71(8):779-795.
51. Thapar A, Jenkins IH, Mehta A, Davies AH. Diagnosis and management of carotid atherosclerosis. BMJ. 2013;346:f1485.
52. Hosseini AA, Simpson RJ, Altaf N, Bath PM, MacSweeney ST, Auer DP. Magnetic Resonance Imaging Plaque Hemorrhage for Risk Stratification in Carotid Artery Disease With Moderate Risk Under Current Medical Therapy. Stroke. 2017;48(3):678-685.
53. Gupta A, Baradaran H, Schweitzer AD, et al. Carotid plaque MRI and stroke risk: a systematic review and meta-analysis. Stroke. 2013;44(11):3071-3077.
54. Barnett HJ, Taylor DW, Eliasziw M, et al. Benefit of carotid endarterectomy in patients with symptomatic moderate or severe stenosis. North American Symptomatic Carotid Endarterectomy Trial Collaborators. N Engl J Med. 1998;339(20):1415-1425.
55. Sigovan M, Bidet C, Bros S, et al. 3D black blood MR angiography of the carotid arteries. A simple sequence for plaque hemorrhage and stenosis evaluation. Magn Reson Imaging. 2017;42:95-100.
56. Rothwell PM, Gibson RJ, Slattery J, Sellar RJ, Warlow CP. Equivalence of measurements of carotid stenosis. A comparison of three methods on 1001 angiograms. European Carotid Surgery Trialists' Collaborative Group. Stroke. 1994;25(12):2435-2439.
57. O'Brien M, Chandra A. Carotid revascularisation: risks and benefits. Vasc Health Risk Manag. 2014;10:403-416.
58. Nambi V, Pedroza C, Kao LS. Carotid intima-media thickness and cardiovascular events. Lancet. 2012;379(9831):2028-2030.
59. Wannarong T, Parraga G, Buchanan D, et al. Progression of carotid plaque volume predicts cardiovascular events. Stroke. 2013;44(7):1859-1865.
60. Spence JD. Measurement of carotid plaque burden. JAMA Neurol. 2015;72(4):383-384.
61. Spence JD, Solo K. Resistant Atherosclerosis: The Need for Monitoring of Plaque Burden. Stroke. 2017;48(6):1624-1629.
62. Muller JE, Abela GS, Nesto RW, Tofler GH. Triggers, acute risk factors and vulnerable plaques: the lexicon of a new frontier. J Am Coll Cardiol. 1994;23(3):809-813.
63. Naghavi M, Libby P, Falk E, et al. From vulnerable plaque to vulnerable patient: a call for new definitions and risk assessment strategies: Part I. Circulation. 2003;108(14):1664-1672.

64. Golledge J, Greenhalgh RM, Davies AH. The symptomatic carotid plaque. Stroke. 2000;31(3):774-781.
65. Nandalur KR, Baskurt E, Hagspiel KD, et al. Carotid artery calcification on CT may independently predict stroke risk. American Journal Of Roentgenology. 2006;186(2):547-552.
66. Elias-Smale SE, Odink AE, Wieberdink RG, et al. Carotid, aortic arch and coronary calcification are related to history of stroke: the Rotterdam Study. Atherosclerosis. 2010;212(2):656-660.
67. Nandalur KR, Hardie AD, Raghavan P, Schipper MJ, Baskurt E, Kramer CM. Composition of the stable carotid plaque: insights from a multidetector computed tomography study of plaque volume. Stroke. 2007;38(3):935-940.
68. Kwee RM. Systematic review on the association between calcification in carotid plaques and clinical ischemic symptoms. Journal Of Vascular Surgery. 2010;51(4):1015-1025.
69. Boussel L, Arora S, Rapp J, et al. Atherosclerotic plaque progression in carotid arteries: monitoring with high-spatial-resolution MR imaging--multicenter trial. Radiology. 2009;252(3):789-796.
70. Troyer A, Saloner D, Pan XM, Velez P, Rapp JH, Assessment of Carotid Stenosis by Comparison with Endarterectomy Plaque Trial I. Major carotid plaque surface irregularities correlate with neurologic symptoms. J Vasc Surg. 2002;35(4):741-747.
71. Willinsky RA, Taylor SM, TerBrugge K, Farb RI, Tomlinson G, Montanera W. Neurologic complications of cerebral angiography: prospective analysis of 2,899 procedures and review of the literature. Radiology. 2003;227(2):522-528.
72. Al-Ameri H, Thomas ML, Yoon A, et al. Complication rate of diagnostic carotid angiography performed by interventional cardiologists. Catheterization & Cardiovascular Interventions. 2009;73(5):661-665.
73. Rothwell PM, Gutnikov SA, Warlow CP, Trialists ECS. Reanalysis of the final results of the European Carotid Surgery Trial. Stroke. 2003;34(2):514-523.
74. Grant EG, Benson CB, Moneta GL, et al. Carotid artery stenosis: grayscale and Doppler ultrasound diagnosis--Society of Radiologists in Ultrasound consensus conference. Ultrasound Q. 2003;19(4):190-198.
75. Jahromi AS, Cina CS, Liu Y, Clase CM. Sensitivity and specificity of color duplex ultrasound measurement in the estimation of internal carotid artery stenosis: a systematic review and meta-analysis. J Vasc Surg. 2005;41(6):962-972.
76. Lukanova DV, Nikolov NK, Genova KZ, Stankev MD, Georgieva EV. The Accuracy of

Noninvasive Imaging Techniques in Diagnosis of Carotid Plaque Morphology. Open Access Maced J Med Sci. 2015;3(2):224-230.
77. Teng ZZ, Feng JX, Zhang YX, et al. A uni-extension study on the ultimate material strength and extreme extensibility of atherosclerotic tissue in human carotid plaques. J Biomech 2015;48(14):3859-3867.
78. Li D, Zhao H, Chen X, et al. Identification of intraplaque haemorrhage in carotid artery by simultaneous non-contrast angiography and intraPlaque haemorrhage (SNAP) imaging: a magnetic resonance vessel wall imaging study. Eur Radiol. 2018;28(4):1681-1686.
79. Josephson SA, Bryant SO, Mak HK, Johnston SC, Dillon WP, Smith WS. Evaluation of carotid stenosis using CT angiography in the initial evaluation of stroke and TIA. Neurology. 2004;63(3):457-460.
80. Netuka D, Belsan T, Broulikova K, et al. Detection of carotid artery stenosis using histological specimens: a comparison of CT angiography, magnetic resonance angiography, digital subtraction angiography and Doppler ultrasonography. Acta Neurochir (Wien). 2016;158(8):1505-1514.
81. Rai S, Thaler DE, Salehi P, Madan N, Leung LY. More to Atherosclerosis Than Stenosis: Symptomatic Carotid Artery With Intraplaque Hemorrhage. Stroke. 2017;48(4):e104-e107.
82. Rasanen HT, Manninen HI, Vanninen RL, Vainio P, Berg M, Saari T. Mild carotid artery atherosclerosis: assessment by 3-dimensional time-of-flight magnetic resonance angiography, with reference to intravascular ultrasound imaging and contrast angiography. Stroke. 1999;30(4):827-833.
83. Anzalone N, Scomazzoni F, Castellano R, et al. Carotid artery stenosis: intraindividual correlations of 3D time-of-flight MR angiography, contrast-enhanced MR angiography, conventional DSA, and rotational angiography for detection and grading. Radiology. 2005;236(1):204-213.
84. Weber J, Veith P, Jung B, et al. MR angiography at 3 Tesla to assess proximal internal carotid artery stenoses: contrast-enhanced or 3D time-of-flight MR angiography? Clin Neuroradiol. 2015;25(1):41-48.
85. Zhao H, Wang J, Liu X, et al. Assessment of carotid artery atherosclerotic disease by using three-dimensional fast black-blood MR imaging: comparison with DSA. Radiology. 2015;274(2):508-516.
86. Brinjikji W, Huston J, 3rd, Rabinstein AA, Kim GM, Lerman A, Lanzino G. Contemporary carotid imaging: from degree of stenosis to plaque vulnerability. J Neurosurg.

2016;124(1):27-42.
87. Nederkoorn PJ, van der Graaf Y, Hunink MG. Duplex ultrasound and magnetic resonance angiography compared with digital subtraction angiography in carotid artery stenosis: a systematic review. Stroke. 2003;34(5):1324-1332.
88. Sardar P, Chatterjee S, Aronow HD, et al. Carotid Artery Stenting Versus Endarterectomy for Stroke Prevention: A Meta-Analysis of Clinical Trials. J Am Coll Cardiol. 2017;69(18):2266-2275.
89. Hobson RW, 2nd, Mackey WC, Ascher E, et al. Management of atherosclerotic carotid artery disease: clinical practice guidelines of the Society for Vascular Surgery. J Vasc Surg. 2008;48(2):480-486.
90. Rothwell PM, Eliasziw M, Gutnikov SA, Warlow CP, Barnett HJ, Carotid Endarterectomy Trialists C. Endarterectomy for symptomatic carotid stenosis in relation to clinical subgroups and timing of surgery. Lancet. 2004;363(9413):915-924.
91. North American Symptomatic Carotid Endarterectomy Trial C, Barnett HJM, Taylor DW, et al. Beneficial effect of carotid endarterectomy in symptomatic patients with high-grade carotid stenosis. N Engl J Med. 1991;325(7):445-453.
92. MRC European Carotid Surgery Trial: interim results for symptomatic patients with severe (70-99%) or with mild (0-29%) carotid stenosis. European Carotid Surgery Trialists' Collaborative Group. Lancet. 1991;337(8752):1235-1243.
93. North American Symptomatic Carotid Endarterectomy Trial. Methods, patient characteristics, and progress. Stroke. 1991;22(6):711-720.
94. Randomised trial of endarterectomy for recently symptomatic carotid stenosis: final results of the MRC European Carotid Surgery Trial (ECST). Lancet. 1998;351(9113):1379-1387.
95. Orrapin S, Rerkasem K. Carotid endarterectomy for symptomatic carotid stenosis. Cochrane Database Syst Rev. 2017;6:CD001081.
96. Leach JR, Rayz VL, Soares B, Wintermark M, Mofrad MR, Saloner D. Carotid atheroma rupture observed in vivo and FSI-predicted stress distribution based on pre-rupture imaging. Ann Biomed Eng. 2010;38(8):2748-2765.
97. Virani SS, Catellier DJ, Pompeii LA, et al. Relation of cholesterol and lipoprotein parameters with carotid artery plaque characteristics: the Atherosclerosis Risk in Communities (ARIC) carotid MRI study. Atherosclerosis. 2011;219(2):596-602.
98. Halliday A, Mansfield A, Marro J, et al. Prevention of disabling and fatal strokes by

successful carotid endarterectomy in patients without recent neurological symptoms: randomised controlled trial. Lancet. 2004;363(9420):1491-1502.
99. Benavente O, Moher D, Pham B. Carotid endarterectomy for asymptomatic carotid stenosis: a meta-analysis. BMJ. 1998;317(7171):1477-1480.
100. Chambers BR, Donnan GA. Carotid endarterectomy for asymptomatic carotid stenosis. Cochrane Database Syst Rev. 2005;19;(4):CD001923..
101. Kernan WN, Ovbiagele B, Black HR, et al. Guidelines for the prevention of stroke in patients with stroke and transient ischemic attack: a guideline for healthcare professionals from the American Heart Association/American Stroke Association. Stroke. 2014;45(7):2160-2236.
102. Schubert T, Bieri O, Pansini M, Stippich C, Santini F. Peak velocity measurements in tortuous arteries with phase contrast magnetic resonance imaging: the effect of multidirectional velocity encoding. Invest Radiol. 2014;49(4):189-194.
103. Tang D, Yang C, Kobayashi S, Ku DN. Steady flow and wall compression in stenotic arteries: a three-dimensional thick-wall model with fluid-wall interactions. J Biomech Eng. 2001;123(6):548-557.
104. Group SC, Ringleb PA, Allenberg J, et al. 30 day results from the SPACE trial of stent-protected angioplasty versus carotid endarterectomy in symptomatic patients: a randomised non-inferiority trial. Lancet. 2006;368(9543):1239-1247.
105. Gurm HS, Yadav JS, Fayad P, et al. Long-term results of carotid stenting versus endarterectomy in high-risk patients. New England Journal Of Medicine. 2008;358(15):1572-1579.
106. Eckstein HH, Ringleb P, Allenberg JR, et al. Results of the Stent-Protected Angioplasty versus Carotid Endarterectomy (SPACE) study to treat symptomatic stenoses at 2 years: a multinational, prospective, randomised trial. Lancet Neurology. 2008;7(10):893-902.
107. Cui L, Han Y, Zhang S, Liu X, Zhang J. Safety of Stenting and Endarterectomy for Asymptomatic Carotid Artery Stenosis: A Meta-Analysis of Randomised Controlled Trials. Eur J Vasc Endovasc Surg. 2018; 55(5):614-624.
108. Diao Z, Jia G, Wu W, Wang C. Carotid endarterectomy versus carotid angioplasty for stroke prevention: a systematic review and meta-analysis. J Cardiothorac Surg. 2016;11:142.
109. Inzitari D, Eliasziw M, Gates P, et al. The causes and risk of stroke in patients with asymptomatic internal-carotid-artery stenosis. North American Symptomatic Carotid Endarterectomy Trial Collaborators. N Engl J Med. 2000;342(23):1693-1700.

110. International Carotid Stenting Study i, Ederle J, Dobson J, et al. Carotid artery stenting compared with endarterectomy in patients with symptomatic carotid stenosis (International Carotid Stenting Study): an interim analysis of a randomised controlled trial. Lancet. 2010;375(9719):985-997.
111. Mas JL, Trinquart L, Leys D, et al. Endarterectomy Versus Angioplasty in Patients with Symptomatic Severe Carotid Stenosis (EVA-3S) trial: results up to 4 years from a randomised, multicentre trial. Lancet Neurol. 2008;7(10):885-892.
112. Meier P, Knapp G, Tamhane U, Chaturvedi S, Gurm HS. Short term and intermediate term comparison of endarterectomy versus stenting for carotid artery stenosis: systematic review and meta-analysis of randomised controlled clinical trials. BMJ. 2010;340:c467.
113. Hill MD, Brooks W, Mackey A, et al. Stroke after carotid stenting and endarterectomy in the Carotid Revascularisation Endarterectomy versus Stenting Trial (CREST). Circulation. 2012;126(25):3054-3061.
114. Silver FL, Mackey A, Clark WM, et al. Safety of stenting and endarterectomy by symptomatic status in the Carotid Revascularisation Endarterectomy Versus Stenting Trial (CREST). Stroke. 2011;42(3):675-680.
115. Howard VJ, Lutsep HL, Mackey A, et al. Influence of sex on outcomes of stenting versus endarterectomy: a subgroup analysis of the Carotid Revascularisation Endarterectomy versus Stenting Trial (CREST). Lancet Neurol. 2011;10(6):530-537.
116. Voeks JH, Howard G, Roubin GS, et al. Age and outcomes after carotid stenting and endarterectomy: the carotid revascularisation endarterectomy versus stenting trial. Stroke. 2011;42(12):3484-3490.
117. Howard DPJ, van Lammeren GW, Rothwell PM, et al. Symptomatic Carotid Atherosclerotic Disease Correlations Between Plaque Composition and Ipsilateral Stroke Risk. Stroke. 2015;46(1):182-189.
118. Lal BK, Beach KW, Roubin GS, et al. Restenosis after carotid artery stenting and endarterectomy: a secondary analysis of CREST, a randomised controlled trial. Lancet Neurol. 2012;11(9):755-763.
119. Chakhtoura EY, Hobson RW, 2nd, Goldstein J, et al. In-stent restenosis after carotid angioplasty-stenting: incidence and management. J Vasc Surg. 2001;33(2):220-225.
120. Arquizan C, Trinquart L, Touboul PJ, et al. Restenosis Is More Frequent After Carotid Stenting Than After Endarterectomy The EVA-3S Study. Stroke. 2011;42(4):1015-1020.
121. Gaudry M, Bartoli JM, Bal L, et al. Anatomical and Technical Factors Influence the Rate

of In-Stent Restenosis following Carotid Artery Stenting for the Treatment of Post-Carotid Endarterectomy Stenosis. PLoS One. 2016;11(9):e0161716.
122. Desiron Q, Detry O, Van Damme H, Creemers E, Limet R. Comparison of results of carotid artery surgery after either direct closure or use of a vein patch. (vol 5, pg 295, 1997). Cardiovascular Surgery. 1998;6(1):97-97.
123. Moore WS, Kempczinski RF, Nelson JJ, Toole JF. Recurrent carotid stenosis : results of the asymptomatic carotid atherosclerosis study. Stroke. 1998;29(10):2018-2025.
124. Tse GTW, Kilkenny MF, Bladin C, Grigg M, Dewey HM. Carotid endarterectomy: the change in practice over 11 years in a stroke centre. ANZ J Surg. 2017 doi: 10.1111/ans.14241.
125. Fokkema M, den Hartog AG, Bots ML, van der Tweel I, Moll FL, de Borst GJ. Stenting versus surgery in patients with carotid stenosis after previous cervical radiation therapy: systematic review and meta-analysis. Stroke. 2012;43(3):793-801.

Chapter 3

Imaging Techniques for Carotid Atherosclerosis

Abstract

In this chapter, the imaging techniques used in this project will be introduced. The basic physical principles of different non-contrast-enhanced magnetic resonance angiography (MRA) sequences used in our project — namely time-of-flight (TOF) MRA, phase-contrast (PC) MRA and black-blood (BB) MRA — will be briefly described, and their advantages and limitations will be discussed. The current clinical applications of these techniques will also be reviewed, along with implications for advanced usage according to relevant studies, with the aim of describing the possible utility of these techniques and to illustrate their potential impacts on clinical and academic fields. In addition, an overview of new imaging techniques appropriate for carotid atherosclerosis will be presented, which may provide insights for the development of imaging modalities in plaque discrimination and may offer guidance for future research.

3.1 Introduction

Magnetic resonance imaging (MRI) is a prevalent medical imaging approach for diagnosing atherosclerosis, due to its non-invasive nature. Compared to computed tomography (CT), another commonly used image modality in clinical practice, MRI requires no exposure to ionizing radiation, which is advantageous in clinical application. MRI can be implemented both in contrast-enhanced and non-contrast-enhanced acquisitions. However, non-contrast-enhanced MRI is more prevalent in routine clinical practice due to the absence of a need for intravenous agent injection, which may pose the risk of nephrogenic systemic fibrosis.

MRA, a particular MRI application, is used to generate images of arteries (and less commonly veins) in order to evaluate them for stenosis, occlusions, aneurysms or other abnormalities. MRA has undergone rapid developments over the last few decades, with high spatial

resolution and temporal resolution being achieved, thereby allowing accurate diagnosis of cardiovascular diseases. To date, MRA can be effectively used to assess the arteries of the neck and brain, the thoracic and abdominal aorta, the renal arteries, and peripheral arteries.

3.2 Time-of-flight magnetic resonance angiography

The TOF signal is derived from the contrast between flowing nuclear spins and stationary tissue spins. The stationary tissue, which is subjected to repeated radiofrequency (RF) excitation pulses with short repetition time (TR), becomes magnetically saturated, which produces reduced signals. The flowing blood, which has not been magnetically saturated, flows into the otherwise saturated slice or slab with suppressed signals, leading to large signal contrast. The fresh blood continuously enters the image slice or slab, replacing magnetically saturated blood. Consequently, a contrast between unsaturated flowing blood and saturated stationary tissue is exhibited. The strength of signal contrast, however, depends on the speed of blood flow. High-speed blood flow, which is free from repeated excitations pulses, manifests the most intensive contrast. Whereas slow-speed, stagnant or retrograde blood flow, which cannot fully replace the saturated protons in blood within the slice or slab, results in relatively low or obscured signal intensities. To differentiate the arteries and veins, a band to pre-saturate blood is normally placed upstream of the flow from the unwanted direction to suppress the flow signal from that direction, while maintaining the signal from the opposite direction [1, 2].

The contrast between blood flow and stationary tissue also depends on the TR and the flip angle. In general, a long TR allows the flowing spins to recover from excitations and hence improves the inflow discrimination effects. However, increased TR also leads to an increased

stationary signal. As such, an intermediate TR should be selected. A large flip angle could enhance suppression of the background tissue's signal, but it can also enhance the magnetic saturation of flowing blood. Consequently these parameters should be carefully selected to achieve a balanced contrast between blood flow and background signal when designing a TOF-MRA protocol.

The images can be acquired in two dimensional (2D) or three dimensional (3D) modes, corresponding to in-plane slice or slab acquisition. In most cases the choice of 2D or 3D mode depends on the vascular structure. The 2D method is preferable for extensive anatomic coverage, such as for the long carotid and peripheral vasculatures [2]. Conversely, for the carotid bifurcation and intracranial vasculatures, the 3D method is commonly applied due to the requirements for sharp images that capture vessel tortuosity. In general, the 3D mode allows higher visibility with fewer artefacts compared to the 2D mode, at the expense of acquisition time [3].

A variety of approaches could be harnessed to reduce the acquisition time, such as magnetisation transfer [4], parallel imaging [5], multiple overlapping thin slab acquisition (MOTSA) [6] and tilted optimized non-saturating excitation (TONE) [4]. Magnetization transfer leads to a diminished signal from macromolecules, which are mostly seen in brain tissues. Parallel imaging is a technique for under-sampling *k*-space through the use of coil sensitivity profiles, which results in substantial reductions in acquisition times at the cost of reduced signal-to-noise ratios (SNRs). MOTSA uses multiple thin 3D slabs, which are slightly overlapped, so that the resulting overall 3D angiogram has less signal saturation than would occur with a single-volume 3D acquisition.

The major disadvantage of TOF-MRA is signal loss due to complex or turbulent flow where flow is slow and parallel to the slice or slab plane. Once the slice or slab is not perpendicular to the vessel, the signal would be unsatisfactory. Some researchers reported that TOF may overestimate the percentage stenosis of pre-occluded arteries due to complex flow [7]. The other noteworthy disadvantage is the poor suppression of signals from stationary tissue when using a small flip angle, so that short-T1 tissues, such as fatty tissue, haematomata and thrombi, may be misrecognized as blood, which might cause artefacts or obscuration in delineating a vessel wall.

In our project, the relatively small region of the carotid bifurcation was the targeted region for imaging acquisition. Under the requirement of obtaining a precise representation of the vasculature for modelling reconstruction, we employed the 3D sampling mode to achieve relatively high signal contrast, and utilized a small flip angle to keep unsaturated spins in the flowing blood so as to reduce saturation effects and thereby enhance the inflow effects [4]. As mentioned before, the small flip angle will also increase the stationary signal. Therefore, other techniques needed to be implemented to reduce the background signal to achieve a good contrast. In our study the parallel imaging technique known as generalized autocalibrating partially parallel acquisitions (GRAPPA) was employed to fulfil the high spatial resolution requirement and simultaneously reduce the acquisition time, making it more practically viable. A pre-saturation band was placed downstream of the carotid artery to eliminate signals from the veins that also carry blood into the image slab.

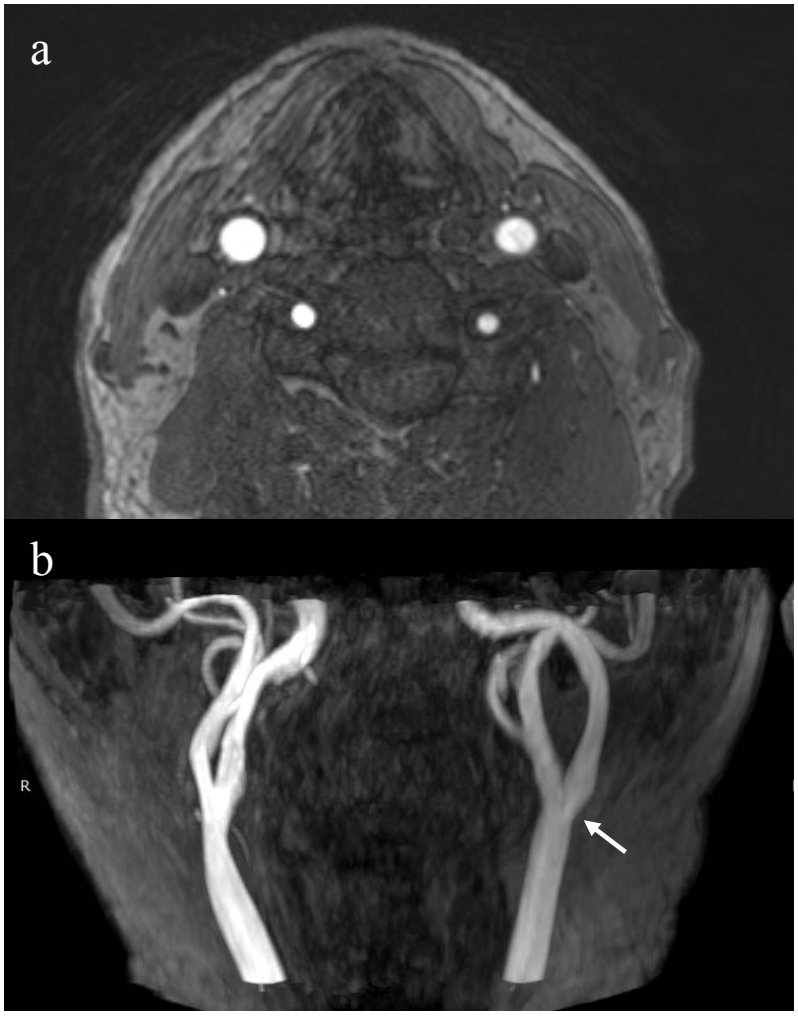

Figure 3-1. Three-dimensional time-of-flight magnetic resonance angiography. A 48-year-old male with carotid atherosclerosis in the left carotid artery (arrow). (a) Cross-sectional imaging shows bilateral common carotid artery. (b) Maximum-intensity projection of bilateral carotid bifurcation.

Clinical application： TOF-MRA is broadly used to examine carotid artery and intracranial vasculatures. It has high signal-to-noise ratio (SNR), particularly for 3D TOF-MRA, and can accurately depict the tortuous properties of vessels. The major application of TOF-MRA in routine clinical practice is in the diagnosis of stenosis or other occlusive diseases, as well as intracranial aneurysms. A study of forty-nine subjects with carotid atherosclerosis that compared TOF-MRA to contrast-enhanced MRA and conventional digital subtraction angiography, with rotational angiography as the reference, suggested that TOF-MRA could be used as the surrogate for stenosis measurement [7].

Advanced application: Although TOF-MRA provides flow-dependent luminal imaging without visualization of the vessel wall, it is still able to discriminate hyper-intensive and hypo-intensive signals at the vessel wall, which allows the differentiation of various plaque compositions with high or dark signals, such as intraplaque haemorrhage (IPH), fibrous caps, and calcification. IPH presents high signals for TOF sequences, which can be discriminated from iso-intensive compositions, such as the lipid-rich necrotic core [8]. A clinical study also showed that hyper-intensity in TOF-MRA was associated with ischaemic stroke in patients with low-grade stenosis [9]. Fibrous caps manifested a low-signal band between bright blood flow and iso-intensive vessel wall [10]. A study by Hatsukami *et al.* [10] reported that TOF-MRA was able to differentiate between different fibrous caps, including thick, thin and disrupted caps, with a consistency of 89% according to histological validation. In following research, Yuan *et al.* [11] further confirmed the ability of TOF to distinguish fibrous caps.

3.3 Phase-contrast magnetic resonance angiography

PC-MRA is a well-known imaging method that can provide the quantification of flow

information *in vivo*. The accuracy and reproducibility of PC-MRA ensures its clinical availability [12]. Compared to ultrasound, it is less user-dependent and has higher image quality.

The principle of PC-MRA is similar to that of TOF-MRA: the contrast between flow spins and stationary spins. Unlike the signal obtained in TOF-MRA, information on the velocity of flow is encoded within phase-contrast MRA, providing the ability not only to visualise the flow but also to quantify the flow. To achieve this, PC-MRA exploits a pair of bipolar gradient pulses, which are basically magnetic field gradients that reverse direction at the midpoint. The paired bipolar gradients can create a velocity-dependent phase shift in flowing or moving spins, but a net zero-shift in stationary spins. However, two data sets are required to subtract flow information: one is a velocity-encoded sequence to generate a velocity-encoded phase image, and the other is a flow-compensated sequence to obtain a magnitude image of the same field-of-view as a reference [13].

On the velocity-encoded phase image, the signal intensity reflects the real magnitude of flow velocity. The signal intensity in the image is independent of the direction of flow and is linearly proportional to the phase shift. The phase shift is measured in degrees and its range is from −180° to +180°. A positive phase shift is represented as a bright signal in an image, whereas a negative phase shift is represented as a dark signal in an image. Quantitative information regarding flow velocity and volumetric flow rate can be derived from this phase image.

On the magnitude image, the signal also correlates to flow velocity. However, it does not include any phase shift, thus the magnitude image is usually used as the anatomic orientation.

The encoding velocity (VENC) is the maximum velocity that the machine can report, corresponding to positive phase shifts. As a user-defined parameter, VENC can be tuned before measuring the flow information. When the velocity in the vessel exceeds the VENC, aliasing will occur. This means that the aberrant velocities will only be mapped within the range of −VENC to +VENC. In this regard, the selected VENC should be able to cover the expected range of velocities. However, the encoding velocity cannot be set arbitrarily high, as the SNR will decrease as a penalty. If a cardiac gate is applied, then the flow information within the cardiac cycle could be obtained. At different time-points in each cardiac cycle, PC-MRA yields a set of frames including velocity and anatomy information.

3D PC-MRA is able to quantify the flow velocity in three directions and, hence, comprises four sets of images: one flow-compensated magnitude image and three velocity-encoded phase maps in three orthogonal directions. 3D PC-MRA allows visualization and quantification of blood flow in all directions within a 3D volume. However, the acquisition of four sets of images requires prolonged scan time, hence limiting the application and prevalence of 3D PC-MRA. In addition, the interpretation of 3D PC-MRA requires expertise and specific software, which impede its routine use in clinical practice. Time-resolved (cine) 3D PC-MRA can support haemodynamic analysis for various vasculatures and extend extra functional information [14]. However, the limited spatial and time resolution precludes the application for haemodynamic evaluation.

In our project, 2D PC-MRA was applied to obtain the velocity of blood flow at three separate points along the carotid bifurcation region. The image slices were carefully located on the common carotid artery (CCA), internal carotid artery (ICA) and external carotid artery (ECA)

to avoid tortuous vessels and the branches, which provide additional flow perpendicular to the longitudinal vessel wall. In some cases, if the slice were misaligned, inaccurate flow and velocity information would be obtained due to the partial volume effect. As the obliquity increased, the measured velocity decreased. However, other authors argued that obliquity does not affect the volumetric flow significantly, because the vessel areas also increase, providing a compensatory effect [15]. It has been demonstrated that obliquities of less than 15° are able to keep the deviations in the magnitude of peak velocity and flow volumetric rate under 10%, which is an acceptable level in clinical practice [16, 17].

The data analysis software used in our project for velocity subtraction was Argus (Siemens, Erlangen, Germany). The contours of vessels of interest were delineated automatically on the magnitude image, then adjusted according to the shape and position of the cross-sectional vessels on the phase image. The region of interest (ROI) can encompass the entire vessel area, as its size could affect the velocity and volumetric flow. For flow estimation, smaller diameters lead to overestimation of the flow; conversely, larger diameters lead to underestimation. However, for peak velocity assessment, a small ROI within the vessel is sufficient, and may yield better results than the entire vessel ROI, as it avoids the arbitrary phase velocity from adjacent tissues. It is proven that peak velocity is more reliable than volumetric flow rate [18, 19]. In this regard, the peak velocity was measured in the current project, rather than the volumetric flow rate.

The VENC value used in our 2D PC-MRA measurements was chosen in accordance with previous reports. In the carotid artery, the VENC is usually set between 100 and 200 cm/s [20]. However, before measuring the flow velocity, different VENC values were tested. If the flow velocity exceeded 200 cm/s, then larger VENC values were applied until the peak

velocity was free from aliasing.

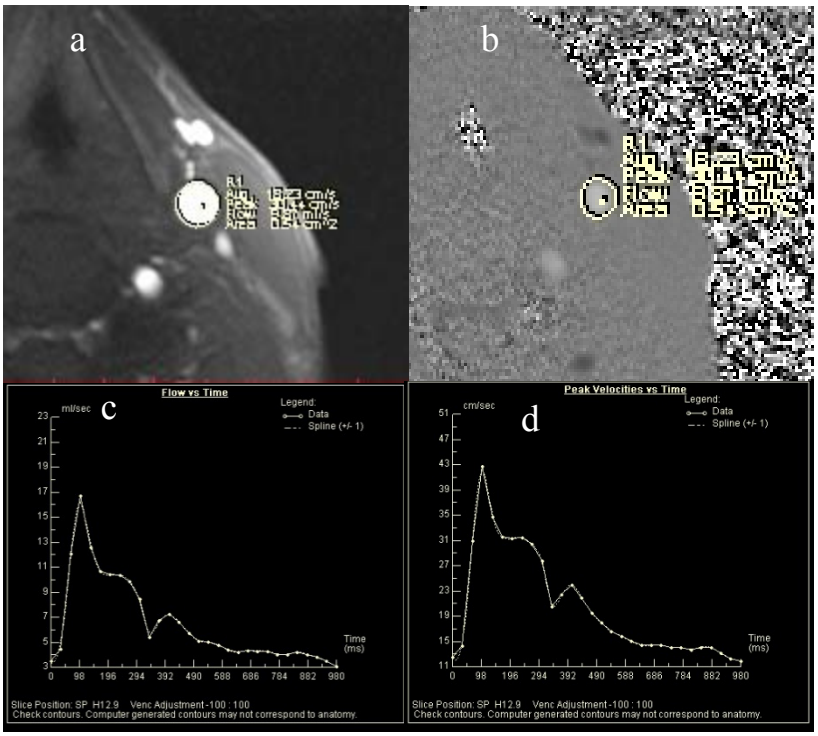

Figure 3-2. Phase-contrast magnetic resonance angiography. Left common carotid artery in a 56-year-old male patient. (a) Magnitude image. (b) Phase image. (c) Flow–time curve. (d) Peak velocity versus time.

Clinical application: The 2D PC-MRA sequence is suitable for intracranial vessels, coronary arteries, vessels in the lower extremities [21], the pulmonary artery [22], renal arteries [23], and carotid arteries. Nevertheless, 2D PC-MRA is clinically underused due to its relatively long scan time — except for the cerebral veins. Although 2D PC-MRA is capable of being used for angiographic imaging, the application of 2D PC-MRA in angiography is still limited due to the low resolution of imaging. A study by Steffens et al. [24] showed that 2D PC-MRA could be used to screen for occlusive diseases in the lower extremities. 2D PC-MRA along with perfusion and diffusion-weighted imaging was also used to prognosticate stroke outcomes.

Owing to PC-MRA's inherent capacity for flow quantification, flow assessment based on 2D PC-MRA is more frequently used in clinical practice. 2D PC-MRA has been shown to provide flow quantification for cerebral arteries and venous flow volume, cerebral spinal fluid measurement [15, 25], arteriovenous malformation [26], carotid stenosis [27] and thoracic dissection [28].

Advanced application: Traditional cine PC-MRA requires the implementation of electrocardiogram (ECG) and respiration gates, resulting in low acquisition efficiency and limited utility. On the other hand, real-time PC-MRA without ECG and respiration control allows the measurement of flow on short timescales and quantification of point-to-point variation [29]. Therefore, real-time PC-MRA could be a promising alternative technique that could overcome the limitations of conventional PC-MRA.

3.4 Black-blood magnetic resonance angiography

Black-blood (BB) MRA, also known as dark blood MRA, is not commonly used as an angiographic imaging modality. It is normally employed to evaluate the vessel wall or intraluminal lesions, because of its ability to suppress the signal from the flowing blood. It is also well recognised as one of the standard sequences in differentiating plaque components.

BB-MRA exploits the fast spin-echo (FSE) sequence to suppress the blood flow signal and create a contrast between the dark lumen and the brighter vessel wall. The FSE sequence employs a double inversion–recovery (DIR) preparatory pulse. At first, a non-selective 180° pulse is applied to magnetize the blood flow, then a section-selective 180° pulse is applied to restore the magnetization of an imaged slice [30]. By properly choosing the inversion time (TI), the inflowing blood can reach the fully saturated condition. The inflowing blood from outside the imaging plane replaces the blood in the imaging plane, resulting in diminished blood signals. Therefore, the vessel wall structure and interface between vessel and lumen can be clearly seen.

Quadruple inversion-recovery (QIR) was also employed in the BB-MRA, which can provide an efficient suppression of a flow signal with TI in a large range. QIR consists of two double-inversion modules followed by two delays [31]. By using an appropriate range of TR, QIR improves the reliability of both post-contrast flow suppression and quantitative estimation of CE with respect to DIR.

The FSE sequence was first developed for single slice acquisition with an ECG gate as a prerequisite, leading to long scan times that impeded its clinical application. With the implementation of non-gated techniques, multiple slices can be simultaneously obtained and hence the scan time is reduced [32]. Implanted with motion-sensitised driven-equilibrium

(MSDE) , FSE sequence can achieve better blood suppression and provide a more accurate depiction of the lumen boundaries by eliminating plaque mimicking artifacts [33]. Later the emergence of a 3D technique was able to greatly reduce the acquisition time by applying various flip angles, to reduce the T2 blurring effect with a long echo train [34-36]. Besides that, the 3D method also allows non-gated techniques and can provide extended coverage of the pertinent anatomic region along with increased spatial resolution [34, 37]. A study based on 83 patients showed that a 3D FSE sequence displayed better image quality compared to that with a 2D FSE sequence, and furthermore allowed calculation of percentage stenosis and the detection of IPH [34].

Clinical application: BB-MRA is typically implemented as T1-weighted (T1w), T2-weighted (T2w) or proton-density-weighted (PDw) imaging. T1w can identify IPH, because the presence of iron decreases the T1 relaxation time, while T2w is mainly used to distinguish fibrous tissues. The combination of different BB-MRA sequences could provide comprehensive understanding of different plaque compositions.

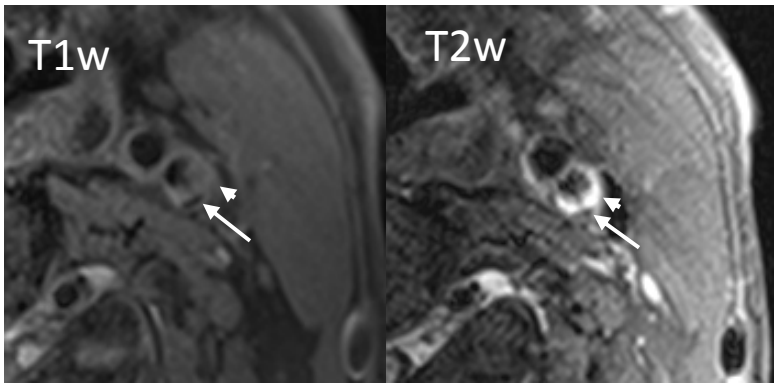

Figure 3-3. Atherosclerotic plaque imaged by black-blood magnetic resonance angiography: T1-weighted (T1w) and T2-weighted (T2w) imaging. Different plaque components including calcification (arrows) and loose matrix (arrow heads) are clearly shown, as well as the interface of vessel wall and lumen.

Advanced application: Recent technical advances allow optimisation of the 3D FSE sequence, which can overcome the inherent limitations of conventional FSE sequences and provide better image qualities. Delay Alternating with Nutation for Tailored Excitation (DANTE) pulse trains can be used to suppress the signal from inflowing spins, while preserving the signal from the stationary spins through motion-sensitive preparation modules [38]. Compared with a conventional FSE sequence, it can further suppress the background signal, providing a sharp contrast for vessel wall visualisation [38, 39]. The Sampling Perfection with Application-optimised Contrast using different angle Evolution (SPACE) technique allows visualisation of the vessel wall structure from different arbitrary perspectives by including non-selective IR pulses and increasing the excitation frequency [40]. Iterative decomposition of water and fat with echo asymmetry and least-squares estimation (IDEAL),

also known as the water–fat separation method, is insensitive to inhomogeneity of the magnetic field compared to DIR pulses, and is insensitive to the radiofrequency field in comparison to chemical shifts [41]. The study by Khosa *et al.* [42] showed that IDEAL can improve the identification of lipid and haemorrhage compared to conventional multi-contrast sequences.

3.4 New imaging techniques in plaque composition discrimination

With the development of computer hardware and MRI techniques, high-spatial-resolution MRI has been investigated and demonstrated to be able to distinguish plaque compositions both *in vitro* and *in vivo*. The conventional MRI sequences for plaque imaging have been introduced in the previous sections of this chapter, together with their advantages and disadvantages. Newly developed plaque imaging sequences have emerged as options complementary to conventional plaque imaging, due to their ability to mitigate the inherent limitations of the conventional techniques. The well-recognised concept of 'vulnerable plaque' has also facilitated the development of new imaging techniques. In the following, several newly emerged MR imaging techniques are discussed.

3.4.1 Magnetisation-prepared rapid-acquisition gradient-echo

Magnetisation-prepared rapid-acquisition gradient-echo (MPRAGE), which is an intrinsically dark blood method, relies on spins flowing along different readout directions. MPRAGE, also known as direct thrombus imaging, exploits the short-T1 effect to identify components with short T1 relaxation times, such as thrombus or IPH [43]. The principle of MPRAGE is to nullify the blood signal through use of a T1-weighted magnetisation-prepared 3D gradient-echo sequence to eliminate the signal from fat. The advantages of this sequence are a water-

selective radiofrequency, an effective inversion recovery time, and the acquisition of images in the coronary plane [43, 44].

MPRAGE has been shown to be able to accurately identify IPH in atherosclerotic plaques. Moody and his co-workers [43] reported the first MPRAGE sequence and demonstrated its advantages in identifying IPH with both sensitivity and specificity of 84%. Ota *et al.* [37] compared MPRAGE to TOF-MRA and a conventional FSE sequence, suggesting that the MPRAGE sequence is superior for the identification of IPH, with a sensitivity of 97% and a specificity of 100%.

The major limitation of MPRAGE is the image quality reduction due to respiration and pulsatile motion artefacts [45]. Motion artefacts can decrease the signal suppression from blood flow and lipid tissue and thereby reduce the SNR, which eventually reduces the contrast between IPH and the vessel wall [46]. Recently, some implementations were developed to limit the motion artefacts by applying cardiac gating with post-processing to obtain cine MPRAGE [47]. 3D inversion–recovery techniques have also been demonstrated to mitigate the motion artefacts of MPRAGE [48].

Advanced application: MPRAGE was initially used to identify IPH in asymptomatic patients by Moody and his co-workers [43]. It was then tested in different magnetic fields of 1.5T and 3.0T, yielding similar accuracy [45]. A study by Saito et al. [49] suggested that MPRAGE could be used to differentiate IPH from lipid–fibrous components. Moreover, the presence of hyperintense lesions on MPRAGE was demonstrated to be strongly associated with ischaemic events [49, 50]. In addition, MPRAGE could be applied before carotid stenting to predict future embolic events and to assist in the selection of distal protection

devices.

3.4.2 Simultaneous non-contrast angiography and intraplaque haemorrhage imaging

Simultaneous non-contrast angiography and intraplaque haemorrhage (SNAP) imaging describes a newly proposed sequence that aims to investigate, with a single scan, carotid stenosis and IPH in patients suffering atherosclerosis [51]. SNAP imaging utilizes a phase-sensitive IR sequence to reconstruct images. The advantage of such IR pulses, in which an interleaved full-matrix-size reference is exploited, is to remove the background phase while preserving the desired magnetized phase [52]. Components with short T1 can be sensed with high positive signals, whereas tissues with long T1 remain dark [51]. Taking advantage of these optimizations, SNAP imaging is able to simultaneously depict vessel walls and blood flow. A study by Wang et al. showed that SNAP imaging was able to represent IPH and vessel wall in a single scan when using an optimized sequence [51]. However, the interleaved full-matrix-size reference has low acquisition efficacy with relatively prolonged scan time. Chen *et al.* [53] used a single *k*-space line as a reference to speed up the acquisition time with similar image quality to the previously described SNAP imaging sequence.

The major merit of SNAP imaging sequences lies in the simultaneous discrimination of two pathologies: carotid stenosis and IPH. As a result, it can be used to depict the morphologic characteristics of atherosclerotic plaques, particularly in ulceration detection [51, 54]. In a comparison with a TOF-MRA sequence, SNAP imaging was insensitive to flow motion due to the utilization of a motion-sensitive IR sequence [51]. Furthermore, SNAP imaging is good for identifying stagnant flow [51]. SNAP imaging has a higher SNR for vessel walls and IPH in comparison to MPRAGE, and was demonstrated to be superior in detection of spotty and scattered IPH [51].

Despite all of the abovementioned advantages, the SNAP imaging sequence has also been demonstrated to have some limitations. It images arteries and veins in one scan, and hence may lead to difficulty in directly visualizing the arterial flow. It is also sensitive to turbulent flow.

Advanced application: The SNAP imaging sequence was demonstrated to be consistent in the measurement of carotid stenosis in comparison to conventional contrast-enhanced MRA [55]. A study by Wang *et al.* [56] showed that a SNAP imaging sequence has a similar ability to detect intracranial stenosis to that of TOF-MRA. Li *et al.* [57] found that SNAP imaging is superior to MPRAGE in identifying haemorrhages, particularly tiny haemorrhages. Compared to conventional multi-contrast sequences, Chen *et al.* [58] found that SNAP imaging had in consistent performance in the detection of intraluminal calcification and ulceration. However, with short acquisition times, SNAP imaging is more clinically practical.

3.4.3 Diffusion-weighted imaging

Diffusion-weighted imaging (DWI) can be used to quantitatively analyse atherosclerotic plaques, despite its limitations of low spatial resolution and partial-volume effects. DWI scans are typically acquired using strong magnetic field gradients to make the magnetic resonance signal sensitive to the molecular motion of water. The ability of water molecules to diffuse is represented by the apparent diffusion coefficient (ADC) [59]. The ADC value thus represents the ability of water to move; however, it also includes the effects of the constraints of physical boundaries or barriers from cell membranes and organelles [60]. DWI is commonly used in the differentiation between benign lesions and malignant ones; however, it has seldom been applied for vessel diagnosis. In addition, due to the pulsatile flow, a conventional DWI

sequence cannot be directly utilized in the diagnosis of atherosclerotic plaques. As such, a 2D interleaved multislice reduced field-of-view single-shot diffusion-weighted echo–planar imaging sequence was developed to reduce the pulsatile artefacts [61, 62].

Advanced application: The application of DWI for atherosclerotic diseases was initially proposed by Toussaint *et al.* and his colleagues [63]. Owing to the different ADC values, DWI is able to differentiate between IPH, fatty necrotic tissue, and other components [63]. An *in vitro* study showed that DWI can achieve good contrast between thrombus and underlying plaque. It furthermore allows efficacious differentiation between plaques and vessel wall [64]. Cappendijk *et al.* [65] found that DWI had the highest SNR in the identification of lipid tissue in comparison with conventional T1w and T2w sequences, using histology as a reference. Furthermore, Clark *et al.* [66, 67] demonstrated that DWI had an excellent contrast when identifying lipid tissues. Later *in vivo* studies also demonstrated that DWI could detect lipid tissue [62, 68, 69], and hence could be used to distinguish lipid and fibrous tissues [69].

Table 3.1 The advantages and disadvantages of different techniques in carotid imaging

	Advantages	Disadvantages
TOF	Widely acknowledged	Signal loss due to stagnant and complex flow
PC	Quantitative flow estimation	Limited spatial and time resolution
BB	Vessel wall visualisation	Long acquisition time
MPRAGE	The assessment of intraplaque haemorrhage	Unavailable for vessel wall visualisation
SNAP	Simultaneous evaluation of intraplaque haemorrhage and vessel wall	Difficult to differential Arterial flow and sensitive to disturb flow
DWI	The differentiation of Lipid core	Low spatial resolution and partial-volume effect

References

1. Huston J, 3rd, Ehman RL. Comparison of time-of-flight and phase-contrast MR neuroangiographic techniques. Radiographics. 1993;13(1):5-19.

2. Miyazaki M, Lee VS. Nonenhanced MR angiography. Radiology. 2008;248(1):20-43.

3. HaiFeng L, YongSheng X, YangQin X, et al. Diagnostic value of 3D time-of-flight magnetic resonance angiography for detecting intracranial aneurysm: a meta-analysis. Neuroradiology. 2017;59(11):1083-1092.

4. Atkinson D, Brant-Zawadzki M, Gillan G, Purdy D, Laub G. Improved MR angiography: magnetization transfer suppression with variable flip angle excitation and increased resolution. Radiology. 1994;190(3):890-894.

5. Hartung MP, Grist TM, Francois CJ. Magnetic resonance angiography: current status and future directions. J Cardiovasc Magn Reson. 2011;13:19.

6. Blatter DD, Parker DL, Robison RO. Cerebral MR angiography with multiple overlapping thin slab acquisition. Part I. Quantitative analysis of vessel visibility. Radiology. 1991;179(3):805-811.

7. Anzalone N, Scomazzoni F, Castellano R, et al. Carotid artery stenosis: intraindividual correlations of 3D time-of-flight MR angiography, contrast-enhanced MR angiography, conventional DSA, and rotational angiography for detection and grading. Radiology. 2005;236(1):204-213.

8. Yuan C, Mitsumori LM, Ferguson MS, et al. In vivo accuracy of multispectral magnetic resonance imaging for identifying lipid-rich necrotic cores and intraplaque hemorrhage in advanced human carotid plaques. Circulation. 2001;104(17):2051-2056.

9. Yamada K, Yoshimura S, Shirakawa M, et al. High intensity signal in the plaque on routine 3D-TOF MRA is associated with ischemic stroke in the patients with low-grade carotid stenosis. J Neurol Sci. 2018;385:164-167.

10. Hatsukami TS, Ross R, Polissar NL, Yuan C. Visualization of fibrous cap thickness and rupture in human atherosclerotic carotid plaque in vivo with high-resolution magnetic resonance imaging. Circulation. 2000;102(9):959-964.

11. Yuan C, Zhang SX, Polissar NL, et al. Identification of fibrous cap rupture with magnetic resonance imaging is highly associated with recent transient ischemic attack or stroke. Circulation. 2002;105(2):181-185.

12. Chatzimavroudis GP, Oshinski JN, Franch RH, Walker PG, Yoganathan AP, Pettigrew RI. Evaluation of the precision of magnetic resonance phase velocity mapping for blood flow measurements. J Cardiovasc Magn Reson. 2001;3(1):11-19.

13. Dumoulin CL. Phase contrast MR angiography techniques. Magn Reson Imaging Clin N Am. 1995;3(3):399-411.

14. Iseda T, Nakano S, Miyahara D, Uchinokura S, Goya T, Wakisaka S. Poststenotic signal attenuation on 3D phase-contrast MR angiography: a useful finding in haemodynamically significant carotid artery stenosis. Neuroradiology. 2000;42(12):868-873.

15. Luetmer PH, Huston J, Friedman JA, et al. Measurement of cerebrospinal fluid flow at the cerebral aqueduct by use of phase-contrast magnetic resonance imaging: technique validation and utility in diagnosing idiopathic normal pressure hydrocephalus. Neurosurgery. 2002;50(3):534-543; discussion 543-534.

16. Lotz J, Meier C, Leppert A, Galanski M. Cardiovascular flow measurement with phase-contrast MR imaging: basic facts and implementation. Radiographics. 2002;22(3):651-671.

17. Tang C, Blatter DD, Parker DL. Accuracy of phase-contrast flow measurements in the presence of partial-volume effects. J Magn Reson Imaging. 1993;3(2):377-385.

18. Kozerke S, Botnar R, Oyre S, Scheidegger MB, Pedersen EM, Boesiger P. Automatic vessel segmentation using active contours in cine phase contrast flow measurements. J Magn Reson Imaging. 1999;10(1):41-51.

19. Moran PR, Moran RA, Karstaedt N. Verification and evaluation of internal flow and motion. True magnetic resonance imaging by the phase gradient modulation method. Radiology. 1985;154(2):433-441.

20. Guo G, Wu RH, Zhang YP, et al. Combination 3D TOP with 2D PC MRA Techique for cerebral blood flow volume measurement. Conf Proc IEEE Eng Med Biol Soc. 2006;1:489-492.

21. Mohajer K, Zhang H, Gurell D, et al. Superficial femoral artery occlusive disease severity correlates with MR cine phase-contrast flow measurements. J Magn Reson Imaging. 2006;23(3):355-360.

22. Sanz J, Kuschnir P, Rius T, et al. Pulmonary arterial hypertension: noninvasive detection with phase-contrast MR imaging. Radiology. 2007;243(1):70-79.

23. de Haan MW, Kouwenhoven M, Kessels AG, van Engelshoven JM. Renal artery blood flow: quantification with breath-hold or respiratory triggered phase-contrast MR imaging. Eur Radiol. 2000;10(7):1133-1137.

24. Liu Y, Karonen JO, Vanninen RL, et al. Acute ischemic stroke: predictive value of 2D phase-contrast MR angiography--serial study with combined diffusion and perfusion MR imaging. Radiology. 2004;231(2):517-527.

25. Miralles M, Dolz JL, Cotillas J, et al. The role of the circle of Willis in carotid occlusion: assessment with phase contrast MR angiography and transcranial duplex. Eur J Vasc Endovasc Surg. 1995;10(4):424-430.

26. Grinstead JW, Sinha S, Tateshima S, Nien YL, Vinuela F. Visualization and quantification of flow and velocity fields in intracranial arteriovenous malformations using phase-contrast MR angiography. AJR Am J Roentgenol. 2006;186(2):553-555.

27. Glor FP, Ariff B, Hughes AD, et al. Image-based carotid flow reconstruction: a comparison between MRI and ultrasound. Physiol Meas. 2004;25(6):1495-1509.

28. Strotzer M, Aebert H, Lenhart M, et al. Morphology and hemodynamics in dissection of the descending aorta. Assessment with MR imaging. Acta Radiol. 2000;41(6):594-600.

29. Sun A, Zhao B, Li Y, He Q, Li R, Yuan C. Real-time phase-contrast flow cardiovascular magnetic resonance with low-rank modeling and parallel imaging. J Cardiovasc Magn Reson. 2017;19(1):19.

30. Yarnykh VL, Yuan C. Multislice double inversion-recovery black-blood imaging with simultaneous slice reinversion. J Magn Reson Imaging. 2003;17(4):478-483.

31. Yarnykh VL, Yuan C. T1-insensitive flow suppression using quadruple inversion-recovery. Magn Reson Med. 2002;48(5):899-905.

32. Song HK, Wright AC, Wolf RL, Wehrli FW. Multislice double inversion pulse sequence for efficient black-blood MRI. Magn Reson Med. 2002;47(3):616-620.

33. Wang J, Yarnykh VL, Hatsukami T, Chu B, Balu N, Yuan C. Improved suppression of plaque-mimicking artifacts in black-blood carotid atherosclerosis imaging using a multislice motion-sensitized driven-equilibrium (MSDE) turbo spin-echo (TSE) sequence. Magn Reson Med. 2007;58(5):973-981.

34. Sigovan M, Bidet C, Bros S, et al. 3D black blood MR angiography of the carotid arteries. A simple sequence for plaque hemorrhage and stenosis evaluation. Magn Reson Imaging. 2017;42:95-100.

35. Narumi S, Sasaki M, Miyazawa H, et al. T1-Weighted Magnetic Resonance Carotid Plaque Imaging: a Comparison between Conventional and Fast Spin-Echo Techniques. J Stroke Cerebrovasc Dis. 2017;26(2):273-279.

36. Takano K, Yamashita S, Takemoto K, et al. Characterization of carotid atherosclerosis with black-blood carotid plaque imaging using variable flip-angle 3D turbo spin-echo: comparison with 2D turbo spin-echo sequences. Eur J Radiol. 2012;81(3):e304-309.

37. Ota H, Yarnykh VL, Ferguson MS, et al. Carotid intraplaque hemorrhage imaging at 3.0-T MR imaging: comparison of the diagnostic performance of three T1-weighted sequences. Radiology. 2010;254(2):551-563.

38. Li L, Miller KL, Jezzard P. DANTE-prepared pulse trains: a novel approach to motion-sensitized and motion-suppressed quantitative magnetic resonance imaging. Magn Reson Med. 2012;68(5):1423-1438.

39. Li L, Chai JT, Biasiolli L, et al. Black-blood multicontrast imaging of carotid arteries with DANTE-prepared 2D and 3D MR imaging. Radiology. 2014;273(2):560-569.

40. Mihai G, Winner MW, Raman SV, Rajagopalan S, Simonetti OP, Chung YC. Assessment of carotid stenosis using three-dimensional T2-weighted dark blood imaging: Initial experience. Journal Of Magnetic Resonance Imaging. 2012;35(2):449-455.

41. Reeder SB, Pineda AR, Wen Z, et al. Iterative decomposition of water and fat with echo asymmetry and least-squares estimation (IDEAL): application with fast spin-echo imaging. Magn Reson Med. 2005;54(3):636-644.

42. Khosa F, Clough RE, Wang X, Madhuranthakam AJ, Greenman RL. The potential role of IDEAL MRI for identification of lipids and hemorrhage in carotid artery plaques. Magn Reson Imaging. 2017;49:25-31.

43. Moody AR, Murphy RE, Morgan PS, et al. Characterization of complicated carotid plaque with magnetic resonance direct thrombus imaging in patients with cerebral ischemia. Circulation. 2003;107(24):3047-3052.

44. Murphy RE, Moody AR, Morgan PS, et al. Prevalence of complicated carotid atheroma as detected by magnetic resonance direct thrombus imaging in patients with suspected carotid artery stenosis and previous acute cerebral ischemia. Circulation. 2003;107(24):3053-3058.

45. Scott McNally J, Yoon HC, Kim SE, et al. Carotid MRI Detection of Intraplaque Hemorrhage at 3T and 1.5T. J Neuroimaging. 2015;25(3):390-396.

46. Bitar R, Moody AR, Leung G, et al. In vivo 3D high-spatial-resolution MR imaging of intraplaque hemorrhage. Radiology. 2008;249(1):259-267.

47. Mendes J, Parker DL, Kim SE, Treiman GS. Reduced blood flow artifact in intraplaque hemorrhage imaging using CineMPRAGE. Magnetic Resonance In Medicine. 2013;69(5):1276-1284.

48. Kim SE, Roberts JA, Eisenmenger LB, et al. Motion-insensitive carotid intraplaque hemorrhage imaging using 3D inversion recovery preparation stack of stars (IR-prep SOS) technique. J Magn Reson Imaging. 2017;45(2):410-417.

49. Saito A, Sasaki M, Ogasawara K, et al. Carotid plaque signal differences among four kinds of T1-weighted magnetic resonance imaging techniques: A histopathological correlation study. Neuroradiology. 2012;54(11):1187-1194.

50. Yamada N, Higashi M, Otsubo R, et al. Association between signal hyperintensity on T1-weighted MR imaging of carotid plaques and ipsilateral ischemic events. AJNR Am J Neuroradiol. 2007;28(2):287-292.

51. Wang J, Bornert P, Zhao H, et al. Simultaneous noncontrast angiography and intraplaque hemorrhage (SNAP) imaging for carotid atherosclerotic disease evaluation. Magn Reson Med. 2013;69(2):337-345.

52. Kellman P, Arai AE, McVeigh ER, Aletras AH. Phase-sensitive inversion recovery for detecting myocardial infarction using gadolinium-delayed hyperenhancement. Magnetic Resonance In Medicine. 2002;47(2):372-383.

53. Chen S, Ning J, Zhao X, et al. Fast simultaneous noncontrast angiography and intraplaque hemorrhage (fSNAP) sequence for carotid artery imaging. Magn Reson Med. 2017;77(2):753-758.

54. Chen S, Zhao H, Li J, et al. Evaluation of carotid atherosclerotic plaque surface characteristics utilizing simultaneous noncontrast angiography and intraplaque hemorrhage (SNAP) technique. J Magn Reson Imaging. 2018;47(3):634-639.

55. Shu H, Sun J, Hatsukami TS, et al. Simultaneous noncontrast angiography and intraplaque hemorrhage (SNAP) imaging: Comparison with contrast-enhanced MR angiography for measuring carotid stenosis. J Magn Reson Imaging. 2017;46(4):1045-1052.

56. Wang J, Guan M, Yamada K, et al. In Vivo Validation of Simultaneous Non-Contrast Angiography and intraPlaque Hemorrhage (SNAP) Magnetic Resonance Angiography: An Intracranial Artery Study. PLoS One. 2016;11(2):e0149130.

57. Li D, Zhao H, Chen X, et al. Identification of intraplaque haemorrhage in carotid artery by simultaneous non-contrast angiography and intraPlaque haemorrhage (SNAP) imaging: a magnetic resonance vessel wall imaging study. Eur Radiol. 2018;28(4):1681-1686.

58. Chen S, Zhao H, Li J, et al. Evaluation of carotid atherosclerotic plaque surface characteristics utilizing simultaneous noncontrast angiography and intraplaque hemorrhage (SNAP) technique. J Magn Reson Imaging. 2018;47(3):634-639.

59. Chawla S, Kim S, Wang S, Poptani H. Diffusion-weighted imaging in head and neck cancers. Future Oncol. 2009;5(7):959-975.

60. Bammer R, Herneth AM, Maier SE, et al. Line scan diffusion imaging of the spine. AJNR Am J Neuroradiol. 2003;24(1):5-12.

61. Jeong EK, Kim SE, Guo J, Kholmovski EG, Parker DL. High-resolution DTI with 2D interleaved multislice reduced FOV single-shot diffusion-weighted EPI (2D ss-rFOV-DWEPI). Magn Reson Med. 2005;54(6):1575-1579.

62. Kim SE, Jeong EK, Shi XF, Morrell G, Treiman GS, Parker DL. Diffusion-weighted imaging of human carotid artery using 2D single-shot interleaved multislice inner volume diffusion-weighted echo planar imaging (2D ss-IMIV-DWEPI) at 3T: diffusion measurement in atherosclerotic plaque. J Magn Reson Imaging. 2009;30(5):1068-1077.

63. Toussaint JF, Southern JF, Fuster V, Kantor HL. Water diffusion properties of human atherosclerosis and thrombosis measured by pulse field gradient nuclear magnetic resonance. Arterioscler Thromb Vasc Biol. 1997;17(3):542-546.

64. Viereck J, Ruberg FL, Qiao Y, et al. MRI of atherothrombosis associated with plaque rupture. Arterioscler Thromb Vasc Biol. 2005;25(1):240-245.

65. Cappendijk VC, Heeneman S, Kessels AG, et al. Comparison of single-sequence T1w TFE MRI with multisequence MRI for the quantification of lipid-rich necrotic core in atherosclerotic plaque. J Magn Reson Imaging. 2008;27(6):1347-1355.

66. Clarke SE, Hammond RR, Mitchell JR, Rutt BK. Quantitative assessment of carotid plaque composition using multicontrast MRI and registered histology. Magnetic Resonance In Medicine. 2003;50(6):1199-1208.

67. Clarke SE, Beletsky V, Hammond RR, Hegele RA, Rutt BK. Validation of automatically classified magnetic resonance images for carotid plaque compositional analysis. Stroke. 2006;37(1):93-97.

68. Qiao Y, Ronen I, Viereck J, Ruberg FL, Hamilton JA. Identification of atherosclerotic lipid deposits by diffusion-weighted imaging. Arterioscler Thromb Vasc Biol. 2007;27(6):1440-1446.

69. Young VE, Patterson AJ, Sadat U, et al. Diffusion-weighted magnetic resonance imaging for the detection of lipid-rich necrotic core in carotid atheroma in vivo. Neuroradiology. 2010;52(10):929-936.

Chapter 4

New MRI Sequence for the Analysis of Atherosclerotic Plaques - Multicontrast Atherosclerosis Characterization (MATCH)

A new MRI sequence was introduced in this chapter, the performance of this new sequence was compared with conventional multicontrast MRI sequence as well as histological reference. This chapter was published as:

Y. Dai, P. Lv, J. Lin, R. Luo, A. Ji, H. Liu, C. Fu. Comparison study between multicontrast atherosclerosis characterization (MATCH) and conventional multicontrast MRI of carotid plaque with histology validation. J Magn Reson Imaging. 2017; 45(3):764-770.

Chapter 4 of this thesis has been removed due to copyright reasons

Chapter 5

Computational Fluid Dynamics Techniques and Applications for Cerebrovascular Diseases

Abstract

In this chapter, computational fluid dynamics (CFD) techniques are introduced and the applications of CFD in cerebrovascular diseases outlined. Afterwards, the detailed steps of the imaged-based CFD methodology used in this project are presented, which include geometric segmentation, model surface reconstruction, and results post-processing.

5.1 Introduction

CFD is a branch of fluid dynamics that provides an effective approach to simulate fluid flows. The simulation of fluid flow is principally achieved by solving the Navier–Stokes equations. CFD models can be derived from either idealized or realistic geometric models. With the advancement of medical imaging techniques over the last decades, patient-specific image data have become available to provide realistic individual information. Therefore, the confluence of medical imaging techniques and CFD has enabled considerable progress in the development and application of image-based CFD methods to human bodies, especially in cardiovascular diseases. With the modern computer techniques and hardware, it is desirable to model the complex blood flows associated with patient-specific geometries as accurately as possible to make a real and significant impact on the management of cardiovascular diseases. However, before the image-based CFD technologies can have significant impacts on routine clinical practice in the diagnosis and assessment of cardiovascular diseases, it is necessary to comprehensively understand the haemodynamic information provided by the simulations.

5.2 The application of CFD in cerebrovascular diseases

It is well known that haemodynamics plays a fundamental role in cerebrovascular diseases. Image-based CFD is capable of representing the realistic haemodynamic environment, and therefore it can be used to investigate the haemodynamic parameters in the diagnosis and

treatment of cerebrovascular diseases.

5.2.1 Intracranial aneurysms and their treatment with endovascular stents

Initiation, enlargement and rupture are the different stages in the natural history of cerebral aneurysms. The regions in which the aneurysms are initiated have been revealed to be associated with high wall shear stress (WSS) as well as high WSS gradient (WSSG) [1, 2]. Regarding the growth and rupture of aneurysms, however, conflicting findings exist, as these conditions have been demonstrated to occur in both low and high WSS regions [3-5].

Some investigators proposed that aneurysms rupture in areas with stagnant flow and low WSS [6, 7]. A study conducted by Shojima *et al.* [8] showed that low WSS regions were mainly located at the dome of the ruptured aneurysm and the value of average WSS in the ruptured region of aneurysms (1.64±1.16 Pa) was lower than that of the vessel region. A recent systematic review [9] including 1257 patients from 22 studies revealed a significantly higher rate of occurrence of low WSS (0–1.5 Pa) in ruptured aneurysms (odds ratio 2.17; 95% confidence interval, 1.73–2.62), and it was suggested that decreased local WSS may be an important predictive parameter for the rupture of intracranial aneurysms. A follow-up study showed that the minimum WSS values were significantly different in ruptured and unruptured aneurysms of the internal carotid artery ($p < 0.001$); this phenomenon, however, had not been observed in aneurysms occurring on the middle cerebral artery [10]. The results suggested that the location of an aneurysm might be one factor leading to the discrepancy.

Contrary to the above proposal, some studies were in favour of the high-WSS theory, which proposes that regions of increased flow and WSS are associated with the rupture of aneurysms [11, 12]. A study by Cebral *et al.* [13] compared the haemodynamic parameters for ruptured

and non-ruptured aneurysms in a rather large number of subjects. The results showed that elevated values of maximum WSS, WSSG and inflow focusing were more likely to occur in the ruptured aneurysms. It was also suggested that high aneurysm–parent artery WSS ratios could lead to the rupture of the aneurysm [14]. However, in a review by Meng *et al.* [15] it was suggested that both theories may possibly be valid and that rupture might occur in both low and high WSS regions. Therefore, understanding of the role that haemodynamics plays in intracranial aneurysm still needs to be strengthened, and more studies are needed to provide explanations of the underlying haemodynamic mechanisms of rupture in intracranial aneurysms.

In addition to the immense investigations into the rupture of intracranial aneurysms, image-based CFD is also applied to analyse the haemodynamic behaviour in the stent treatment of intracranial aneurysms [16]. It can also be utilised to investigate the effects of different stent designs on the flow pattern and inflow disruption in cerebral aneurysms [17], to perform 'virtual testing' of different stent shapes, sizes and materials in realistic arterial geometries [18], and to predict the haemodynamic changes after stenting and the outcomes of the intervention [16].

5.2.2 Carotid atherosclerosis

The carotid bifurcation has been intensively investigated due to the ease of accessibility in combination with its clinical relevance to cerebrovascular diseases. It has facilitated image-based CFD studies by serving as a prototype for the study of disturbed flow patterns. Therefore an image-based CFD method has been introduced in this study to explore the haemodynamic characteristics of the carotid bifurcation.

5.2.3 Image-based CFD of the carotid artery

Various MRI sequences have been used to explore the ability of image-based CFD methods for haemodynamic analysis. Contrast-enhanced MRI was commonly used, due to its excellent contrast between vessels and surrounding tissues. However, numerous studies have exploited non-contrast-enhanced MRA to provide geometric information. TOF-MRA was first used to construct computational models of a normal carotid artery by Zha *et al.* [19]. Steinman *et al.* [20] applied black-blood MRA in the construction of their geometric models and exploited PC-MRI to provide boundary conditions. The simulation results showed that low WSS mainly occurred in the region of the carotid bulb. Thomas *et al.* [21] also used black-blood MRA and PC-MRA to simulate carotid haemodynamics, characterised in terms of WSS, time-averaged WSS, WSSG, time-averaged WSSG, and oscillatory shear index. The results revealed that the reproducibility of image-based model reconstruction is mainly dependant on the segmentation process. However, the ability of different non-contrast-enhanced MRA sequences to construct the geometric models has not been reported so far, although it would probably be an interesting topic.

Geometrical characteristics are considered to exert influence on flow patterns. A variety of geometrical factors have been investigated and proposed as plausible indicators of atherosclerosis, such as bifurcation angle, planarity, differences in area ratios, tortuosity, *etc*. A study of various geometries in both synthetic and volunteer models showed that the bifurcation angle had a negative correlation with WSS [22]. A recent CFD study, in which multivariate regression analysis was used, concluded that only the tortuosity of the ICA and the proximal ICA area ratios were significant determinants of disturbed flow patterns [23]. Another study reported that the proximal ICA radius and ICA angle were related to the haemodynamic changes [24]. A further study, based on MRI scans, showed that the

bifurcation area ratio and the tortuosity of the ICA were independent predictors of carotid wall thickening [25]. Other geometric parameters, such as surface curvatures, vascular radius, and rate of change of the vascular radius, were also explored and considered to be linked to the haemodynamic parameters [26]. Although the results from these studies showed that geometric characteristics have correlations with haemodynamics, due to the lack of larger cohort studies firm conclusions are not available yet.

5.2.4 Haemodynamics after treatment

The haemodynamic changes after treatment, either invasive or non-invasive, have been explored by several studies. Lu *et al.* [27] found that after carotid stenting, the turbulent flow in the stenosis was restored to a laminar flow. The major haemodynamic parameters, including velocity, lumen diameter, residual area, peak systolic velocity, and diastolic velocity, were altered significantly. Likewise, Schirmer *et al.* [28] also presented results showing laminar flow restoration after stenting, and WSS and WSSG decreased significantly after stenting. In a follow-up study after medicine treatment, the results showed that the plaque thickness as well as plaque components were negatively associated with WSS, and a moderate association was found between the plaque thickness and WSS [29]. However, few studies focused on the haemodynamic changes after carotid endarterectomy [30], which will be discussed afterwards in our study.

Despite the successful carotid revascularisation, restenosis is still an issue that causes treatment failure. As haemodynamics is involved in the onset and progress of atherosclerosis, it is also considered to contribute to restenosis. A previous study showed that the distributions of WSS and WSSG were different in the cases with restenosis compared with those in the non-restenosis group [31]. However, the haemodynamic mechanism remains unclear, and

longitudinal study as well as animal studies are necessary to provide further understanding of restenosis after revascularisation.

Imaged-based CFD can be used to analyse patient-specific haemodynamic conditions in cerebrovascular diseases. It can also promote further understanding of the natural development and treatment of cerebrovascular diseases. However, there still are some unconcerned issues. Firstly, the artery geometries for use in image-based CFD can be reconstructed from different image modalities, including computed tomography angiography (CTA) or different sequences of magnetic resonance angiography (MRA), which may lead to a difference in geometries. Secondly, patient-specific boundary conditions were not available in some studies, for various reasons, which may affect the accuracy of the haemodynamic results. As such, a realistic and systematic image-based CFD method needs to be proposed to quantitatively evaluate the haemodynamic information; the result would be a tool to desirably and reliably aid clinicians in decision-making for diagnosis or treatment.

5.3 CFD procedures in this project

As mentioned above, the quality of patient-specific angiograms is essential to guarantee the quality of CFD simulation. In clinical, the image data are mainly obtained from ultrasound, CTA, MRA or DSA, *etc*. Due to the low resolution of ultrasound and the radiation exposure of CTA and DSA, recent studies have focused on MRA and have demonstrated that MRA is able to provide realistic geometric conditions for the CFD simulations of arterial haemodynamics. Moreover, the reproducibility of such MRA-based CFD techniques has also been investigated and confirmed in a previous study [21].Therefore, in this study, TOF-MRA, a non-contrast measure tool, has been applied to obtain the artery geometries. In order to precisely measure the blood flow, PC- MRA was applied at the inlets and outlets to measure patient-specific

flow conditions. The CFD process in this study was included the following steps: 1. Artery structure segmentation; 2. Surface reconstruction; 3. Computational simulation; 4. Post-processing.

5.3.1 Artery structure segmentation

Image-based segmentation methods have made noticeable progress in the simulation of realistic blood flow constructed from 3D medical imaging data over the last decade [19, 32, 33]. The segmentation process can be performed in either a manual or a semi-automatic way [34]. A commercial software application, MIMICS 16.0 (Materialise, Leuven, Belgium), was used in our project to perform the segmentation process. We obtained 3D geometries from TOF-MRA, which is a commonly used sequence in routine clinical practice. To accurately segment the geometries, the following steps were implemented. Firstly, the contrast of images from TOF-MRA was adjusted to make the arterial lumen distinct from the surrounding tissue. The upper and lower grayscale thresholds were then selected and adjusted, and the lumen area was identified through the use of greyscale thresholds. Manual modification of the lumen area was applied to remove branches or any erroneous features. Finally, a reconstructed 3D surface model of the carotid bifurcation was completed at this stage. The model was next smoothed and then trimmed in order to generate the flat inlet and outlet boundaries for the subsequent step.

5.3.2 Meshing generation

After the segmentation process, body-fitted structured or unstructured grids were generated around the complex geometrics to mesh the constructed models. Structured grids are usually considered to be more accurate compared to unstructured grids. However, due to the complex

geometry, unstructured grids, comprising tetrahedral, hexahedral, pyramidal or hybrid elements, were used in any appropriate combinations in this study.

The quality of grid accounts for the accuracy of the flow solution and meeting of the convergence criteria [34]. Specifically, the grids should be smooth; that is, there should be no large differences in the volume or in the aspect ratio of adjacent grid cells, and the grids should be as regular as possible. Factors such as size, type and location of the cells are correlated with the quality of grid. To meet the requirements, we applied small grid sizes in the stenosed regions of atherosclerotic models (**Figure 5-1a**). The general quality of the mesh was then checked and improved, with a general mesh quality > 0.3 considered to be satisfactory.

The utilisation of a combination of a prism layer together with a hexahedral or hybrid mesh is considered to provide the best precision for WSS evaluation [35]. Therefore a prism-layer was placed in the near-wall regions in order to reduce such errors (**Figure 5-1b**). For the first prism layer, the thickness of the grid was set to 0.1 mm. The total number of prism layers was 6, with a growth factor of 1.2.

For each model we used ICEM CFD (ANSYS Inc., Canonsburg, USA) to generate the grids in the general mesh as well as in the prism layers. The total number of elements in the grids ranged from 3 to 6 million based on different carotid models.

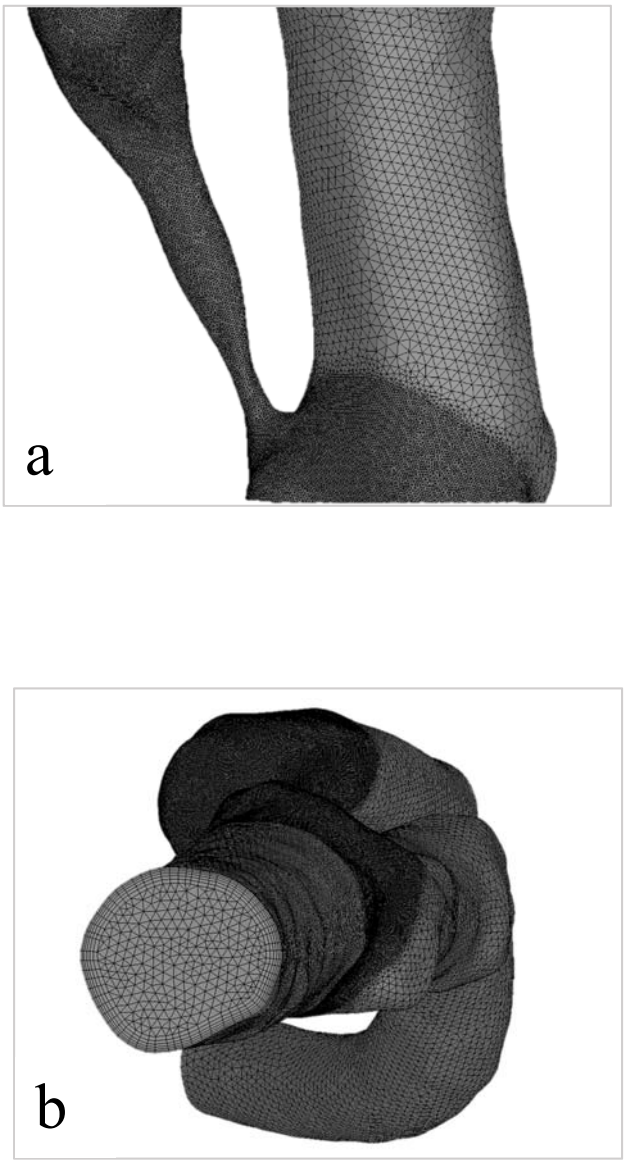

Figure 5-1. Meshing of the carotid bifurcation. (a) Demonstration of the fine meshing in the region of the stenosis. (b). A close look at the grid at the inlet of the carotid artery, the boundary-layer mesh.

5.3.3 Boundary conditions

Inlet boundary condition

For the inlet boundary conditions, the distribution of all flow variables needs to be specified at the inlet boundaries. Inlet flow velocity is the type of boundary condition commonly specified. Flow or pressure waveforms obtained from ultrasound or PC-MRA are also commonly seen as the inlet boundary conditions. In our study we provided the velocity measured by PC-MRA as a physiological parameter for the inlet boundary condition.

Outlet boundary conditions

Many empirical and theoretical methods have been proposed to resolve the outlet boundary conditions. Murray's law has been used to estimate the flow ratio of daughter arteries in the carotid bifurcation [36, 37]. However, as Murray law's does not hold for stenotic carotids, a formula for flow distribution was proposed by Groen *et al.* [38] from the experience of a relatively large number of subjects, which is considered to be accurate and suitable for stenotic carotids.

Some theoretical conditions were also proposed to determine the outlet boundary conditions. The zero pressure outlet or traction-free boundary condition is used in various models due to its simplicity. Commonly, the zero pressure boundary condition assumes that the vessel is cut and exposed to atmospheric conditions, thereby it neglects the changes in pressure and flow rate by wave reflection from downstream vessels, resulting in considerable difference from actual blood flow [39]. Although in many studies the outflow boundary is considered to be zero pressunre, this method is likely to produce different results compared to clinical measurements [40]. The other well-known outlet condition uses impedance boundary models, such as 0D and 1D models, which attempt to capture the resistance of the proximal and distal

arteries of the boundary as well as the capacitance of the downstream vessels [41]. Recently, the Minimum Energy Loss theory was proposed and recommended for application to the cardiovascular system, as it could provide better results compared with clinical data [42]. However, these assumptions were proposed for different situations when the physiological measurements were not readily available.

In this project, the patient-specific physiological parameters of velocity measured by PC-MRA were used as the inlet boundary condition at the CCA. To avoid the bias from PC-MRA measurements, zero pressure condition was applied at the ECA outlet while the velocity measured by PC-MRA was applied at the ICA outlet. As a calibration test, the simulated results at ECA was compared with the velocity which measured by PC-MRA. **Figure 5-2** illustrates the locations where the inlet and outlet boundary conditions were measured around the carotid bifurcations.

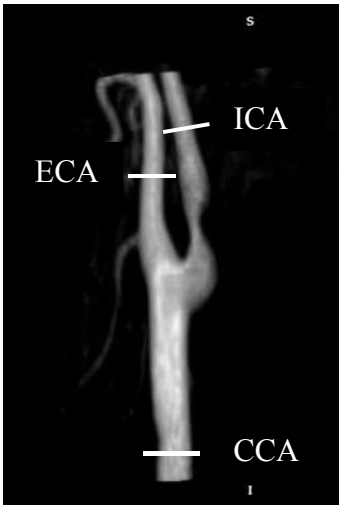

Figure 5-2. Illustration of the locations of the inlet and outlets on a scan acquired by phase-contrast magnetic resonance angiography. At the inlet of the common carotid artery (CCA), the measurement plan is about 2 cm from the bifurcation, whereas at the outlet of internal carotid artery (ICA), the measurement plane is about 1 cm distal to the stenosis. At the outlet of the external carotid artery (ECA), the measurement plane is about 1 to 2 cm distal to the bifurcation, to avoid the branches.

5.3.4 Blood flow model

Researchers have dedicated their efforts to develop accurate methods for modelling the circulatory system by simplifying or approximating properties that are difficult to precisely imitate. Since the complicated vessel shape of the entire vascular system can neither be measured nor be realized exactly, the usage of simple flow modelling conditions is inevitable,

The blood can be assumed to be a Newtonian or non-Newtonian fluid. The assumption of regarding blood as a Newtonian fluid is a simplified method, which ignores its characteristics and treats it as a water-like liquid. In many previous studies, the blood was assumed to be a

Newtonian fluid [31, 43]. However, the Newtonian blood behaviour is only valid when the shear rate is over 100 s^{-1}, which tends to occur in large arteries [44]. In most cases, non-Newtonian blood models can provide more accurate blood flow behaviour, particularly in stenotic vessels [43]. In our project, the majority of research subjects have stenotic carotids, so it is appropriate to apply a non-Newtonian blood model for the sake of precise simulation. Besides that, the blood is considered to be incompressible and non-slipping at the walls, as has been assumed in a previous study [31].

Under physiological conditions, arterial vessels are compliant and deformable. For the purpose of simplifying the simulation process and due to the unavailability of arterial wall materials, a rigid-wall boundary was applied in simulating blood flow in the carotid artery. However, rigid and compliant vessel boundaries were compared in a previous study, and the results showed that the distributions of flow and the shear patterns were similar [19]. In line with the previous study, a rigid-wall boundary was applied in our project [31].

A steady-state flow model was applied for this project, despite the pulsatile nature of physiological blood flow. Vincent *et al.* [45] conducted an animal study in which pulsatile effects were ignored; consequently, their conclusions were based on steady-state results. Their results revealed that steady-state flow could be used as a simplified mode of pulsatile flow. A phantom study showed that under steady-state flow conditions the velocity and WSS simulated from CFD correlate well with those measured by particle imaging velocimetry (PIV) and PC-MRA [46]. In addition, a steady-state flow analysis of cerebrovascular flow demonstrated that it could provide reasonable information with the advantages of time-efficiency and time-independency [47]. In a study by Hsiao *et al.* [48] the haemodynamics in different flow models was investigated, comprising steady-state and pulsatile flow for intra-

stent blood flow. Their study showed that the distribution of WSS was similar in the two flow modes, with a relatively low time consumption for simulation of the steady-state flow condition. In our project, we investigated the haemodynamic changes based on a relatively large number of subjects for the sake of generalized application and high time-efficiency. Therefore, the steady-state flow mode was selected for the abovementioned reasons.

5.3.5 Governing Equations

Flow simulations are based on the governing equations that reflect the conservation laws for the fluid's physical properties. The basic equations are the three physical laws of conservation:

Conservation of Mass: Continuity Equation

$$\frac{\partial u}{\partial t} + \boldsymbol{\nabla} \cdot (\boldsymbol{u}) = 0 \qquad (5\text{-}1)$$

The equation can be simplified in incompressible flow:

$$\boldsymbol{\nabla} \cdot \boldsymbol{u} = 0 \qquad (5\text{-}2)$$

where ρ [kg/m^3] is the density, $\boldsymbol{u}$ [m/s] is the velocity.

Conservation of Momentum: Momentum Equation (Newton's Second Law)

The conservation equations correspond to the incompressible Navier–Stokes equation:

$$\rho\left(\frac{\partial \boldsymbol{u}}{\partial t} + \boldsymbol{u} \cdot \boldsymbol{\nabla u}\right) = -\boldsymbol{\nabla} p + \boldsymbol{\nabla} \cdot \boldsymbol{\tau} + \boldsymbol{F} \qquad (5\text{-}3)$$

where ρ is the density, $\boldsymbol{u}$ is the velocity field, p [Pa] is the pressure, t is a point in the time domain, $\boldsymbol{\tau}$ [Pa] is shear stress, and $\boldsymbol{F}$ represents any externally applied body forces such as gravity.

5.3.6 Convergence

For a steady-state simulation, we need to ensure that the solution at least satisfies the following two conditions:

1) Residual Maximum error values have been reduced to an acceptable value (typically 10^{-5}).
2) Monitor points for our values of interest have reached a steady solution.

In our project, iterative convergence was guaranteed by requiring the RMS residuals for the continuity and momentum equations to be less than 10^{-5} within 1000 time steps.

5.3.7 Numerical discretisation

Finite-volume-based analysis is one of the prominent approaches that can be efficiently used to simulate cardiovascular biomechanics problems in patient-specific three-dimensional vascular models. In the current project, solutions were generated with a commercial software application, ANSYS CFX 15.0 (ANSYS Inc., Canonsburg, USA) by the use of the finite-element method.

5.3.8 Post-processing

Haemodynamic parameters applied in this project

Wall shear stress (WSS)

WSS is a friction force that blood flow exerts on endothelial cells lining the inner vessel wall [49]. As a key regulator of vascular biology, WSS regulates the inflammatory status of the endothelium and thus determines the location of plaque development [50, 51]. The magnitude

of WSS can be determined by calculating the gradient of the local blood flow velocity close to the vessel wall multiplied by the blood viscosity.

$$\text{WSS} = \tau_w = \mu\frac{\partial u}{\partial y} \quad (5\text{-}4)$$

where μ is the dynamic viscosity, u is the velocity parallel to the wall and y is the unit vector perpendicular to the wall.

Wall shear stress gradient (WSSG)

WSSG represents the spatial rate of change of WSS [31].

$$\text{WSSG} = \sqrt{\left(\frac{\partial \tau w}{\partial x}\right)^2 + \left(\frac{\partial \tau w}{\partial y}\right)^2} \quad (5\text{-}5)$$

Where x and y are the local tangential and normal direction to the wall, respectively. In the present study, y is not available in the current study because a vessel wall was simulated as a rigid wall.

Physiological effects

As described above, the WSS is mainly exerted on the endothelium, the inner wall of the vessel. Endothelial cells can sense the mechanical force arising from WSS, and then convert it into signals that are sent to cells, triggering a series of cellular signals generated by smooth muscle cells [52]. A variety of studies have provided evidence that the WSS must be maintained within certain ranges in order to maintain the vascular physiology [49, 50, 53, 54]. The physiological levels of WSS have been investigated in humans as well as in animals [19, 32, 55], and it is normally acknowledged that under certain conditions, such as undisturbed laminar flow of large arteries, the time-averaged WSS levels are around 1.5 Pa. However, the

physiological levels of WSS are different throughout the entire arterial vasculature, due to the fact that it depends on the proximity to the aortic root, with arteries located closer experiencing the highest levels of WSS [56]. So far, WSS cannot be measured directly, and therefore the veracity of these indirect calculations relies on the accuracy of flow measurements and the precision of the imaging modalities used [57].

In vitro and animal experiments have demonstrated that high WSS influences the orientation of endothelial cells and the subsequent production of molecules that inhibit coagulation, permit migration of leukocytes, and induce smooth muscle cell proliferation, promoting endothelial cell survival [49]. Conversely, low WSS shifts the profile of secreted factors and expressed surface molecules to one that favours the opposite effects, thereby contributing to the development of atherosclerosis [49, 58].

It has been suggested that high WSSG often accompanies by high WSS [59], and high WSSG combined with high WSS promotes the loss of intercellular adhesion, which in turn causes endothelial cell dysfunction [60].

The output of haemodynamic parameters included velocity, WSS and WSSG (**Figure 5-3)**. The contours of these parameters were plotted to depict their distributions in the atherosclerotic carotids, which can provide the visualisation for the discussion of carotid artery haemodynamics in this study.

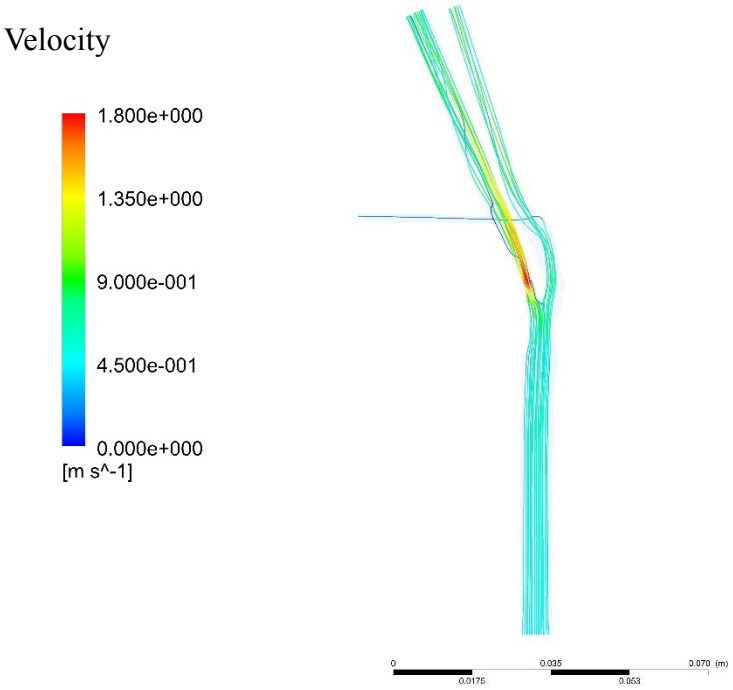

a. Velocity streamlines

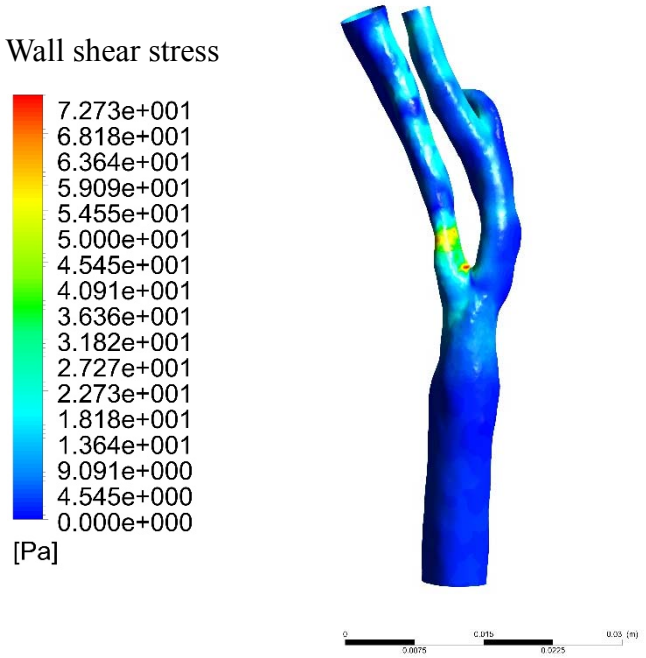

b. Wall shear stress

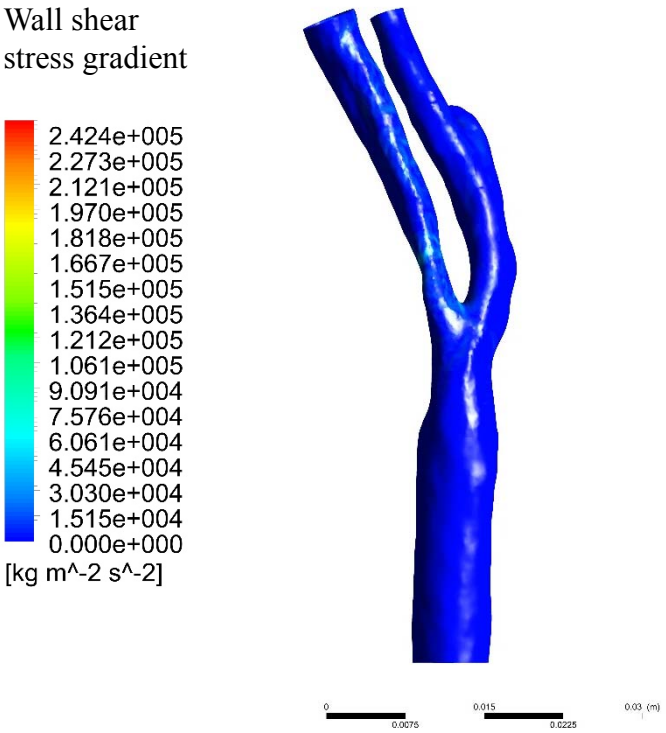

c. Wall shear stress gradient

Figure 5-3. Illustration of haemodynamic outputs for a severely stenotic carotid bifurcation: (a) velocity streamline, (b) the distribution of wall shear stress (WSS) and (c) the wall shear stress gradient (WSSG). We can see the disturbance of flow in the stenosis region through the velocity streamlines, as well as the unevenly distributed wall shear stress and its gradient in the same region.

5.3.9 Validation

Validation is the process to confirm the results of the simulation outcomes or to evaluate the results to ensure compliance with specific requirements. CFD simulations are based on n simulations, therefore, the validation of the results is necessary. In general, the available validation methods includes PIV or clinical data validation. PIV can concurrently acquire 2D velocity information across an entire plane, making it possible to determine the in-plane 2D flow structures with excellent spatial and temporal resolutions. However, the model construction is time-consuming and costly. Clinical data validation is another way to ensure the results are valid, as has been proved by many studies [42, 55, 61]. Validation studies comparing simulated intra-aneurysmal flow patterns with those measured using 2D or 4D PC-MRA reported good agreements and thereby encourage the continued advancement of CFD [62-64]. A recent study also showed that with proper encoding velocity, the measurements from PIV and PC-MRA have good agreement on velocities at the inlet and the throat of stenotic arteries [65].

In our study, we employed clinical data to validate the CFD simulation. The velocity measured at the ECA by PC-MRA was compared to the velocity computed by CFD simulation. We analysed the correlation between two sets of data and the results were demonstrated in the following chapters.

5.4 Conclusion

The haemodynamics of cerebrovascular has been well investigated, however, the previous research have not well acknowledged the influence that haemodynamics exerted on plaque components and the haemodynamic changes after endarterectomy. In this regard, our study will try to make efforts on these aspects, aiming to have further understanding on these fields.

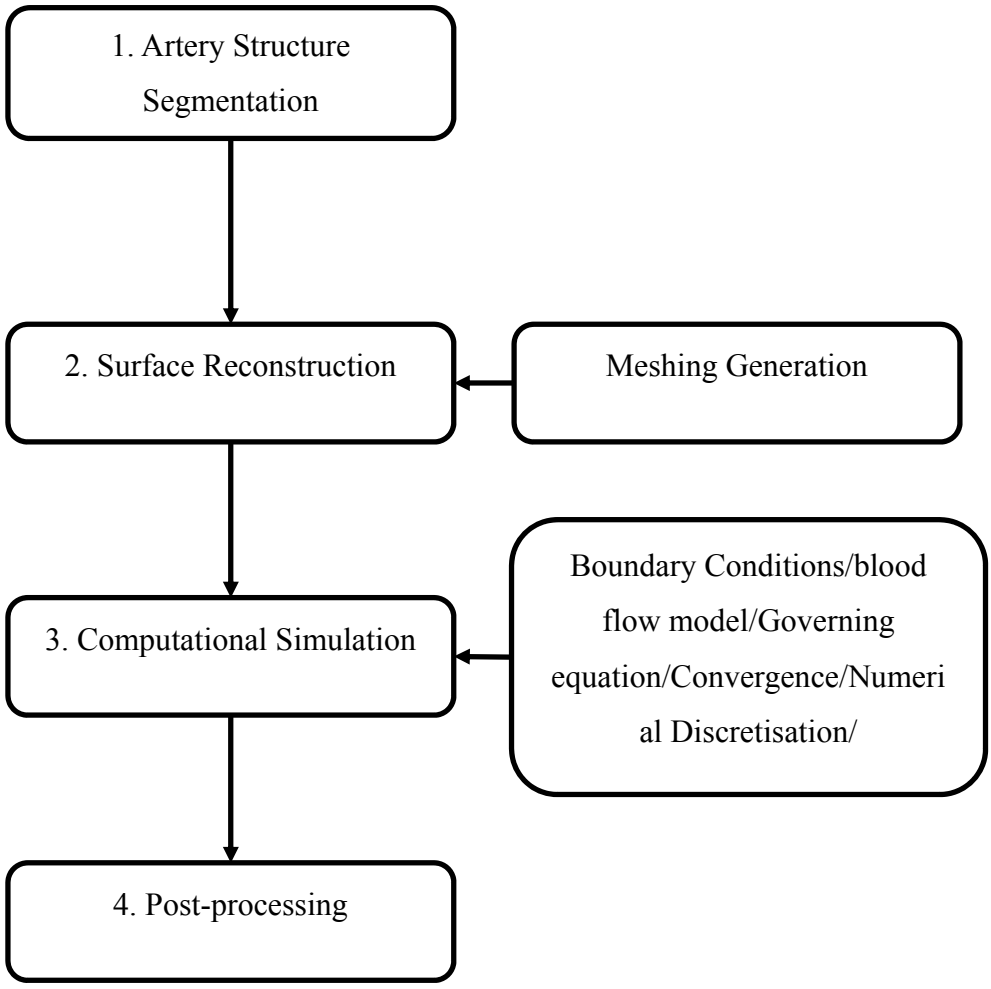

Figure 5-4. Flow chart shows the procedures of computational fluid simulation processed in this project.

References:

1. Gao L, Hoi YM, Swartz DD, Kolega J, Siddiqui A, Meng H. Nascent aneurysm formation at the basilar terminus induced by hemodynamics. Stroke. 2008;39(7):2085-2090.

2. Kulcsar Z, Ugron A, Marosfoi M, Berentei Z, Paal G, Szikora I. Hemodynamics of cerebral aneurysm initiation: the role of wall shear stress and spatial wall shear stress gradient. AJNR Am J Neuroradiol. 2011;32(3):587-594.

3. Boussel L, Rayz V, McCulloch C, et al. Aneurysm Growth Occurs at Region of Low Wall Shear Stress Patient-Specific Correlation of Hemodynamics and Growth in a Longitudinal Study. Stroke. 2008;39(11):2997-3002.

4. Castro M, Putman C, Radaelli A, Frangi A, Cebral J. Hemodynamics and rupture of terminal cerebral aneurysms. Acad Radiol. 2009;16(10):1201-1207.

5. Shojima M, Nemoto S, Morita A, Oshima M, Watanabe E, Saito N. Role of shear stress in the blister formation of cerebral aneurysms. Neurosurgery. 2010;67(5):1268-1274.

6. Omodaka S, Sugiyama S, Inoue T, et al. Local Hemodynamics at the Rupture Point of Cerebral Aneurysms Determined by Computational Fluid Dynamics Analysis. Cerebrovascular Diseases. 2012;34(2):121-129.

7. Tanoue T, Tateshima S, Villablanca JP, Vinuela F, Tanishita K. Wall shear stress distribution inside growing cerebral aneurysm. AJNR Am J Neuroradiol. 2011;32(9):1732-1737.

8. Shojima M, Oshima M, Takagi K, et al. Magnitude and role of wall shear stress on cerebral aneurysm: computational fluid dynamic study of 20 middle cerebral artery aneurysms. Stroke. 2004;35(11):2500-2505.

9. Zhou G, Zhu Y, Yin Y, Su M, Li M. Association of wall shear stress with intracranial aneurysm rupture: systematic review and meta-analysis. Sci Rep. 2017;7(1):5331.

10. Takao H, Murayama Y, Otsuka S, et al. Hemodynamic differences between unruptured and ruptured intracranial aneurysms during observation. Stroke. 2012;43(5):1436-1439.

11. Castro MA, Putman CM, Sheridan MJ, Cebral JR. Hemodynamic patterns of anterior communicating artery aneurysms: a possible association with rupture. AJNR Am J Neuroradiol. 2009;30(2):297-302.

12. Mut F, Lohner R, Chien AC, et al. Computational hemodynamics framework for the analysis of cerebral aneurysms. International Journal for Numerical Methods In Biomedical Engineering. 2011;27(6):822-839.

13. Cebral JR, Mut F, Weir J, Putman C. Quantitative characterization of the hemodynamic environment in ruptured and unruptured brain aneurysms. AJNR Am J Neuroradiol. 2011;32(1):145-151.
14. Qiu TL, Jin GL, Xing HY, Lu HT. Association between hemodynamics, morphology, and rupture risk of intracranial aneurysms: a computational fluid modeling study. Neurological Sciences. 2017;38(6):1009-1018.
15. Meng H, Tutino VM, Xiang J, Siddiqui A. High WSS or low WSS? Complex interactions of hemodynamics with intracranial aneurysm initiation, growth, and rupture: toward a unifying hypothesis. AJNR Am J Neuroradiol. 2014;35(7):1254-1262.
16. Zhang Y, Chong W, Qian Y. Investigation of intracranial aneurysm hemodynamics following flow diverter stent treatment. Med Eng Phys. 2013;35(5):608-615.
17. Radaellia AG, Augsburger L, Cebral JR, et al. Reproducibility of haemodynamical simulations in a subject-specific stented aneurysm model - A report on the Virtual Intracranial Stenting Challenge 2007. Journal Of Biomechanics. 2008;41(10):2069-2081.
18. Zhang M, Li Y, Zhao X, et al. Haemodynamic effects of stent diameter and compaction ratio on flow-diversion treatment of intracranial aneurysms: A numerical study of a successful and an unsuccessful case. J Biomech. 2017;58:179-186.
19. Zhao SZ, Xu XY, Hughes AD, et al. Blood flow and vessel mechanics in a physiologically realistic model of a human carotid arterial bifurcation. J Biomech. 2000;33(8):975-984.
20. Steinman DA, Thomas JB, Ladak HM, Milner JS, Rutt BK, Spence JD. Reconstruction of carotid bifurcation hemodynamics and wall thickness using computational fluid dynamics and MRI. Magn Reson Med. 2002;47(1):149-159.
21. Thomas JB, Milner JS, Rutt BK, Steinman DA. Reproducibility of image-based computational fluid dynamics models of the human carotid bifurcation. Ann Biomed Eng. 2003;31(2):132-141.
22. Saho T, Onishi H. Evaluation of the impact of carotid artery bifurcation angle on hemodynamics by use of computational fluid dynamics: a simulation and volunteer study. Radiol Phys Technol. 2016;9(2):277-285.
23. Lee SW, Antiga L, Spence JD, Steinman DA. Geometry of the carotid bifurcation predicts its exposure to disturbed flow. Stroke. 2008;39(8):2341-2347.
24. Phan TG, Beare RJ, Jolley D, et al. Carotid artery anatomy and geometry as risk factors for carotid atherosclerotic disease. Stroke. 2012;43(6):1596-1601.

25. Bijari PB, Wasserman BA, Steinman DA. Carotid bifurcation geometry is an independent predictor of early wall thickening at the carotid bulb. Stroke. 2014;45(2):473-478.
26. Chen Y, Canton G, Kerwin WS, Chiu B. Modeling hemodynamic forces in carotid artery based on local geometric features. Med Biol Eng Comput. 2016;54(9):1437-1452.
27. Lu CJ, Kao HL, Sun Y, et al. The hemodynamic effects of internal carotid artery stenting: a study with color-coded duplex sonography. Cerebrovasc Dis. 2003;15(4):264-269.
28. Schirmer CM, Malek AM. Patient based computational fluid dynamic characterization of carotid bifurcation stenosis before and after endovascular revascularisation. J Neurointerv Surg. 2012;4(6):448-454.
29. LaDisa JF, Jr., Bowers M, Harmann L, et al. Time-efficient patient-specific quantification of regional carotid artery fluid dynamics and spatial correlation with plaque burden. Med Phys. 2010;37(2):784-792.
30. Guerciotti B, Vergara C, Azzimonti L, et al. Computational study of the fluid-dynamics in carotids before and after endarterectomy. J Biomech. 2016;49(1):26-38.
31. Uemiya N, Lee CJ, Ishihara S, Yamane F, Zhang Y, Qian Y. Analysis of restenosis after carotid artery stenting: preliminary results using computational fluid dynamics based on three-dimensional angiography. J Clin Neurosci. 2013;20(11):1582-1587.
32. Schirmer CM, Malek AM. Computational fluid dynamic characterization of carotid bifurcation stenosis in patient-based geometries. Brain Behav. 2012;2(1):42-52.
33. Dong J, Inthavong K, Tu J. Image-based computational hemodynamics evaluation of atherosclerotic carotid bifurcation models. Comput Biol Med. 2013;43(10):1353-1362.
34. Renner J, Najafabadi HN, Modin D, Lanne T, Karlsson M. Subject-specific aortic wall shear stress estimations using semi-automatic segmentation. Clinical Physiology & Functional Imaging. 2012;32(6):481-491.
35. Cane F, Verhegghe B, De Beule M, et al. From 4D Medical Images (CT, MRI, and Ultrasound) to 4D Structured Mesh Models of the Left Ventricular Endocardium for Patient-Specific Simulations. Biomed Res Int. 2018; doi.org/10.1155/2018/7030718.
36. Groen HC, Gijsen FJ, van der Lugt A, et al. Plaque rupture in the carotid artery is localized at the high shear stress region: a case report. Stroke. 2007;38(8):2379-2381.
37. Sherman TF. On connecting large vessels to small. The meaning of Murray's law. J Gen Physiol. 1981;78(4):431-453.
38. Huang XY, Teng ZZ, Canton G, Ferguson M, Yuan C, Tang D. Intraplaque hemorrhage is associated with higher structural stresses in human atherosclerotic plaques: an in vivo MRI-

based 3d fluid-structure interaction study. Biomedical Engineering Online. 2010;9:86. doi: 10.1186/1475-925X-9-86..
39. Moon JY, Suh DC, Lee YS, Kim YW, Lee JS. Considerations of blood properties, outlet boundary conditions and energy loss approaches in computational fluid dynamics modeling. Neurointervention. 2014;9(1):1-8.
40. Vignon-Clementel IE, Figueroa CA, Jansen KE, Taylor CA. Outflow boundary conditions for 3D simulations of non-periodic blood flow and pressure fields in deformable arteries. Comput Methods Biomech Biomed Engin. 2010;13(5):625-640.
41. Ohhara Y, Oshima M, Iwai T, et al. Investigation of blood flow in the external carotid artery and its branches with a new 0D peripheral model. Biomed Eng Online. 2016;15:16.
42. Lee CJ, Uemiya N, Ishihara S, Zhang Y, Qian Y. A comparison of estimation methods for computational fluid dynamics outflow boundary conditions using patient-specific carotid artery. Proc Inst Mech Eng H. 2013;227(6):663-671.
43. Soares AA, Gonzaga S, Oliveira C, Simoes A, Rouboa AI. Computational fluid dynamics in abdominal aorta bifurcation: non-Newtonian versus Newtonian blood flow in a real case study. Comput Methods Biomech Biomed Engin. 2017;20(8):822-831.
44. Berger SA, Jou LD. Flows in stenotic vessels. Annual Review Of Fluid Mechanics. 2000;32:347-382.
45. Vincent PE, Plata AM, Hunt AAE, Weinberg PD, Sherwin SJ. Blood flow in the rabbit aortic arch and descending thoracic aorta. Journal Of the Royal Society Interface. 2011;8(65):1708-1719.
46. Khodarahmi I. Comparing velocity and fluid shear stress in a stenotic phantom with steady flow: phase-contrast MRI, particle image velocimetry and computational fluid dynamics. MAGMA. 2015;28(4):385-393.
47. Mantha AR, Benndorf G, Hernandez A, Metcalfe RW. Stability of pulsatile blood flow at the ostium of cerebral aneurysms. Journal of Biomechanics. 2009;42(8):1081-1087.
48. Hsiao HM, Lee KH, Liao YC, Cheng YC. Hemodynamic Simulation of Intra-stent Blood Flow. Iumrs International Conference In Asia 2011. 2012;36:128-136.
49. Kwak BR, Back M, Bochaton-Piallat ML, et al. Biomechanical factors in atherosclerosis: mechanisms and clinical implications. Eur Heart J. 2014;35(43):3013-3020, 3020a-3020d.
50. Malek AM, Alper SL, Izumo S. Hemodynamic shear stress and its role in atherosclerosis. JAMA. 1999;282(21):2035-2042.
51. Chiu JJ, Usami S, Chien S. Vascular endothelial responses to altered shear stress:

pathologic implications for atherosclerosis. Ann Med. 2009;41(1):19-28.
52. Fulton D, Gratton JP, McCabe TJ, et al. Regulation of endothelium-derived nitric oxide production by the protein kinase Akt. Nature. 1999;399(6736):597-601.
53. Qiu J, Lei D, Hu J, et al. Effect of intraplaque angiogenesis to atherosclerotic rupture-prone plaque induced by high shear stress in rabbit model. Regen Biomater. 2017;4(4):215-222.
54. Wang Y, Qiu J, Luo S, et al. High shear stress induces atherosclerotic vulnerable plaque formation through angiogenesis. Regen Biomater. 2016;3(4):257-267.
55. Gharahi H, Zambrano BA, Zhu DC, DeMarco JK, Baek S. Computational fluid dynamic simulation of human carotid artery bifurcation based on anatomy and volumetric blood flow rate measured with magnetic resonance imaging. Int J Adv Eng Sci Appl Math. 2016;8(1):40-60.
56. Cheng C, Helderman F, Tempel D, et al. Large variations in absolute wall shear stress levels within one species and between species. Atherosclerosis. 2007;195(2):225-235.
57. Szajer J, Ho-Shon K. A comparison of 4D flow MRI-derived wall shear stress with computational fluid dynamics methods for intracranial aneurysms and carotid bifurcations - A review. Magn Reson Imaging. 2017;48:62-69.
58. Evans PC, Kwak BR. Biomechanical factors in cardiovascular disease. Cardiovasc Res. 2013;99(2):229-231.
59. Dolan JM, Kolega J, Meng H. High wall shear stress and spatial gradients in vascular pathology: a review. Ann Biomed Eng. 2013;41(7):1411-1427.
60. Wang Z, Kolega J, Hoi Y, et al. Molecular alterations associated with aneurysmal remodeling are localized in the high hemodynamic stress region of a created carotid bifurcation. Neurosurgery. 2009;65(1):169-177.
61. Cebral J, Mut F, Sforza D, et al. Clinical Application of Image-Based CFD for Cerebral Aneurysms. Int J Numer Method Biomed Eng. 2011;27(7):977-992.
62. Endres J, Kowarschik M, Redel T, et al. A Workflow for Patient-Individualized Virtual Angiogram Generation Based on CFD Simulation. Comput Math Methods Med. 2012; doi:10.1155/2012/306765.
63. Sun Q, Groth A, Aach T. Comprehensive validation of computational fluid dynamics simulations of in-vivo blood flow in patient-specific cerebral aneurysms. Medical Physics. 2012;39(2):742-754.
64. Boussel L, Rayz V, Martin A, et al. Phase-Contrast Magnetic Resonance Imaging

Measurements in Intracranial Aneurysms In Vivo of Flow Patterns, Velocity Fields, and Wall Shear Stress: Comparison with Computational Fluid Dynamics. Magnetic Resonance In Medicine. 2009;61(2):409-417.
65. Khodarahmi I, Shakeri M, Kotys-Traughber M, Fischer S, Sharp MK, Amini AA. In vitro validation of flow measurement with phase contrast MRI at 3 tesla using stereoscopic particle image velocimetry and stereoscopic particle image velocimetry-based computational fluid dynamics. J Magn Reson Imaging. 2014;39(6):1477-1485.

Chapter 6

Associations between Local Haemodynamics and Carotid Intraplaque Haemorrhage with Different Stenosis Severities

This chapter is to provide insights for clinicians by investigating the relationships between intraplaque haemorrhage and local haemodynamics. This chapter was submitted as:

Y. Dai, M. Zhang, Y. Li, P. Lv, A. Ji, X. Bai, Y. Qian, J. Lin. Associations between local haemodynamics and carotid intraplaque haemorrhage with different stenosis severities: a preliminary study based on MRI and CFD. Submitted to "Journal of Clinical Neuroscience".

Abstract

Background and purpose： The relationship between carotid blood flow and carotid intraplaque haemorrhage (IPH) has not yet been fully understood. This study was to investigate the associations between local haemodynamics and carotid plaques with IPH related to stenosis severity.

Material and methods： Fifty-nine patients with carotid atherosclerosis were received non-contrast-enhanced MRI examinations and computational fluid dynamics (CFD) analysis. The carotids were categorised into two: IPH and non-IPH groups, according to the presence of IPH. For each group, carotids were then classified as: mild (<50%), moderate (50-69%) and severe (≥70%) subgroups. The maximum wall shear stress (mWSS) between the IPH and non-IPH groups were calculated and compared by independent t-test, and the relationship between the mWSS and IPH volume was explored by Pearson correlation.

Results： Fifty-four atherosclerotic carotids were subject to plaque and CFD analysis, and five carotids were excluded due to unrecognisable plaques. No significant difference of baseline characteristics was found between the IPH (21 carotids) and non-IPH (33 carotids) group. While mWSS was significantly higher in the IPH group than that in the non-IPH group of the mild ($P = 0.001$) and moderate stenosis ($P = 0.002$), it showed no significant difference in the severe stenosis ($P = 0.42$). Furthermore, for carotids with stenosis less than 70%, a good correlation ($r = 0.763$, $P < 0.001$) was shown between the mWSS and IPH volume, whereas no significant difference was found for carotids with stenosis over 70%.

Conclusion： The mWSS is significantly associated with IPH for the carotids with stenosis less than 70%, and this association tends to be prominent in cases with mild stenosis. The

mWSS might be a potential quantitative parameter for the risk stratification of carotid atherosclerosis.

Key words: carotid atherosclerosis, computational fluid dynamics, magnetic resonance imaging, intraplaque haemorrhage, wall shear stress

6.1 Introduction

Stroke is one of the leading causes of death and disability worldwide. Carotid atherosclerosis is the major cause of stroke and its proper treatment can considerably reduce the risk of stroke [1, 2]. Current guidelines have established the severity of stenosis as the primary surrogate for stroke risk and indication of intervention [3]. Internal carotid arteries (ICA) with over 70% stenosis or stenosis between 50 to 69% with symptoms are recommended for revascularisation. However, large randomised clinical trials indicated that patients with stenosis under 50% also carried the risk of cerebrovascular events [3, 4]. Therefore, unstable plaques in the carotid arteries are prone to embolisation, regardless of the degree of stenosis [5].

Carotid intraplaque haemorrhage (IPH) has been recognised as a determinant of plaque instability [6]. IPH is thought to be developed from the leakage of plaque microvessels [7]. The accumulation of free cholesterol and erythrocytes from microvessels leads to plaque progress and rupture [8]. Numerous follow-up studies have shown that IPH is associated with an increased risk of the subsequent ischemic infarction and stroke [9-11]. The advent of high-resolution magnetic resonance imaging (MRI) has enabled the characterisation of plaque components *in vivo* and especially the identification of IPH [12, 13].

In addition to IPH, carotid haemodynamics may also play an important role in plaque rupture. Plaque rupture may be caused by increased wall shear stress (WSS) via triggering the molecular mechanism on endothelial cells [14]. A clinical study with ten month follow-ups showed that carotid plaque ruptured in the areas exposed to elevated WSS [15]. High WSS is also thought to be able to induce the formation of vulnerable plaque compositions through angiogenesis [16]. Tuenter *et al.* [17] demonstrated that IPH was related to the maximum WSS on carotid arteries with mild stenosis. However, these studies either had small number of cases or were correlation studies, which were in a lack of quantitative investigation of the associations between IPH and haemodynamics. As such findings may provide further information on the vulnerability of the carotid plaque, it is therefore critical for the risk stratifications and preventions from stroke. In this study, we investigate the haemodynamics of carotid arteries by using computational fluids dynamics (CFD), which is a commonly used numerical method to estimate the blood flow in vascular diseases. Furthermore, we investigated the associations between local haemodynamics and carotid IPH under different severities of stenosis.

6.2 Material and methods

6.2.1 Patient data

From July 2015 to June 2016, 59 patients (48 males, 9 females; age range, 45-79 years; mean age ± SD, 66.6 ± 7.5 years) suspected with carotid atherosclerosis were recruited. The study was approved by local institutional ethic boards, with informed consent obtained from all participants.

6.2.2 MR imaging acquisition protocols

All patients suspected with carotid atherosclerosis received MRI examinations by using a 3.0-T MRI scanner (Magnetom Verio; Siemens, Erlangen, Germany) with an 8-channel carotid artery coil (Shanghai Chenguang Medical Technologies, Shanghai, China). MRI sequences comprised of three-dimensional (3D) time-of-flight (TOF) magnetic resonance angiography (MRA), two-dimensional (2D) phase-contrast (PC) MRA, and conventional multi-contrast plaque sequence which includes plaque TOF, T1-weighted (T1w), T2-weighted (T2w) images. The parameters of each MRI sequence were listed as following:

1. TOF-MRA: repetition time/echo time (TR/TE) 83/8.1 ms, flip angle 8°, thickness 2mm, field-of-view (FOV) 160 × 160 mm, matrix 256 × 256, acquisition time 1:40 minutes. The coverage centred at carotid bifurcation for around 7cm length.
2. PC-MRA: TR/TE 13/4ms, slice thickness 1.0 mm, FOV 140×140 mm, matrix 256×256, encoded velocity was generally set at a range of 100-200 cm/s, acquisition time about 1:30 minutes.
3. Multi-contrast plaque sequence: T2w turbo spin-echo (TSE): TR/TE 4000/59 ms, echo spacing 15.1, echo train length 18, bandwidth 133 Hz/pixel, flip angle 180°, acquisition time 3:40 min; T1w TSE: TR/TE 800/12 ms, acquisition time 3:20 min; TOF: TR/TE 26/3.23 ms, flip angle 25°, acquisition time 2:33 minutes. All plaque sequences have a FOV of 160 × 160 mm, slice thickness of 2 mm, matrix of 256 × 256, in-plane resolution of 0.63 × 0.63 mm^2, and longitudinal coverage of 36 mm.

6.2.3 MR image interpretation

Image quality was assessed by a reviewer (X.B.) following a 4-score standard [18]. Images with insufficient quality (image score ≤ 2) were excluded from further plaque components analysis.

MR images with sufficient quality (score > 2) were independently reviewed by two experienced radiologists (A.J. and P. L., with 2 years and 7 years experiences in cardiovascular imaging diagnosis). At the first step, the percentage of carotid stenosis was measured on TOF-MRA, following the North American Symptomatic Carotid Endarterectomy Trial (NASCET) criteria [19]. Plaque characterisation were performed on plaques with slices more than 2 and thickness larger than 2mm. Secondly, two observers reviewed the cross-sectional images to characterise the plaques. Then plaques were categorised into the IPH and the non-IPH groups according to the presence of IPH. The IPH plaque is defined as a hyperintense region within the plaque on TOF and T1w, hyperintense or isointense on T2w sequences [7], and the non-IPH plaque is defined as the plaque with the absence of IPH. Each group was then classified into three subgroups based on the stenosis percentage: mild (<50%), moderate (50-69%) and severe (≥70%). Finally, the volume of IPH was reconstructed and calculated on T1w images.

6.2.4 Computational fluid dynamics

We applied the same CFD simulation protocol to study the local haemodynamics as reported in our previous study [20]. Firstly, a commercial software Mimics 16.0 (Materialise Company, Leuven, Belgium) was used to generate the 3D geometry of the carotid bifurcation. The reconstructed geometry was then imported into ICEM 15.0 (ANSYS, Lebanon, NH, USA) as a stereolithography (STL) file for mesh generation with the total mesh elements ranged from 1 to 6 million across from different models. After that, a software CFX 15.0 (ANSYS, Lebanon, NH, USA) was implemented for numerical simulations, in which the flow was assumed to be steady and incompressible and the blood was considered as a non-Newtonian fluid with a density of 1050 kg/m^3 and viscosity of 0.0035 Pa·s [21]. The vascular wall was

assumed to be rigid and a non-slip boundary condition was composed. To model a fully-developed flow condition, the inlet and outlet were extended respectively to the length of 20 times the vascular diameter. We imposed the mean velocity measured from PC-MRA at the CCA inlet and the ICA outlet as boundary conditions, and applied zero pressure condition at ECA outlet. All the simulations converged to the target criteria of 1×10^{-5} for the normalised continuity and velocity residuals. The maximum wall shear stress (mWSS) on the surface of IPH and through the stenotic segments of non-IPH carotids was calculated.

6.2.5 Statistical analysis

The variability of inter-observer was analysed by intraclass correlation coefficient (ICC). ICC value greater than 0.8 was defined as excellent [22]. The difference of baseline characteristics between the IPH and the non-IPH groups was analysed by using independent t-test (continuous variables) or chi-square test (categorised variables). The difference of mWSS between the IPH and non-IPH groups was compared by using independent t-test, and so were the difference among three subgroups with different stenosis severities. The relationship between IPH volume and mWSS was explored by using Pearson correlation. The correlations were interpreted as the following categories according to the value of r: poor (0-0.2), fair (0.2-0.4), moderate (0.4-0.6), good (0.6-0.8), and excellent (> 0.8) [23]. Continuous variables were recorded as mean value ± standard deviation (SD). The data were analysed using SPSS statistical software 22.0 (IBM, Chicago, IL, USA). Two-sided tests were performed and $P < 0.05$ was considered statistically significant.

6.3 Results

6.3.1 Image quality

Of the 59 patients, 3 patients were excluded due to insufficient image quality (image score

≤2), and 2 patients were excluded due to the small size of plaques. Finally, 54 carotid arteries from 54 patients (45 males, 9 females; age range, 45-79 years; mean age ± SD, 66.6 ± 7.7 years) with diagnostic image quality were included. The image quality was excellent in 36 arteries and good in 18 arteries, with a mean score of 3.67 ± 0.48. The inter-observer variabilities in measuring carotid stenosis, identifying IPH, and quantifying the IPH volume were 0.930 (95% confidence interval [CI], 0.884 - 0.956), 0.901(95% CI, 0.840 - 0.939) and 0.902 (95% CI, 0.775 - 0.959), respectively.

6.3.2 Clinical characteristics

Twenty-one carotids were categorised into the IPH group, and 33 carotids were included in the non-IPH group. For carotids with mild, moderate and severe stenosis, the incidences of IPH were 40.0% (6/15), 26.7% (4/15), and 45.8% (11/24), respectively. The baseline characteristics of the patients were summarised and compared between the IPH and the non-IPH groups (**Table 6-1**).

Table 6-1 Baseline characteristics of patients between the IPH and the non-IPH groups.

Variables	IPH group (n = 21)	Non-IPH group (n = 33)	P values
Gender	21M	28M	0.322
Age	66.27±7.96	66.81±7.58	0.802
Smokers (ever)	5	9	0.657
Hypertension	13	25	0.132
Hyperlipidaemia	4	2	0.170
HDL-Cholesterol (mmol/L)	1.01±0.38	1.21±0.61	0.177
Total cholesterol (mmol/L)	3.47±0.97	3.45±0.77	0.939
Stains user	1	3	0.506
Diabetes	7	6	0.270
Cerebrovascular events	19	23	0.208

n indicates subjects number; IPH intraplaque haemorrhage; M, male; HDL, high density lipoprotein

6.3.3 Lumen and flow characteristics

We compared the stenosis severity and mass flowrate of ICA between the IPH and the non-IPH groups. No significant difference of stenosis percentage was found between the two groups in the mild (44.2 ± 5.4% vs. 42.0 ± 5.0%, P = 0.444), moderate (66.1 ± 4.0 % vs. 61.6 ± 6.5 %, P = 0.233), and severe stenosis (83.7 ± 6.5% vs. 80.3 ± 6.9%, P = 0.227). There is no significant difference of mass flowrate between the two groups in the mild (0.197 ± 0.07 $kg.s^{-1}$ vs. 0.196 ± 0.09 $kg.s^{-1}$, P = 0.983), moderate (0.167 ± 0.05 $kg.s^{-1}$vs. 0.175 ± 0.08 $kg.s^{-1}$, P = 0.845) and severe stenosis (0.105 ± 0.06 $kg.s^{-1}$ vs. 0.120 ± 0.10 $kg.s^{-1}$, P = 0.664).

6.3.4 Quantitative analysis of the association between IPH and carotid haemodynamics

The mWSS was significantly higher in the IPH group with mild stenosis compared with that in the non-IPH group (41.7 ± 18.4 Pa vs. 11.4 ± 7.2 Pa, P = 0.001) (**Table 6-2**). Likewise, we observed an increased mWSS in carotids with IPH under moderate stenosis (85.0 ± 14.3 Pa vs. 39.8 ± 21.9 Pa, P = 0.002) (**Figure 6-1**), whereas the mWSS exhibited no significant difference between the two groups in carotids with severe stenosis (218.4 ± 165.4 Pa vs. 280.6 ± 199.2 Pa, P = 0.42).

Table 6-2. Maximum wall shear stress between IPH and non-IPH carotids under different stenosis.

	Mild	**Moderate**	**Severe**
IPH group (Pa)	41.7 ± 18.4	85.0 ± 14.3	218.4 ± 165.4
Non-IPH group(Pa)	11.4 ± 7.2	39.8 ± 21.9	280.6 ± 199.2
P value	< 0.001	0.002	0.42

IPH, intraplaque haemorrhage

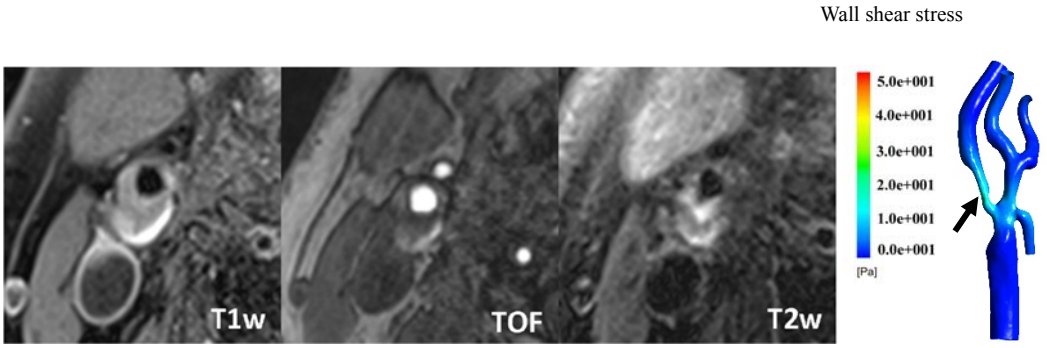

Figure 6-1. Intraplaque haemorrhage (IPH) shows hyper-intensive signal on T1w, TOF and T2w. The maximum wall shear stress was calculated on the surface of IPH (black arrow).

The levels of mWSS were also compared between different stenosis severities in the IPH group. The mWSS in the severe stenosis was higher than that in the moderate stenosis (218.4 ± 165.4 vs. 85.0 ± 14.3, P = 0.037), and the latter was higher than that in the mild stenosis (85.0 ± 14.3 vs. 41.7 ± 18.4, P = 0.005).

To better investigate the difference of mWSS, we calculate the delta value of the difference (ΔD ± SD) between the IPH and non-IPH group, which was shown in **Figure 6-2**. The results indicated that ΔD gradually increased in the mild and moderate stenosis (stenosis < 70%) with relatively small SD values (SD < 14.5). In contrast, ΔD was below zero in severe stenosis (stenosis > 70%), with a large SD value (SD >165.4). This suggest that the IPH may not be in direct correlation with mWSS when the stenosis of ICA is over 70%.

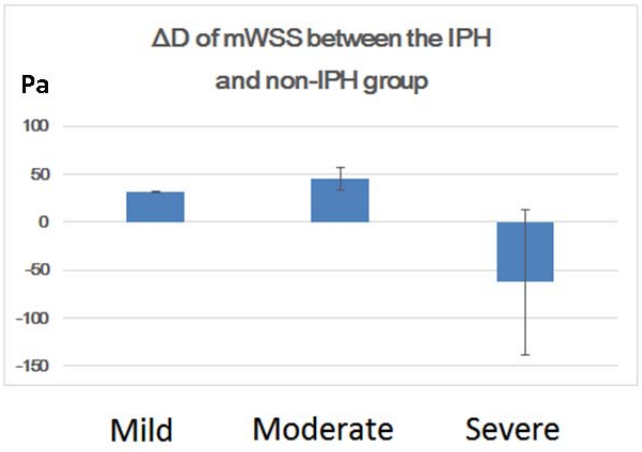

Figure 6-2. Delta value of the difference (ΔD) and its standard deviation of the maximum wall shear stress (mWSS) between intraplaque haemorrhage (IPH) and non-IPH plaques in the mild, moderate and severe stenosis, respectively.

6.3.5 Relationships between the IPH volume and local haemodynamics

The relationship between the mWSS and the volume of IPH was present in **Figure 6-3**. For cases with stenosis less than 70%, a good correlation ($r = 0.763$, $P < 0.001$) was found between the mWSS and IPH volume, whereas no significant difference ($r = 0.376$, $P = 0.253$) was found in the cases with stenosis larger than 70%.

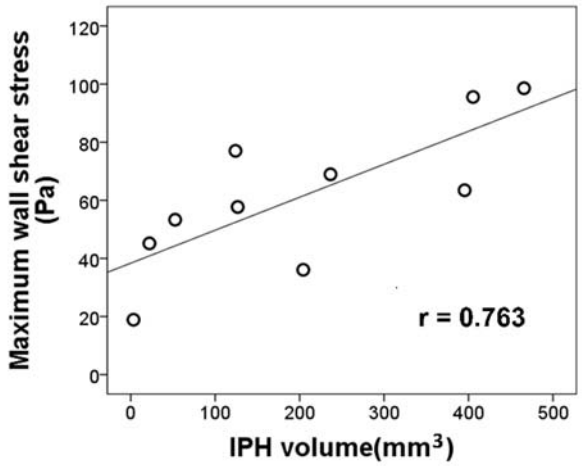

(a)

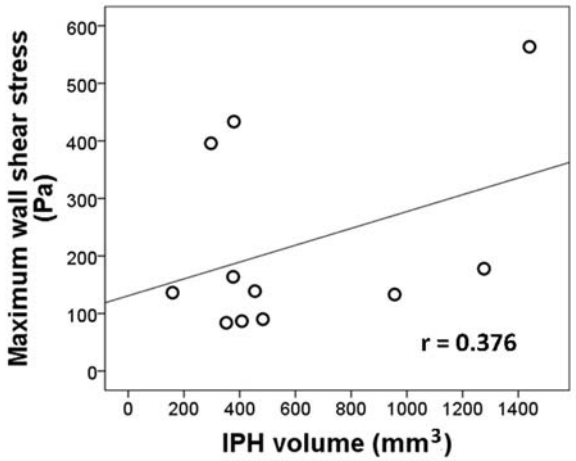

(b)

Figure 6-3. The correlation between the volume of intraplaque haemorrhage (IPH) and maximum wall shear stress in carotids with stenosis under 70% (a) was good ($r = 0.763$, $P < 0.001$), whereas no statistically correlation ($r = 0.376$, $P = 0.253$) was found for carotids with stenosis over 70% .

6.4 Discussion

Through the use of unenhanced MRI and CFD simulation, the current study quantitatively investigated the relationships between carotid plagues with the presence of IPH and local haemodynamics. Our results demonstrated that for the ICA with stenosis less than 70%, mWSS was significantly higher in the IPH group than that in the non-IPH group, and the volume of IPH was significantly correlated to the mWSS. Our study indicates that the mWSS may be a promising parameter to predict the stability of carotid plaques.

As the blood flow alteration might have effects on the WSS, we compared the stenosis severity and mass flowrate between the IPH and non-IPH group. These results showed no significant difference of stenosis percentage and mass flowrate between the two groups, which indicated that the stenosis severities and ICA flowrates had limited effects on the associations between the mWSS and IPH.

For the cases with artery stenosis less than 70%, we found that the mWSS in the IPH group was higher than that from non-IPH group. The results suggested that the mWSS might be a valued parameter to predict and evaluate the stability of plaques for carotids at the condition of stenosis less than 70%. However, the underlying mechanisms between intraplaque haemorrhage and WSS has not been fully investiaged. A previous study conducted by Lu et al[24] showed that the deformation of neovessels affected by the local hemodynamics. The severity of neovessel deformation under stress and stretch is related to its tortuosity, perimeter and the distance to the lumen. Therefore, it is reasonable to believe that higher WSS would have more influence on the deformation neovessels and consequently cause the leakage of neovessels which then formed haemorrhage inside plaques. In this regard, the mWSS is a

sensitive parameter to predict the stability of plaque, and might be used as an indirect indicator to estimate the risks of cerebral ischemic events.

On the other hand, however, in the cases of ICA with stenosis larger than 70%, there was no significant difference of mWSS between IPH and non-IPH two groups. It indicates that IPH might not be simply affected by the local haemodynamic condition. Other factors, such as the permeability of neovessels or the cellular mediators inside the plaque, might also have influence on the occurrence and even the growth of IPH [25]. In addition, it needs to be taken into consideration that the signals of T1w may be attenuated following the changes of IPH compositions, since the deposition of hemosiderin may be difficult to be distinguished from calcifications on MRI images [26], and thus IPH might be misclassified and the volume IPH may be underestimated. This is particularly remarked in carotids with severe stenosis, the plaque of size is usually developed to be large. We suppose these reasons may lead to affect the quality of mWSS to diagnose IPH in the cases of carotids stenosis larger than 70%. In generally, however, almost the cases of carotid stenosis >70% are to be treated.

Our results indicated that the haemodynamic change may have influence on the formation of IPH. This finding may support the decision making for the treatment of carotid atherosclerosis. The current critical ICA stenosis of 70% has been questioned [27]. Our results suggest that the severity of stenosis is definitely crucial and can provide guidance the further treatments. Besides, this study may could also provide doctors with further decision-making for patients with the severity of carotid stenosis under 70%. Currently, high-resolution MRI for detecting carotid plaque is not a daily routine for patients suspected with carotid atherosclerosis. Without the analysis of plaque compositions, the severity of stenosis and high mWSS would provide information for the stability of plaques. We suggest that anti-

atherosclerosis treatment should be raised in cases with higher mWSS. However, the threshold of the mWSS value would provide clear and definite guidance for doctors. In this study, due to the lack of pathological evidence, the cut-off values for the plaques with IPH could not be provided. Further study with large subjects' number and pathology evidence is critical for clinical application.

Our results indicated that there was an observable haemodynamics change in plaques with IPH for the ICA with stenosis less than 70%. This finding may support the current guidelines for the treatment of carotid atherosclerosis, as the severity of stenosis 70% in the ICA is the major criterion for the revascularisation, although this has also been questioned by a recently systematic review [26].

There are some limitations in our study. First of all, the vascular wall in CFD simulation was to assume be rigid, and this may lead to an overestimation of the absolute value of WSS on plaques with IPH, as these plaques are usually softer than those with other compositions. However, the impact of the assumption should be minor, as the compliance of wall had negligible effects on the shear stress [27]. Secondly, we were in lack of the historical confirmation of IPH identified on MRI as some patients were treated with stent or still being monitored as their stenosis were moderate. However, the accuracy of using MRI to identify IPH has been proved by a previous study [28], it should therefore be considered acceptable to use MRI diagnosis as a substitute. Thirdly, plaque comprised of other components, such as lipid necrotic core, were not considered in the current study. However, as showed by a previous study, lipid necrotic core mostly located in low WSS region, which is in different regions compared with that in our study [29]. Finally, the age of IPH was not explored in this

study. This is because our intention was only to investigate the non-chronic IPH that appears as the hyperintensive signals on MRI sequences, which was demonstrated to be related to the subsequent neurological events [10].

6.5 Conclusion

Our study suggested that mWSS was associated with the occurrence of IPH in carotid with stenosis less than 70%, and this association tended to be prominent in the mild stenosis. The combination of MRI and CFD could provide comprehensive information to quantitatively analyse the local haemodynamics, which might assist in evaluating the plaque vulnerability and thereby predicting the stroke risks.

Reference

1. Rothwell PM, Eliasziw M, Gutnikov SA, et al. Analysis of pooled data from the randomised controlled trials of endarterectomy for symptomatic carotid stenosis. Lancet. 2003;361(9352):107-116.

2. Barrett KM, Brott TG. Stroke Caused by Extracranial Disease. Circ Res. 2017;120(3):496-501.

3. Barnett HJ, Taylor DW, Eliasziw M, et al. Benefit of carotid endarterectomy in patients with symptomatic moderate or severe stenosis. North American Symptomatic Carotid Endarterectomy Trial Collaborators. N Engl J Med. 1998;339(20):1415-1425.

4. Rothwell PM, Gutnikov SA, Warlow CP, Trialists ECS. Reanalysis of the final results of the European Carotid Surgery Trial. Stroke. 2003;34(2):514-523.

5. Millon A, Mathevet JL, Boussel L, et al. High-resolution magnetic resonance imaging of carotid atherosclerosis identifies vulnerable carotid plaques. J Vasc Surg. 2013;57(4):1046-1051.

6. Gupta A, Baradaran H, Schweitzer AD, et al. Carotid plaque MRI and stroke risk: a systematic review and meta-analysis. Stroke. 2013;44(11):3071-3077.

7. Saam T, Ferguson MS, Yarnykh VL, et al. Quantitative evaluation of carotid plaque composition by in vivo MRI. Arterioscler Thromb Vasc Biol. 2005;25(1):234-239.

8. Virmani R, Kolodgie FD, Burke AP, et al. Atherosclerotic plaque progression and vulnerability to rupture: angiogenesis as a source of intraplaque hemorrhage. Arterioscler Thromb Vasc Biol. 2005;25(10):2054-2061.

9. Takaya N, Yuan C, Chu BC, et al. Association between carotid plaque characteristics and subsequent ischemic cerebrovascular events - A prospective assessment with MRI - Initial results. Stroke. 2006;37(3):818-823.

10. Yamada N, Higashi M, Otsubo R, et al. Association between signal hyperintensity on T1-weighted MR imaging of carotid plaques and ipsilateral ischemic events. AJNR Am J Neuroradiol. 2007;28(2):287-292.

11. Hosseini AA, Simpson RJ, Altaf N, Bath PM, MacSweeney ST, Auer DP. Magnetic Resonance Imaging Plaque Hemorrhage for Risk Stratification in Carotid Artery Disease With Moderate Risk Under Current Medical Therapy. Stroke. 2017;48(3):678-685.

12. Puppini G, Furlan F, Cirota N, et al. Characterisation of carotid atherosclerotic plaque: comparison between magnetic resonance imaging and histology. Radiol Med. 2006;111(7):921-930.

13. Underhill HR, Yarnykh VL, Hatsukami TS, et al. Carotid plaque morphology and composition: initial comparison between 1.5- and 3.0-T magnetic field strengths. Radiology. 2008;248(2):550-560.

14. Qiu J, Lei D, Hu J, et al. Effect of intraplaque angiogenesis to atherosclerotic rupture-prone plaque induced by high shear stress in rabbit model. Regen Biomater. 2017;4(4):215-222.

15. Groen HC, Gijsen FJ, van der Lugt A, et al. Plaque rupture in the carotid artery is localized at the high shear stress region: a case report. Stroke. 2007;38(8):2379-2381.

16. Eshtehardi P, Brown AJ, Bhargava A, et al. High wall shear stress and high-risk plaque: an emerging concept. Int J Cardiovasc Imaging. 2017;33(7):1089-1099.

17. Tuenter A, Selwaness M, Arias Lorza A, et al. High shear stress relates to intraplaque haemorrhage in asymptomatic carotid plaques. Atherosclerosis. 2016;251:348-354.

18. Ota H, Yarnykh VL, Ferguson MS, et al. Carotid intraplaque hemorrhage imaging at 3.0-T MR imaging: comparison of the diagnostic performance of three T1-weighted sequences. Radiology. 2010;254(2):551-563.

19. Staikov IN, Arnold M, Mattle HP, et al. Comparison of the ECST, CC, and NASCET grading methods and ultrasound for assessing carotid stenosis. European Carotid Surgery Trial. North American Symptomatic Carotid Endarterectomy Trial. J Neurol. 2000;247(9):681-686.

20. Dai Y, Lv P, Javadzadegan A, Tang X, Qian Y, Lin J. Hemodynamic analysis of carotid artery after endarterectomy: a preliminary and quantitative imaging study based on computational fluid dynamics and magnetic resonance angiography. Quant Imaging Med Surg. 2018;8(4):399-409.

21. Uemiya N, Lee CJ, Ishihara S, Yamane F, Zhang Y, Qian Y. Analysis of restenosis after carotid artery stenting: preliminary results using computational fluid dynamics based on three-dimensional angiography. J Clin Neurosci. 2013;20(11):1582-1587.

22. Ernst M, Kriston L, Groth M, Frolich AM, Fiehler J, Buhk JH. Factors Influencing Confidence in Diagnostic Ratings and Retreatment Recommendations in Coiled Aneurysms. AJNR Am J Neuroradiol. 2018;39(5):869-874.

23. Qi H, Sun J, Qiao H, et al. Carotid Intraplaque Hemorrhage Imaging with Quantitative Vessel Wall T1 Mapping: Technical Development and Initial Experience. Radiology. 2018;287(1):276-284.

24. Lu J, Duan W, Qiao A. Finite element analysis of mechanics of neovessels with intraplaque hemorrhage in carotid atherosclerosis. Biomed Eng Online. 2015;14 Suppl 1:S3.

25. Parma L, Baganha F, Quax PHA, de Vries MR. Plaque angiogenesis and intraplaque hemorrhage in atherosclerosis. Eur J Pharmacol. 2017;816:107-115.

26. Chu B, Kampschulte A, Ferguson MS, et al. Hemorrhage in the atherosclerotic carotid plaque: a high-resolution MRI study. Stroke. 2004;35(5):1079-1084.

27. Abbott AL, Paraskevas KI, Kakkos SK, et al. Systematic Review of Guidelines for the Management of Asymptomatic and Symptomatic Carotid Stenosis. Stroke. 2015;46(11):3288-3301.

28. Friedman MH, Bargeron CB, Duncan DD, Hutchins GM, Mark FF. Effects of arterial compliance and non-Newtonian rheology on correlations between intimal thickness and wall shear. J Biomech Eng. 1992;114(3):317-320.

29. Wentzel JJ, Schuurbiers JC, Gonzalo Lopez N, et al. In vivo assessment of the relationship between shear stress and necrotic core in early and advanced coronary artery disease. EuroIntervention. 2013;9(8):989-995.

Chapter 7

Haemodynamic Analysis of Carotid Artery after Endarterectomy

In this chapter, CFD simulation with non-contrast-enhanced MRA has been applied to provide the assessment for the post-surgery outcomes. This chapter was published as:

Y. Dai, Y. Qian, P. Lv, A. Javadzadegan, X. Tang, Y. Qian, J. Lin. Haeomdyanmics analysis of carotid artery after endarterectomy: A study based on CFD and MRA. Quantitative Imaging in Medicine and Surgery. 2018; 8(4):399-409.

Abstract

Background: The carotid blood flow following carotid endarterectomy (CEA) is not fully understood. Computational fluid dynamics (CFD) is a promising method to study blood flow. This study is to investigate local haemodynamic characteristics after CEA via the use of unenhanced magnetic resonance angiography (MRA) and CFD.

Materials and Methods: Eight carotid arteries with atherosclerosis and sixteen normal carotid arteries were included in this study. Time-of-flight (TOF) and phase-contrast (PC) MRA were applied for the measurement of three-dimensional artery geometries and velocity profile under CFD simulation. The haemodynamic parameters of the proximal internal carotid artery (ICA) including velocity, ICA/common carotid artery (CCA) velocity ratio, mean, maximum, minimum and gradient of wall shear stress (WSS_{mean}, WSS_{max}, WSS_{min} and WSSG) were calculated before and after CEA. Morphological characteristics of the carotid including bifurcation angle, tortuosity and planarity were also analysed.

Results: Compared with pre-CEA, there was a significant reduction in post-CEA velocity, WSS_{max}, WSS_{mean}, and WSSG, by 87.24% ± 13.38%, 86.86% ± 14.97%, 57.32% ± 56.71% and 69.74% ± 37.03% respectively, whereas WSS_{min} was almost unchanged. ICA/ CCA velocity ratios increased significantly after CEA. We also found that the post-CEA flow conditions were positively remodelled to approximate the conditions in normal arteries. The correlation between PC-MRA and CFD was excellent for the measurement of maximum velocity at the external carotid artery ($r = 0.846$).

Conclusions: Our preliminary results indicated that major flow dynamics were restored shortly following CEA, and CFD based on MRA measurements could be useful for

quantitative evaluation of haemodynamic outcomes after CEA.

Key words

Carotid atherosclerosis; wall shear stress; computational fluid dynamics; magnetic resonance angiography

7.1 Introduction

Carotid atherosclerosis is a major cause of stroke and transient ischemic attack. For patients with carotid atherosclerosis, carotid endarterectomy (CEA) or the surgical removal of the plaque is recommended as an effective method to reduce the risk of stroke [1], with the morphological correction of carotid stenosis. The effectiveness of CEA is largely evaluated via the measurement of luminal changes on imaging examinations or by reductions in cerebrovascular events during follow-up assessments. However, until now there have been only a limited number of studies focused on the evaluation of haemodynamic recovery following CEA.

Wall shear stress (WSS), a force of blood flow against the vessel wall, plays a critical role in the development of atherosclerotic plaque. Low and oscillator wall shear stress are both linked with the initiation and progress of the atherosclerosis plaque [2], while high wall shear stress may be associated with plaque vulnerability [3]. Schirmer *et al*. showed that WSS began to approach normal levels following carotid stenting [4]. Uemiya *et al.* reported that local haemodynamics altered after endarterectomy and stenting [5]. Whether or not haemodynamics can be restored after CEA remains poorly understood [6]. Furthermore, in order to better understand the mechanisms of restenosis after revascularisation, it is also

critical to study and monitor the local haemodynamic alterations after intervention.

Computational fluids dynamics (CFD) is an accepted method for *in vivo* haemodynamic analysis and has been extensively used in cardiovascular studies. CFD techniques can be utilized to simulate blood flows based on patient specific three-dimensional (3D) geometry derived from medical imaging. A number of studies have proved that the CFD method is a powerful and reliable tool for the haemodynamic analysis of carotid stenosis [7, 8]. Recently, Guerciotti B *et al.* used CFD to investigate the haemodynamic effects of CEA on carotid bifurcation, however, a normal control was not available in that study for comparison [9].

Time-of-flight magnetic resonance angiography (TOF-MRA) is an unenhanced luminal angiography technique commonly used for morphological evaluation of carotid stenosis in clinical practice, especially in patients who have a risk of adverse reactions to contrast media or in those with impaired renal function [10]. Phase contrast magnetic resonance angiography (PC-MRA) is another unenhanced MRA modality that provides *in vivo* blood velocity measurements [8]. In this study, we employed CFD methods based on TOF- and PC-MRA measurements to quantitatively analyse carotid flows both before and after CEA, with normal carotid arteries as a control group for comparison.

7.2 Materials and Methods

7.2.1 Subjects

Eight patients (7 males, 1 female; age range, 51-75 years; mean age ± SD, 65.5 ± 7.8 years) diagnosed with carotid atherosclerosis, who underwent CEA were recruited. The degree of stenosis within all eight arteries was over 70%, with mean stenosis 84.21 ± 8.87%. Three of the treated arteries were right-sided, whilst five were left-sided. The stenosis was located at

the proximal internal carotid artery (ICA) or carotid bulb. All operations were carried out by the same vascular surgeon (X.T). Ten volunteers with 16 normal carotid arteries (9 males, 1 female; age range, 41-76 years; mean age ± SD, 48.2 ± 10.9 years) were enrolled as a control group in this study. The study was approved of by the local institutional ethic board, with informed consent obtained from all participants.

7.2.2 MRA protocols and analysis

All patients with carotid atherosclerosis underwent MRA twice, one week prior to and 15 days post CEA operation. MRA was performed using a 3.0-T magnetic resonance imaging scanner (Magnetom Verio; Siemens, Erlangen, Germany) with an 8-channel carotid artery coil (Chenguang Technology, Shanghai, China).

MRA sequences included 3D TOF-MRA and a two-dimensional (2D) time-resolved PC-MRA sequence triggered by an electrocardiogram gating. The parameters for TOF-MRA were: repetition time/echo time (TR/TE) 26/3.23 ms, flip angle 25°, thickness 2mm, field-of-view (FOV) 160 ×160 mm, matrix 256 × 256, and acquisition time 2.33 minutes. The longitudinal coverage of TOF-MRA was approximately 7 cm including the distal common carotid artery (CCA), carotid bifurcation, the proximal ICA and the proximal external carotid artery (ECA). The parameters for PC-MRA sequence were as following: TR/TE 13/4 ms, slice thickness 1.0 mm, FOV 140 × 140 mm, matrix 256 × 256. The maximum velocity was targeted in this study, thus the encoded velocity was set at a range between 100-200 cm/s [11, 12].

7.2.3 MRA processing

The measurement of PC-MRA was performed independently by two experienced radiologists (Y.D, P. L.), with the mean values from the two measurements recorded.

2D PC-MRA was applied to obtain the velocities in the vicinity of the carotid bifurcation. Velocity was measured at different points at the CCA, ICA and ECA respectively. These measurement points were 2 cm proximal to the carotid bifurcation at CCA and 2 cm distal to stenosis at ICA, or about 3 cm distal to the carotid bifurcation of the normal ICA. On ECA, the measurement point was 1-2 cm distal to the bifurcation where no major branches arose, with measurement planes orthogonal to the long axis of the target vessels.

Two sets of cross-sectional images including magnitude images and phase images were obtained from PC-MRA. Region of interest (ROI) was drawn on the magnitude image, with velocity information extracted from the phase image corresponding to the ROI on the magnitude image. Mean velocity from the cardiac circle was recorded at each measurement point.

7.2.4 Computational fluid dynamics

The 3D geometry of carotid bifurcation was reconstructed based on 3D TOF-MRA data using commercial software Mimics 16.0 (Materialise Company, Leuven, Belgium). The 3D reconstructed geometry was then imported as a stereolithography (STL) file into ICEM 15.0 (ANSYS, Lebanon, NH, USA) for CFD mesh generation. A boundary layer mesh with a growth factor of 1.2 was used to improve the accuracy for the measurement of near-wall haemodynamic parameters. The total mesh size ranged from 1.6 to 3 million hexahedral and prism elements. To minimise the effects of boundary conditions on flow behaviour, the vessel was extended at the inlet and outlet to a length that is 20 times of the vessel diameter. All CFD simulations were normally converged and reached the criteria of residual target 1×10^{-5}.

Blood was considered as a non-Newtonian fluid with a density of 1050 kg/m^3 and a viscosity of 0.0035 Pa·s [5]. CFX 15.0 (ANSYS, Lebanon, NH, USA) was implemented for fluid-flow modelling, with the flow assumed to be steady and incompressible [13]. The vessel walls were assumed to be rigid with non-slip boundary conditions. The velocity at CCA measured via PC-MRA was averaged over a cardiac cycle and used as the inlet boundary condition. As the stenotic segment was located at ICA, measured average velocity at the ICA was imposed as the outlet boundary condition, with a zero pressure condition applied at the outlet of the ECA.

Flow velocity ratios of ICA to CCA were calculated and compared among pre-, post-CEA and normal carotid arteries. The velocity, WSS in mean (WSS_{mean}), maximum (WSS_{max}), minimum (WSS_{min}), as well as WSS gradient (WSSG) were calculated both pre- and post-CEA, and compared to those of the control group. Velocity was defined as the maximum velocity at the most stenotic area within ICA pre-CEA. At post-CEA arteries, the velocity was measured at the same locations as pre-CEA, and for health arteries the velocity was calculated at ICA about 1 cm distal to the bifurcation. The WSS_{mean}, WSS_{max}, WSS_{min} and WSSG of ICA were calculated at the same locations respectively.

7.2.5 Morphology of bifurcation

Morphological characteristics were analysed using Solid Edge ST9 (Siemens PLM Software, Plano, Texas, USA). Geometric factors including bifurcation angle, tortuosity and planarity angle were analysed in this study. These geometric factors were defined using the method described in our previous study [5]. Tortuosity was defined using a formula L/D-1, where L is the length of the centre line from CCA to ICA end point, and D is the straight line distance between these two points. Bifurcation angle was defined as the angles between the centre

lines of ICA and ECA when viewed from the front. The planarity angle was defined as the angle between ECA and ICA in the lateral view.

7.2.6 Statistical Analysis

The demographic data from the patients and healthy subjects were compared by using chi-square test (categorised variables) and independent t test (continuous variables). Inter-observer reproducibility with respect to the velocity measured by PC-MRA was analysed using interclass correlation coefficient (ICC). The results of both haemodynamic and morphological characteristics including velocity, velocity ratio of ICA/CCA, WSS_{max}, WSS_{mean}, WSS_{min}, WSSG, bifurcation angle, tortuosity and planarity both before and after CEA were compared using the non-parametric paired test. The haemodynamic and morphological parameters of pre- and post-CEA arteries, as well as of healthy arteries were compared via the use of independent t-tests. Pearson correlation was used to examine the correlation between PC-MRA and CFD simulation in the measurement of velocity at the ECA. The coefficient ratio $r > 0.80$ was considered as an excellent correlation [14]. The mean value ± standard deviation (SD) was computed for all data. Two-sided tests were performed and $P < 0.05$ was considered statistically significant. SPSS 22.0 statistical software (IBM, Chicago, IL, USA) was used for statistical analysis.

7.3 Results

The demographic data from eight patients with carotid atherosclerosis and ten volunteers were listed and compared in **Table 7-1**. The inter-observer reliability of the velocity measurement obtained from PC-MRA was excellent. (Pre-CEA CCA, ICC = 0.970; pre-CEA ICA, ICC = 0.859; pre-CEA ECA, ICC = 0.976; post-CEA CCA, ICC = 0.988; post-CEA ICA, ICC = 0.938; post-CEA ECA, ICC = 0.944; normal CCA, ICC = 0.979; normal ICA, ICA = 0.946;

normal ECA, ICC = 0.952).

Table 7-1 Baseline characteristics of the patients with carotid atherosclerosis and the controls

Variables	CEA patients (n = 8)	Control group (n =10）	P values
Age (years)	65.5 ± 7.8	48.2 ± 10.9	0.002
Gender	7 Males	9 Males	0.867
Smoker (ever)	5	0	0.005
Diabetes	2	0	0.094
Hypertension	6	1	0.003
Systolic Blood Pressure (mmHg)	156.3 ± 22.0	119.0 ± 8.8	< 0.001
Diastolic Blood Pressure (mmHg)	101.9 ± 13.1	78.6 ± 8.3	< 0.001
Hyperlipidemia	1	0	0.25
HDL-Cholesterol (mmol/L)	1.06 ± 0.14	1.13 ± 0.27	0.166
Total Cholesterol (mmol/L)	3.58 ± 0.89	2.97 ± 0.88	0.487
Statins user	0	0	-

n indicates the number of subjects; HDL, high density lipoprotein

Table 7-2. Flow comparison between pre-, post-CEA and normal carotids

Flow parameters	Pre-CEA (n=8)	Post-CEA (n=8)	Normal carotids (n=16)	P value		
				Pre- vs. Post-CEA	Pre-CEA vs. normal carotids	Post-CEA vs. normal carotids
Velocity	3.07 ± 1.53	0.48 ± 0.21	116.33 ± 97.67	5.44 ± 3.88	3199.33 ± 3405.31	0.02 ± 0.02
ICA/CCA velocity ratio	0.28 ± 0.13	0.68 ± 0.21	9.99 ± 11.35	1.76 ± 1.69	443.79 ± 511.41	0.2 ± 0.2
WSSmax(Pa)	0.22 ± 0.09	0.76 ± 0.14	13.67 ± 9.47	1.71 ± 0.98	331.78 ± 239.83	0.08 ± 0.08
WSSmean(Pa)	0.012	0.025	0.012	0.017	0.012	0.575
WSSG(Pa/s)	< 0.001	0.001	< 0.001	< 0.001	0.002	0.050
WSSmin(Pa)	0.176	0.283	0.409	0.144	0.393	0.897

n indicates the number of subjects. CEA, carotid endarterectomy, ICA, internal carotid artery; CCA, common carotid artery.

The bifurcation angle, tortuosity and planarity in pre-CEA, post-CEA and normal arteries were analysed and compared (**Table 7-3**). No significant difference was found in bifurcation angle, tortuosity and planarity between pre-CEA and post-CEA arteries. However, the bifurcation angles of pre-CEA carotids were smaller than those of normal carotids. In addition, we found that all cases had an increased bifurcation angle after surgery with the exception of one case. Compared with pre-CEA results, four post-CEA cases showed increased bifurcation tortuosity, while the other four decreased tortuosity. Four cases had larger planarity whilst the other cases had smaller one. We also observed an interesting phenomenon that post-surgery arteries which had relatively smaller tortuosities created relatively higher WSS values at carotid bifurcation (**Figure 7-5**).

Pearson correlation coefficient showed excellent agreement ($r = 0.846$, $P < 0.001$) between the results of CFD and PC-MRA in the measurement of velocity at the ECA (**Figure 7-6**)

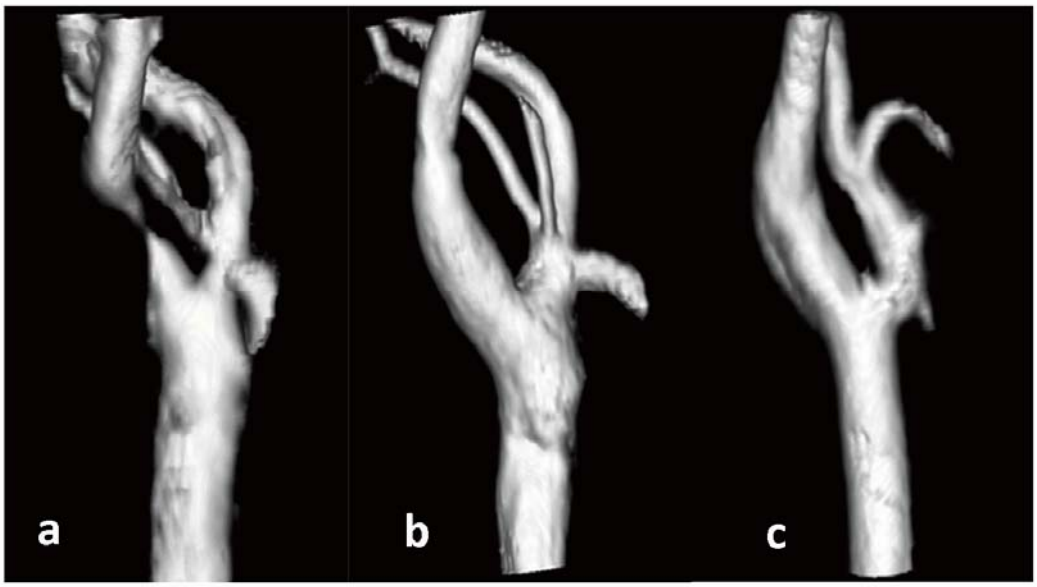

Figure 7-1. 3D TOF-MRA images generated from pre-CEA (a), post-CEA (b) and normal carotids (c). Pre- and post-CEA carotids are from a 59-year-old male with severe stenosis at the proximal internal carotid artery 3 days before and 5 days after CEA. The normal carotid is from a 48-year-old healthy male. 3D, three-dimensional; TOF-MRA, time-of-flight magnetic resonance angiography; CEA, carotid endarterectomy.

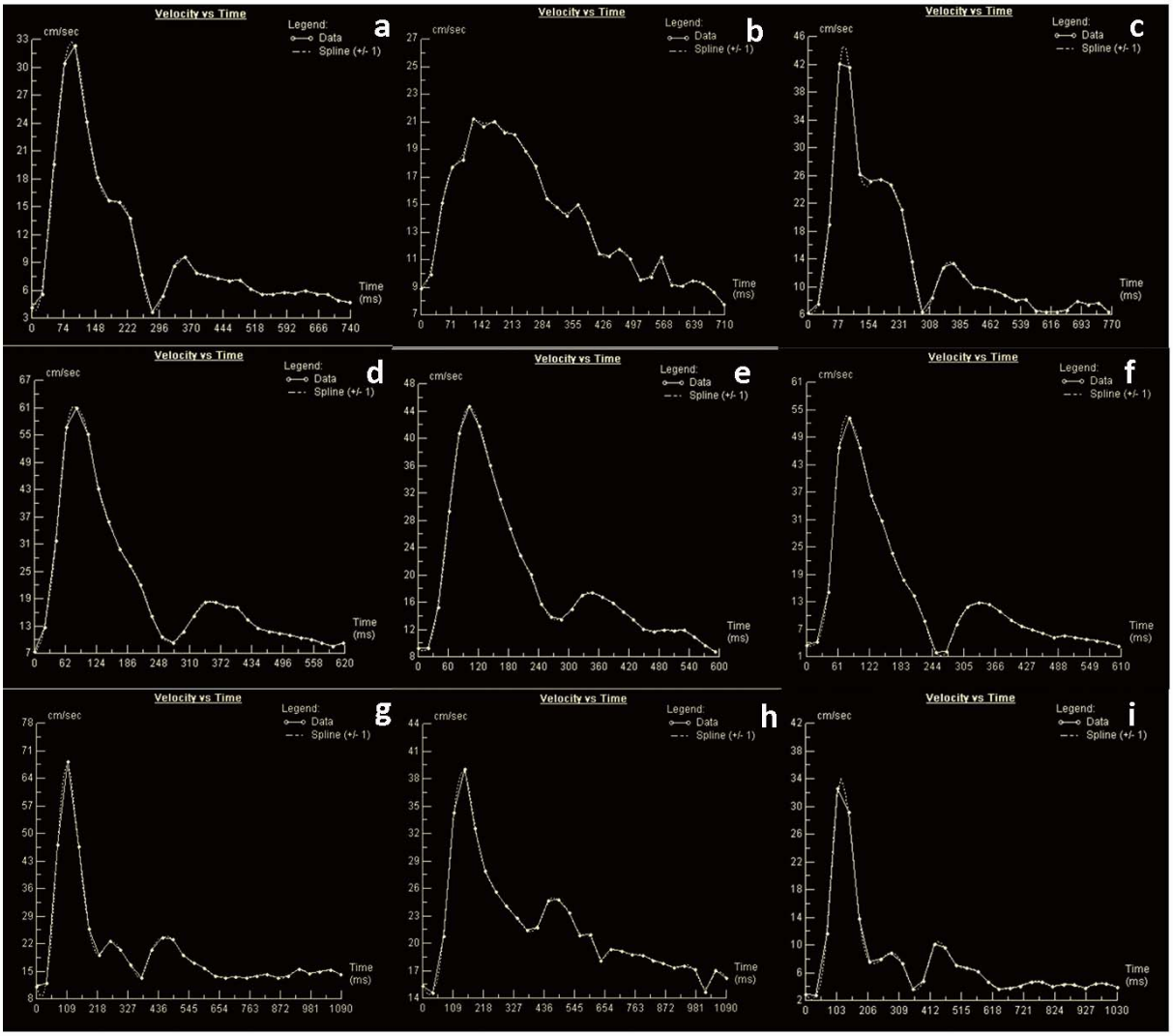

Figure 7-2. Velocities measured by PC-MRA. a-c show velocities from CCA (a), ICA (b) and ECA (c) of a pre-CEA carotid (the same artery as Fig.1a). The velocities of the post-CEA carotid (the same artery as Fig.1b) in CCA (d), ICA (e) and ECA (f) are shown. The velocities of a normal carotid (the same artery as Fig.1c) measured in CCA (g), ICA (h) and ECA (i) are demonstrated. PC-MRA, phase-contrast magnetic resonance angiography; CCA, common carotid artery; ICA, internal carotid artery; ECA, external carotid artery

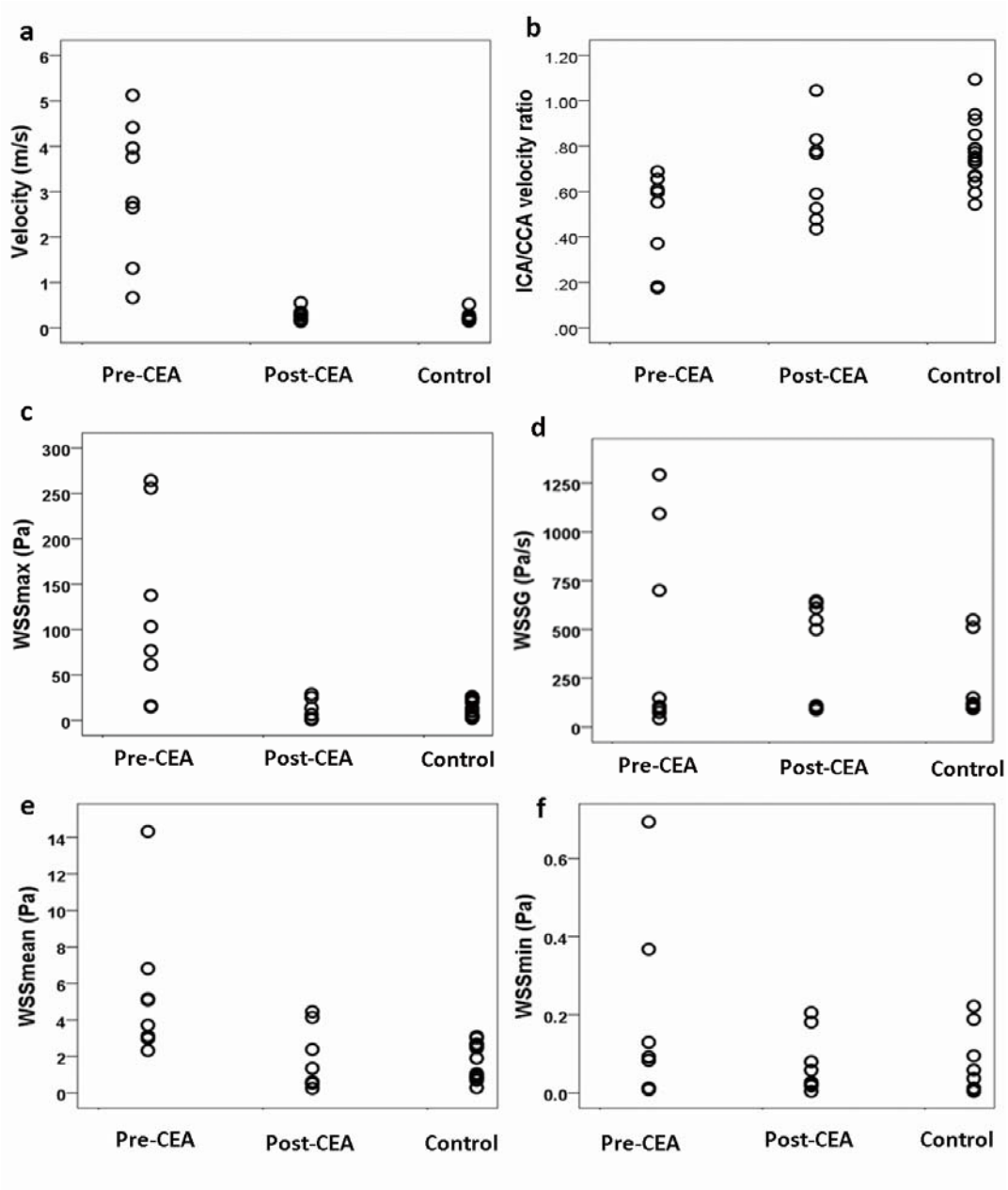

Figure 7-3. Scatter plots show the haemodynamic parameters of velocity (a), ICA/CCA velocity ratio (b), WSS_{max} (c), WSSG (d), WSS_{mean} (e) and WSS_{min} (f) from eight stenotic carotids before and after CEA and sixteen normal carotids (Control). ICA, internal carotid artery; CCA, common carotid artery; WSS, wall shear stress; WSSG, wall shear stress gradient.

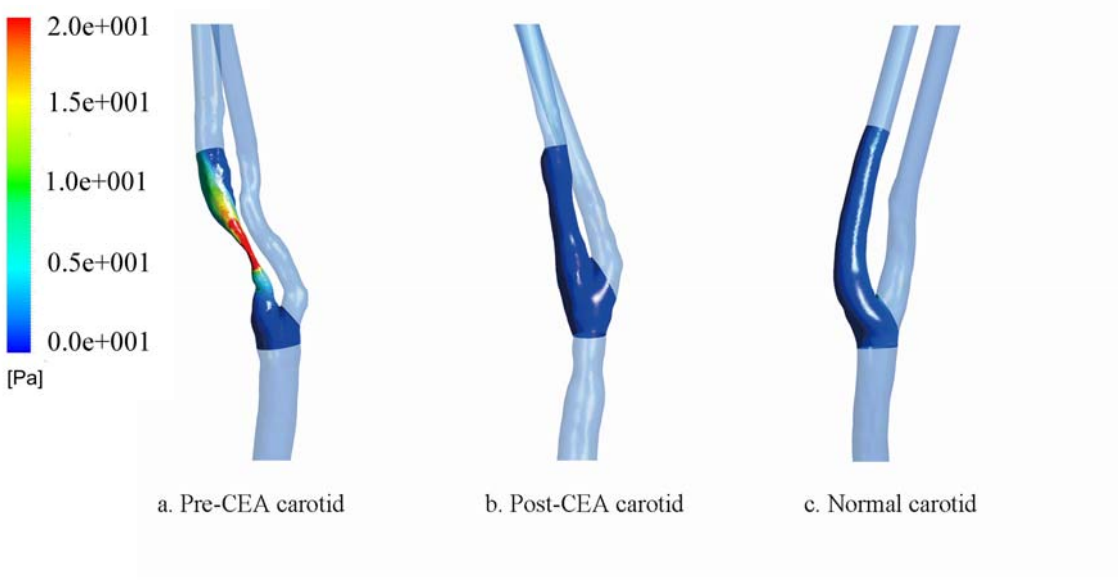

Figure 7-4. Wall shear stress map showed that the distribution of wall shear stress was demonstrated on a pre-CEA (a), post-CEA (b) and normal carotid (c). Wall shear stress increases significantly at stenotic area of pre-CEA carotid. In contrast, the wall shear stress profile after CEA from the same patient is similar to that of a normal carotid. CEA, carotid endarterectomy.

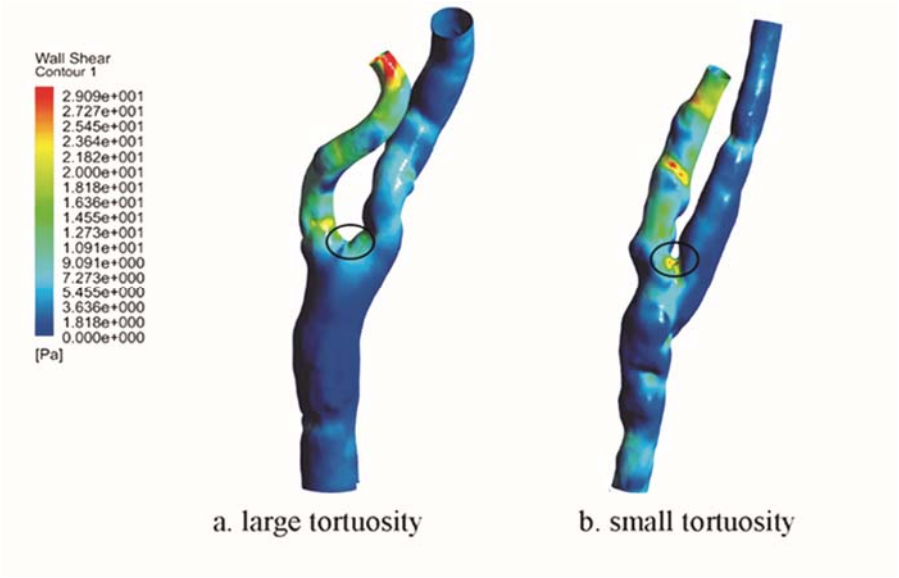

Figure 7-5. Wall shear stress map demonstrated that (a) the carotid with large tortuosity showed relatively low wall shear stress at bifurcation area (circle), while the carotid with small tortuosity showed relatively high wall shear stress at bifurcation (b).

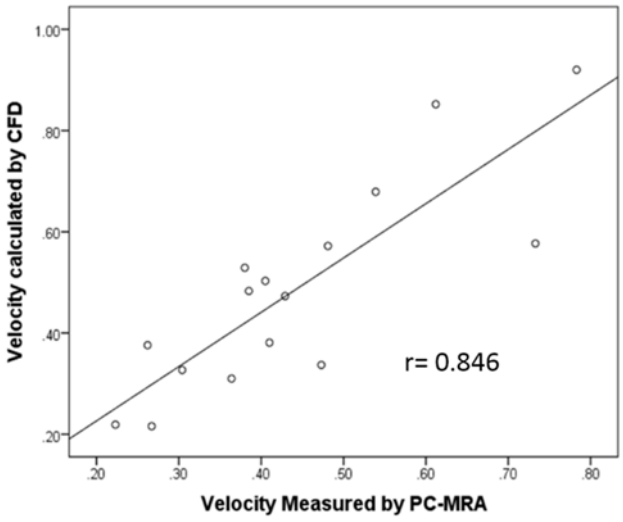

Figure 7-6. There is an excellent agreement between CFD and PC-MRA in measurement of the velocity at external carotid artery. CFD, computational fluid dynamics; PC-MRA, phase-contrast magnetic resonance angiography.

7.4 Discussion

This preliminary study showed that velocity, ICA/CCA velocity ratio, WSS_{max}, WSS_{mean} and WSSG significantly altered after CEA. With normal arteries as a control group, these main haemodynamic parameters of post-CEA arteries were recovered to those normal levels. In addition, we found that bifurcation angle alternations before and after CEA had connections with haemodynamic changes. Based on our results, we can draw a conclusion that the application of unenhanced MRA combined with CFD could provide comprehensive understanding for both flow dynamic and morphological alterations after CEA. The combination of unenhanced MRA and CFD method may greatly facilitate the blood flow follow-up studies after surgery, as it is non-invasive and safe.

Four-dimensional (4D) flow MRI is able to measure both velocity and WSS at the carotid bifurcation (8, 20). Harloff *et al.* [6] compared flow parameters before and after CEA via the use of 4D flow MRI and found that regional WSS decreased after CEA surgery. An earlier study explored similar techniques and showed that the distribution of WSS within stenotic arteries differed greatly from normal arteries, and that the flow distribution in post-operative arteries returned to values that closely resembled pre-operative conditions [15]. Compared with CFD, limitations in 4D flow MRI such as lower spatial and temporal resolution, and relatively poorer delineations in vessel surfaces may hamper the computation of absolute haemodynamic values [13, 16]. Furthermore, 4D flow MRI measurements require relatively long acquisition times depending on the patient's heart rate [13, 16] whilst special software that are not yet widely available, may limit its clinical application [17].

CFD has been applied in the haemodynamic assessment of blood flow. Accurate CFD simulation depends on patient-specific anatomy and flow boundary conditions. In real clinical

scenarios, however, flow boundary conditions are not always available[18]. As a result, the boundary conditions for CFD simulation were typically assumed with statistic or mean values obtained from the literature [7, 19]. This may create inaccuracies on an individual basis, especially at areas with complex geometry, which may lead to errors in the simulation of outcomes. In this study, however, we employed flow results from PC-MRA to assess individual flow boundary conditions. With this patient-specific measurement, our results and comparison studies increase in reliability and clinical relevance.

Using CFD technique, Guerciotti *et al.* [9] showed that both peak velocity and maximum WSS decreased significantly after CEA in patients with severe stenosis. However, since the study lacked a comparison with normal artery haemodynamics, the extent of the haemodynamic recovery after CEA could not be reliably appreciated. Due to localized dilatation at the carotid bifurcation and insufficient understanding of the flow dynamics following CEA, the establishment of a normal control is paramount for the accurate interpretation of CFD measurements. In this study, we found that both the magnitude and distribution of WSS at the bifurcation after CEA were similar to those of controls. We found that both carotid geometry and flow were recovered shortly after CEA, with local post-operative dilatation seemingly having little effect on the flow.

The recurrence rate of stenosis after CEA was approximately 4.1% - 5.8% [20]. Since flow dynamics plays a critical role in the development and progression of atherosclerosis, its alteration may also lead to restenosis after revascularisation surgery. CFD would be a valuable tool to inspect flow after CEA. However, a longer period of observation will be necessary to confirm carotid geometry remodelling and flow alternation which may lead to restenosis.

In order to inspect concordance between CFD simulations and PC-MRA measurements, we performed a correlation study for velocity measurements at the ECA. An excellent correlation was shown between PC-MRA measurements and CFD simulation. The small differences between the two measurements could be attributed to the errors from PC-MRA, caused by dephasing effects at the stenosis. However, a deviation of less than 10% by PC MRA was considered acceptable [8]. Additionally, small arteries which branched off the ECA were not included in CFD modelling, another potential reason to explain the velocity differences between the two methods.

From the comparisons of morphological characteristics, we observed the bifurcation angles of pre-surgery arteries were smaller than those normal ones. Although no significant difference was found in bifurcation angles between pre-CEA and post-CEA carotids, in seven arteries they increased after CEA. We believe that CEA could increase the bifurcation angle in most carotids with stenosis located at proximal ICA and carotid bulb. Our study also showed that no significant difference between tortuosity and planarity between pre-CEA and post-CEA arteries. It appeared that surgery might have different impacts on tortuosity and planarity of different carotids. Further studies with more cases are necessary to verify our observations.

Morphologic characteristics are thought to contribute to local haemodynamics. In our study, we found that the WSS differed between post-CEA cases with different tortuosities. In cases featuring small tortuosities, WSS values were higher at the bifurcation following surgery. As shown in a previous study, restenosis after carotid stenting occurred more frequently in arteries with smaller tortuosities [5]. We speculate that carotids with small tortuosity might have a higher risk of restenosis after CEA, although follow-up observations are required to support this assumption. We suggest that morphological analysis could also provide extra

information for follow-up assessment of carotid artery after surgical intervention.

There were some limitations in this study. The vessel wall surface was assumed to be rigid, and CFD simulation was performed as a steady flow. Although carotid flow is pulsatile, its vessel surface displacement is typically less than 10% [21]. A previous study demonstrated that the rigid wall assumption had little effect on WSS calculation when the vessel wall displacement was small [22]. Besides, the ages between the control group and the study group did not totally match, which may cause bias on the comparison of haemodynamics parameters. Therefore, an age-matched study would be convincible. Another limitation was that long-term follow-up was not available and the study was limited by a small number of cases. Although haemodynamic recovery after CEA was convincingly demonstrated through intra-individual and inter-individual comparison in this study, a large population of patients and a longer time of follow-up would be necessary to further observe its consequences.

7.5 Conclusion

For carotid arteries with severe stenosis, major flow dynamics at bifurcation was found to be restored shortly after CEA. CFD simulation based on unenhanced MRAs was able to effectively evaluate haemodynamic changes both before and after CEA. It is a promising technique in the assessment and follow-up of the patient-specific effectiveness of revascularisation.

References

1. Biller J, Feinberg WM, Castaldo JE, et al. Guidelines for carotid endarterectomy: a statement for healthcare professionals from a Special Writing Group of the Stroke Council, American Heart Association. Circulation. 1998;97(5):501-509.

2. Thim T, Hagensen MK, Horlyck A, et al. Wall shear stress and local plaque development in stenosed carotid arteries of hypercholesterolemic minipigs. J Cardiovasc Dis Res. 2012;3(2):76-83.

3. Tuenter A, Selwaness M, Arias Lorza A, et al. High shear stress relates to intraplaque haemorrhage in asymptomatic carotid plaques. Atherosclerosis. 2016;251:348-354.

4. Schirmer CM, Malek AM. Patient based computational fluid dynamic characterization of carotid bifurcation stenosis before and after endovascular revascularisation. J Neurointerv Surg. 2012;4(6):448-454.

5. Uemiya N, Lee CJ, Ishihara S, Yamane F, Zhang Y, Qian Y. Analysis of restenosis after carotid artery stenting: preliminary results using computational fluid dynamics based on three-dimensional angiography. J Clin Neurosci. 2013;20(11):1582-1587.

6. Harloff A, Berg S, Barker AJ, et al. Wall shear stress distribution at the carotid bifurcation: influence of eversion carotid endarterectomy. Eur Radiol. 2013;23(12):3361-3369.

7. Gharahi H, Zambrano BA, Zhu DC, DeMarco JK, Baek S. Computational fluid dynamic simulation of human carotid artery bifurcation based on anatomy and volumetric blood flow rate measured with magnetic resonance imaging. Int J Adv Eng Sci Appl Math. 2016;8(1):40-60.

8. Calderon-Arnulphi M, Amin-Hanjani S, Alaraj A, et al. In vivo evaluation of quantitative MR angiography in a canine carotid artery stenosis model. AJNR Am J Neuroradiol. 2011;32(8):1552-1559.

9. Guerciotti B, Vergara C, Azzimonti L, et al. Computational study of the fluid-dynamics in carotids before and after endarterectomy. J Biomech. 2016;49(1):26-38.

10. Debrey SM, Yu H, Lynch JK, et al. Diagnostic accuracy of magnetic resonance

angiography for internal carotid artery disease: a systematic review and meta-analysis. Stroke. 2008;39(8):2237-2248.

11. Harloff A, Zech T, Wegent F, Strecker C, Weiller C, Markl M. Comparison of blood flow velocity quantification by 4D flow MR imaging with ultrasound at the carotid bifurcation. AJNR Am J Neuroradiol. 2013;34(7):1407-1413.

12. Khodarahmi I. Comparing velocity and fluid shear stress in a stenotic phantom with steady flow: phase-contrast MRI, particle image velocimetry and computational fluid dynamics. MAGMA. 2015;28(4):385-393.

13. Cibis M, Potters WV, Selwaness M, et al. Relation between wall shear stress and carotid artery wall thickening MRI versus CFD. J Biomech. 2016;49(5):735-741.

14. Kwee RM, Teule GJ, van Oostenbrugge RJ, et al. Multimodality imaging of carotid artery plaques: 18F-fluoro-2-deoxyglucose positron emission tomography, computed tomography, and magnetic resonance imaging. Stroke. 2009;40(12):3718-3724.

15. Markl M, Wegent F, Zech T, et al. In vivo wall shear stress distribution in the carotid artery: effect of bifurcation geometry, internal carotid artery stenosis, and recanalization therapy. Circ Cardiovasc Imaging. 2010;3(6):647-655.

16. Cibis M, Potters WV, Gijsen FJ, et al. Wall shear stress calculations based on 3D cine phase contrast MRI and computational fluid dynamics: a comparison study in healthy carotid arteries. NMR Biomed. 2014;27(7):826-834.

17. Markl M, Schnell S, Wu C, et al. Advanced flow MRI: emerging techniques and applications. Clin Radiol. 2016;71(8):779-795.

18. Dong J, Inthavong K, Tu J. Image-based computational hemodynamics evaluation of atherosclerotic carotid bifurcation models. Comput Biol Med. 2013;43(10):1353-1362.

19. Ohhara Y, Oshima M, Iwai T, et al. Investigation of blood flow in the external carotid artery and its branches with a new 0D peripheral model. Biomed Eng Online. 2016;15:16.

20. Kumar R, Batchelder A, Saratzis A, et al. Restenosis after Carotid Interventions and Its Relationship with Recurrent Ipsilateral Stroke: A Systematic Review and Meta-analysis. Eur J Vasc Endovasc Surg. 2017;53(6):766-775.

21. Cinthio M, Ahlgren AR, Bergkvist J, Jansson T, Persson HW, Lindstrom K. Longitudinal movements and resulting shear strain of the arterial wall. Am J Physiol Heart Circ Physiol. 2006;291(1):H394-402.
22. Zhao SZ, Xu XY, Hughes AD, et al. Blood flow and vessel mechanics in a physiologically realistic model of a human carotid arterial bifurcation. J Biomech. 2000;33(8):975-984.

Chapter 8

Conclusions and Future Directions

8.1 Conclusion

The morphological evaluation of carotid atherosclerotic plaques is critical for the risk stratification of stroke. The advancement of magnetic resonance imaging (MRI) has allowed comprehensive morphological evaluations of atherosclerotic plaques. However, conventional multi-contrast MRI requires relatively long acquisition time and is poorly suited for the interpretation of plaque components; therefore, conventional multi-contrast MRI has limited application in clinical practice. In this regard, the conventional multi-contrast MRI techniques need to be optimised, so that they can find broad application in clinical practice.

A new multi-contrast MRI sequence named 'MATCH' has been introduced and validated in this study. MATCH has the potential to be a substitute for conventional multi-contrast MRI sequences, as MATCH is time-efficient and well suited for the interpretation of plaque components. The MATCH sequence was first introduced by Fan *et al.* [1]; however, with application to only a small number of subjects and without any histological confirmations, its ability to characterise plaque components needed to be further addressed. We conducted a large cohort study using MATCH to characterise the major plaque components, and we also provided histological evidence to validate the performance. The results demonstrated that MATCH is superior to conventional multi-contrast MRI, particularly in the identification of tiny and scattered calcifications. Our study indicates that MATCH is more advantageous than conventional multi-contrast MRI, so it can therefore replace conventional multi-contrast MRI and is applicable in clinical practice.

The progress in advanced imaging techniques has also encouraged the development of image-based computational fluid dynamics (CFD). Image-based CFD can provide patient-specific

haemodynamic information and functional assessment, beyond the morphological evaluations.

Our second contribution is that I, in collaboration with my co-workers, developed a new methodology via the use of non-contrast-enhanced MRI and CFD to explore the relationship between intraplaque haemorrhage (IPH) in carotid arteries and the local haemodynamics. The relationship between IPH and haemodynamics has not been fully understood due to the lack of characterisation tools. In this part of my research I found that there were associations between IPH and maximum wall shear stress (mWSS). The associations were observed in the carotids with stenosis of less than 70%, and the associations tended to be prominent in the mild stenosis cases. Our results indicate that the mWSS can used as a quantitative parameter to evaluate plaque vulnerability in the early stage of atherosclerosis, and thereby to predict the future risks of stroke. The exploration of the relationships between IPH and mWSS also promotes the understanding of the connections between plaque components and local haemodynamics, thereby providing insights for future works.

The third contribution of this work is to provide a methodology to assess the outcomes of carotid endarterectomy (CEA). Currently the post-surgery assessments mainly depend upon morphological evaluation, whereas functional assessment is not yet available in clinical practice. Despite successful operations, vascular restenosis occurred in some cases, but the causes remain unknown. In this study I proposed a methodology that combines non-contrast-enhanced MRA with CFD to provide functional assessments after surgery. I found that in the short term after CEA, the local haemodynamic perturbations can be recovered in cases with successful operations. The results indicate that the proposed methodology could provide

quantitative haemodynamic information to help predict the outcomes of surgery. Furthermore, the assessment of these haemodynamics might have potential to enhance the understanding of the underlying mechanisms of vascular restenosis.

8.2 Future directions

8.2.1 The optimisation of MATCH

Despite the many merits of the current MATCH sequence presented in our study, there are some limitations of MATCH, including that the image quality is not excellent for all cases. Therefore, the sequence can be optimised in terms of the image quality. Besides that, the acquisition time of the current MATCH sequence still can be shortened. The acquisition time of the current MATCH sequence is around 5:30 minutes, which is only half that of the conventional sequence; nevertheless it could be reduced through an optimisation process. Furthermore, the performance of MATCH in plaque characterisation needs to be further confirmed: the relatively large number of subjects in the present study proved the ability of MATCH in the characterisation of plaque components; however, studies of even larger subject numbers from multiple institutions are necessary to facilitate the clinical application of MATCH.

8.2.2 Evidence-based study

Although it was demonstrated in this work that haemodynamics has the potential to evaluate plaque vulnerability, the threshold of the mWSS has not been provided due to the relatively small subjects and lack of histological evidence for intraplque haemorrhage. Therefore, large evidence-based studies should be conducted to verify our results and to provide thresholds for the haemodynamic parameters. With this knowledge, the haemodynamic parameters would be

able to provide guidance for the clinicians to make predictions before the treatment.

8.2.3 Longitudinal follow-ups

The underlying mechanism of restenosis after carotid revascularisation remains unclear. It is acknowledged that haemodynamics might be able to explain the underlying mechanisms of restenosis, as it contributes to the initiation and progress of atherosclerosis. Therefore it is necessary to conduct follow-up studies after revascularisation for the dynamic observation of vascular restenosis.

8.2.4 Other haemodynamic parameter

Other haemodynamic parameter need to be introduced to the study of carotid atherosclerosis in order to further understand of local haemodynamics of carotid atherosclerosis. Energy loss (EL) is a biomechanical parameter that represents the relative amount of energy absorbed by the vasculature during the cardiac cycle [2]. EL has been applied in predicting the rupture of intracranial aneurysms [3], and in studying aortic aneurysms [4] and congenital heart diseases [5]. It has been demonstrated that EL can be a better predictor in the rupture of intracranial aneurysm compared to wall shear stress [6]. Therefore, it would be interesting to apply EL analysis to carotid atherosclerosis, especially in the rupture of atherosclerotic plaques.

EL can be calculated from the following equation [7]:

$$\mathrm{EL} = \sum_{i=1}^{n_{\mathrm{in}}} Q_{\mathrm{in},i}\left(\frac{p_i}{\rho} + \frac{1}{2}{v_i}^2\right) - \sum_{i=1}^{n_{\mathrm{out}}} Q_{\mathrm{out},j}\left(\frac{p_j}{\rho} + \frac{1}{2}{v_j}^2\right) \qquad (8\text{-}1)$$

where Q denotes mass flow rate, p is static pressure, ρ is fluid density, v is inflow or outflow velocity; and i and j are indices referring to locations in the measurement domain.

Reference

1. Fan Z, Yu W, Xie Y, et al. Multi-contrast atherosclerosis characterization (MATCH) of carotid plaque with a single 5-min scan: technical development and clinical feasibility. J Cardiovasc Magn Reson. 2014;16:53.

2. Moon JY, Suh DC, Lee YS, Kim YW, Lee JS. Considerations of blood properties, outlet boundary conditions and energy loss approaches in computational fluid dynamics modeling. Neurointervention. 2014;9(1):1-8.

3. Qian Y, Takao H, Umezu M, Murayama Y. Risk analysis of unruptured aneurysms using computational fluid dynamics technology: preliminary results. AJNR Am J Neuroradiol. 2011;32(10):1948-1955.

4. Chung J, Lachapelle K, Wener E, et al. Energy loss, a novel biomechanical parameter, correlates with aortic aneurysm size and histopathologic findings. J Thorac Cardiovasc Surg. 2014;148(3):1082-1088.

5. Qian Y, Liu JL, Itatani K, Miyaji K, Umezu M. Computational hemodynamic analysis in congenital heart disease: simulation of the Norwood procedure. Ann Biomed Eng. 2010;38(7):2302-2313.

6. Takao H, Murayama Y, Otsuka S, et al. Hemodynamic differences between unruptured and ruptured intracranial aneurysms during observation. Stroke. 2012;43(5):1436-1439.

7. Zhang M, Li Y, Zhao X, et al. Haemodynamic effects of stent diameter and compaction ratio on flow-diversion treatment of intracranial aneurysms: A numerical study of a successful and an unsuccessful case. J Biomech. 2017;58:179-186.

Appendix of this thesis has been removed as they may contain sensitive/confidential content